Design and fabrication of functionalized high porous poly(lactic acid)-based scaffolds for tissue engineering

Xavier Puñet Ortiz

Design and Fabrication of Functionalized High Porous Poly(lactic acid)-based Scaffolds for Tissue Engineering

Author: Xavier Punet

Universitat Politècnica de Catalunya, Barcelona, España

Director: Dr. Miguel Ángel Mateos-Timoneda

UPC tutor: Dr. Elisabeth Engel

Programa de Doctorat en Enginyeria Biomèdica

Departament d'Enginyeria Biomèdica

Universitat Politècnica de Catalunya

Barcelona, 2015

Tesi presentada per a obtenir el títol de Doctor per la Universitat Politècnica de Catalunya

Vol. 1 de 1 Vol.

Per als meus pares, Montse i Xavi,
amb tot l'amor i gratitud

"Every one of us is, in the cosmic perspective, precious. If a human disagrees with you, let him live. In a hundred billion galaxies, you will not find another."

—Carl Sagan, Cosmos

CONTENTS

ABSTRACT

Intelligent scaffolds are designed to trigger the healing regeneration process through the controlled released or disposition of bioactive signals. The fabrication of intelligent scaffolds needs the development of novel techniques able to introduce biomimetic properties on the final product through easy and scalable techniques. This thesis is focused on the characterization and development of two versatile techniques for the fabrication of intelligent scaffolds. The first technique is based on the biofunctionalization of polymeric surfaces with synthetic polypeptides (elastin-like recombinamers) for the improvement of cell-surface interactions. The second technique is based on the fabrication of highly porous poly(lactic) acid scaffolds with a nano-fibrous structure that resembles the natural extracellular matrix by means of a novel non-toxic, cheap and easy process.

RESUMEN

Los andamios inteligentes son diseñados para activar los procesos de regeneración a través de la dosificación o disposición controlada de señales bioactivas. Sin embargo es necesario desarrollar nuevas técnicas capaces de introducir propiedades biomemiméticas en dichos andamios a través de metodologías sencillas e industrializables. La presente tesis se centra en la caracterización y desarrollo de dos técnicas versátiles para la fabricación de andamios inteligentes. La primera técnica se basa en la biofuncionalización de superficies poliméricas con polipéptidos sintéticos (*elastin-like recombinamers*) para la mejora de las interacciones entre las células y la superficie del material. La segunda técnica se basa en la fabricación de andamios de ácido poli(láctico) altamente porosos, con una estructura nano-fibrosa que mimetiza la matriz extracelular, a través de procesos fáciles, económicos y no tóxicos.

LIST OF FIGURES

LIST OF TABLES

LIST OF ABBREVIATIONS

2D - Two Dimensional
3D - Three Dimensional
ACL - Anterior Cruciate Ligament
AFM - Atomic Force Microscopy
ALP - Alkaline Phosphatase
AR - Aspect ratio
Arg - Arginine
Asp - Aspartic acid
ATMP - Advanced Therapy Medicinal Product
BSA - Bovine Serum Albumin
CaP - Calcium Phosphate
CAT - Committee for Advanced Therapies
CATMP - Combined Advanced Therapy Medicinal Product
CE - European Conformity
CL - Caprolactone
COGS - Cost of Goods Sold
CT - Computed Tomography
DNA - Deoxyribonucleic Acid
ECM - Extracellular Matrix
EDC - 1-Ethyl-3-(3-dimethylaminopropyl)carbodiimide
ELISA - Enzyme-Linked ImmunoSorbent Assay
ELR - Elastin-like Recombinamer
EMA - European Medicines Agency
EtLac - Ethyl Lactate
FBS - Fetal Bovine Serum
FDA - Food and Drug Administration
FITC - Fluorescein Isothiocyanate
Fn - Fibronectin
FTE - Full Time Equivalent
G_6RGDS - RGD short peptide sequence
G_6RGE - Scramble short peptide sequence (negative control)
GAGs - Glycosaminoglycans
Gly - Glycine
GMP - Good Manufacturing Practices
GTMP - Gene Therapy Medicinal Product
HA - Hydroxyapatite
HMW - High Molecular Weight
$HRGD_6$ - Elastin-like recombinamer with RGD sequence
HUVEC - Human Umbilical Vein Endothelial Cells
IH - Intimal Hyperplasia
IK_{24} - Elastin-like recombinamer without RGD sequence (negative control)
LDH - Lactate Dehydrogenase
LDI - Lysine Diisocyanate
MAA - Marketing Authorization Application
MMP - Metalloproteases
MRI - Magnetic Resonance Imaging
MSC - Mesenchymal Stromal Cell
Mw - Molecular Weight
NaOH - Sodium Hydroxide
NHS - N-hydroxysuccinimide
O.N. - Overnight
PBS - Phosphate-buffered Saline
PCL - Polycaprolactone
PDL - Population Doubling Levels
PDMS - Polydimethylsiloxane
PEG - Polyethylene glycol
PFA - Paraformaldehyde
PGA - Polyglycolic acid
PGS - Polyglycerol sebacate
PLA - Polylactic acid

PLCL - Poly(L-lactide-co- ε -caprolactone)

PLGA - Poly(lactic-co-glycolic) acid

PMMA - Poly(methyl methacrylate)

PTFE - Polytetrafluoroethylene

PTMC - Poly(trimethylene carbonate)

PU - Polyurethane

PVA - Poly(vinyl alcohol)

PWV - Pulse Wave Velocity

Ra - Average Roughness

RGD - Arginine-Glycine-Aspartic acid

RNA - Ribonucleic Acid

ROI - Return on Investments

SCTP - Somatic Cell Therapy Product

SD - Standard Deviation

SEM - Scanning Electron Microscopy

Ser - Serine

SFF - Solid Free-Form

SMC - Smooth Muscles Cells

SME - Small- and Medium-sized Enterprises

TCP - Tissue Culture Polystyrene Plate

TEP - Tissue Engineered Product

Tg - Glass Transition Temperature

T_{GEL} - Gel Temperature

t_{gel} - Gelation Time

THF - Tetrahydrofuran

TOF-SIMS - Time-of-Flight Secondary Ion Mass Spectrometry

UV - Ultraviolet

VEGF - Vascular Endothelial Growth Factor

VP - Value Proposition

CHAPTER 1

1. GENERAL INTRODUCTION

The regenerative therapies market appeared more than two decades ago, however, business success has been limited to few products. Indeed, most innovative projects tend to fail during the clinical trials or are not able to attract funding. Nowadays there is a deep gap between the huge amount of investments spent on tissue engineering research and the actual retribution on society health and wealth. Given the smaller market sizes, long testing times, specific niches and involved technology, regenerative medicine market is ruled by different business models than pharmaceuticals. Actually, the development of regenerative medicine products is generally undergone by small- and medium- sized companies that normally emerge from public research. Thus, in order to increase the ratio of successful research that truly jumps from the bench to the bedside, strong efforts have been devoted to raise awareness throughout researchers on the key aspects that they need to assess during the development stage.

The work presented in this manuscript collects the results of the investigations realized on the area of scaffold design and fabrication for tissue engineering purposes. The efforts of this work are oriented on expose and characterize fabrication methodologies for the development of biomedical devices that may easily overcome the difficulties found on the path toward the market.

This thesis focuses on the development of two different combinable approaches for the fabrication and design of polymeric scaffolds for regenerative therapies. The first approach explores the use of elastin-like recombinamers (ELRs) as a methodology for enhancing cell-surface interactions. The second approach is focused on the development of a novel methodology for the fabrication of highly porous scaffolds by means of phase-separation processes between poly(lactic acid) (PLA) polymer and ethyl lactate (EtLac) solvent. Both approaches are envisaged to be used on the fabrication of scaffolds for the clinics. Thus, they are

based on biocompatible, green, reproducible, scalable and cheap techniques that, nevertheless, present high potential and versatility to be implemented on different clinical situations.

Briefly, the goals of the thesis are resumed as follows:

- Study and characterization of polymeric surfaces functionalized with ELRs to enhance cell-biomaterial interactions.
- Comparative study of the cellular response on polymeric surfaces functionalized with ELRs versus short peptides.
- Development and characterization of a scaffold fabrication method using the PLA-EtLac system properties.
- Characterization of the scaffolds properties obtained from the processing of PLA-EtLac system.
- Fabrication and characterization of a PLA vessel graft fabricated with the PLA-EtLac system and functionalized with ELRs.

In Chapter 2 an overview of tissue engineering market is given and the key concepts of scaffold development such as design, manufacturing and mimicking strategies are assessed.

In Chapter 3 the effect of ELR functionalization on non-biodegradable polymeric poly(methyl methacrylate) surfaces shows improved cell-biomaterial interaction compared to short peptide functionalization. In these studies, the unspecific adsorption of bovine serum albumin (BSA) protein is used to show the competitive advantage of ELR functionalization against short peptides.

In Chapter 4 the studies from Chapter 3 are reproduced on biodegradable polymeric PLA surfaces. ELR surface functionalization processes are deeper studied under the atomic force microscope. ELR non-fouling capacity is detected and correlated with the improved cellular response.

In Chapter 5 a novel scaffold fabrication methodology is developed. The system comprised by PLA polymer and EtLac solvent shows unexpected gelation properties, which are used to mould three-dimensional structures that can be precipitated to fabricate scaffolds. This study characterizes the gelation process through rheometric techniques, and analyses the physical properties of the obtained scaffolds.

In Chapter 6 both approaches, the use of ELRs and the novel scaffold fabrication methodology, are implemented on the fabrication of small-calibre vessel grafts. This study describes the mechanical properties of obtained vessel grafts, as well as first in vitro cell response.

Finally, Chapter 7 summarizes the overall conclusions resulted from the presented work and depict the future perspectives.

CHAPTER 2

2. INTRODUCTION AND STATE OF THE ART

2.1. Tissue Engineering: Born and Evolution of a New Industry

Humanity has been using active substances as medicaments from their very first steps. Actually, the use of natural active products to cure, prevent or palliate illnesses is not a specific competence of humanity, and many animals do it as well, whether in an instinctive manner or through a cultural knowledge. Thus, medicine existed and has been improving life quality and life expectancy from the very ancient times. However, the beginning of what we know as modern medicine, based on the knowledge of testable and reproducible results, is placed on the 18th century with the discovery of the smallpox vaccine introduced by Edward Jenner. Next centuries were characterized for the expansion of the medical field and the achievement of important milestones, which lead medicine to flourish into many specialized fields. Soon, the large and crescent population of the industrialized world created an active demand on health products, giving birth in such a way to a new market that was quickly covered by the new-born pharmaceutical industries.

Up to now we have been observing a sophistication of the medicine that has been able to eradicate serious health menaces or transform serious health problems into chronic diseases compatible with a normal and worthy life. Nowadays most people from the developed world can enjoy a life expectancy larger than some decades ago, and most diseases concerning the average human being are those that result from a long life expectancy. Thus, it is possible to find complex illnesses that concentrate most of the attention and resources of recent medicine investments. Cancer, neurodegenerative processes, and all illnesses or injuries that involve tissue lost or tissue lost function are examples of health threats on the scope of medicine. Such illnesses, due to the high intrinsic complexity of the involved systems, only can be faced from a

very transversal point of view. Thus, tissue engineering evolved to develop tools to give solution to these news problems.

According to Viola et al. [1], the term 'tissue engineering' first appeared in PubMed literature in 1984 'Transactions of the American Ophthalmological Society' [2]. But the most used definition of tissue engineering was given in 1993 by Langer and Vacanti as

'an interdisciplinary field that applies the principles of engineering and life sciences towards the development of biological substitutes that restore, maintain or improve tissue function' [3].

References to replacement of tissues and organs, however, travel back to 1938, in the book 'The Culture of Organs', written by Alexis Carrel and Charles Lindsberg [4]. But substitutive medicine did not make the first attempts until the decade between 1955 and 1965, with the development of artificial hips, artificial lungs, external haemodialysis and pacemakers. Later, with the emergence of the stem cell technology, the term tissue engineering evolved into the broader area of regenerative medicine, which was an expression coined by William Hazletine in the late 1990s [5]. The definition of regenerative medicine is often stated as

'self-healing process through the endogenous recruitment or the exogenous delivery of appropriate cells, biomolecules and supporting structures'.

Differences between the terms tissue engineering and regenerative medicine are vague, and most of the times are used without distinction.

Parallel to research development, in the early 1990s, a new industry appeared in the context of a nascent tissue engineering market. The growth and evolution of this market, due to its ups and downs, have been widely studied (Figure 1) [6-8]. During the first decade, tissue engineering industry lived its bests times and expectations. In 1994 the total worldwide private sector related to tissue engineering industry activity was valued in $246 million, with a number of start-up companies rounding the 40s and a total number of employees circa the 1500 FTEs (Full-time equivalents). Few years later, in 2000, the annual expenditure raised to $610 million, with 73 counted firms and 3080 FTEs. During this period, the spending grew at an annual rate of 16% and the aggregate private sector investment exceeded the $3.5 billion. At this time, the capital value of the 16 publicly traded start-ups achieved the $2.6 billion. This 'boom' on the 1990s, characterized by high investments and a large growth on the capital value of publicly traded firms (especially in US), was hyped in part by media. For instance, in 1999, LIFE

initiative (Living Implants from Engineering, USA) promised engineered human organs within 10 years [9]. In 1999 a television report in *Good Morning America* stated tissue engineering 'as the greatest achievement of the twentieth century' [10]. And, in 2000, *Time* magazine elevated tissue engineering to the hottest new job for the twenty-first century [11].

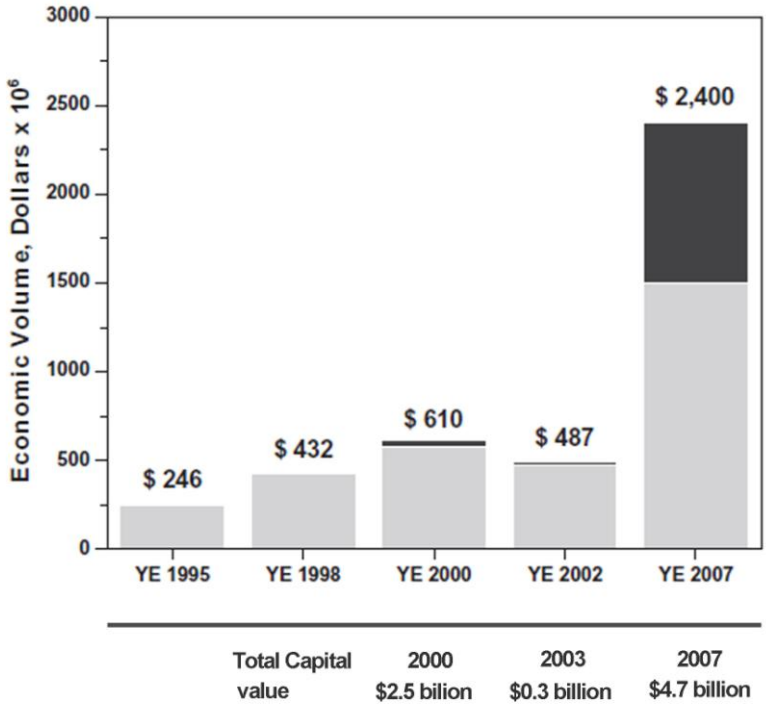

Figure 1. Growth of the worldwide economic value of tissue engineering and regenerative medicine since 1995. Grey colour refers to the development stage spending portion; dark colour refers to the sales spending portion. The total capital value of the 16 publicly traded tissue-engineering start-ups is shown below. Adapted from [7].

However, it has been proved that expectations were glossed over. Between 2001 and 2003 tissue engineering suffered a strong worldwide recession, owing to a combination of factors like the dot-com crash, the failed product launches and the disappointing results from Food and Drug Administration (FDA) clinical trials. Thus, investors were disenchanted, and the market spending, which were growing until now at a 16% rate, declined between 2000 and 2002 by 20%. During these years, 19 counted firms closed or applied for bankruptcy (like the big companies Organogenesis and Advanced Tissue Science), 27 other start-ups downsized significantly, and the capital value of publicly traded tissue engineering firms felt from $2.5 billion in 2000 to $0.3 billion in 2003, which represented an 88% lost. The industrial panorama got restructured and investments on big firms started to recede in favour of investment on small and medium-sized firms (perceived as lower risk).

During the next years tissue engineering industry showed resilience and started to settle down. In 2007, the total worldwide private sector activity stood for $2.4 billion, the number of start-ups raised to 171 and the number of employees achieved the 6100 FTEs. The capital value recovered from $0.3 billion in 2003 to $4.7 billion in 2007. Interestingly, in 2007, from the total private sector activity, $1.3 billion belonged to product sales, showing that this time, tissue engineering industry was supported by commercial profits. From this counted profits, most part was related to acellular products like INFUSE (a recombinant morphogenic bone protein product from Medtronic), with sales valued in $700 million, and other regenerative biomaterials like SIS (an extracellular matrix derived from pig), with sales valued in $240 million. Accounting for the firms in the commercial phase in 2007, 12 were cell- plus biomaterial-based and 6 were only biomaterial-based, from the overall 47 firms with commercial products.

The tissue engineering market in 2007 achieved a stable commercial-stage in which a large part of the economic activity represented product sales (compared to the 5% in 2002). Following years, the field become more diversified, with much of the successful economic activity found in acellular products. However, despite this success, tissue engineering industry still has a lot of setbacks. Indeed, most regenerative products are costly to manufacture and extremely difficult to carry through the regulatory approval. This situation causes that most of the money invested by governments and private sectors on the research and development of regenerative medicine is not translated into social health and, therefore, recovered.

Due to the fast development of regenerative medicine, governments have to continuously design new regulatory systems to fit into the new paradigms of medicine while dealing with the new ethical issues, the development of the new industries and markets, the desperate need of organs and tissue replacements, and the patient protection. Governments are struggling to adapt to the new era of medicine. Actually, the definition and classification of products and the way they actuate are sometimes so diffuse, that specific commissions are created to fit those borderline products into one or another piece of legislation. But the awareness on the new conformation that medicine is adopting is something that not only attains to governments, but to all implied agents. Thus researchers have to change their paradigms as well.

Nowadays, the strategies to face regenerative medicine challenges are multiple, but the successful commercialization of products is still hard owing to a lack of investment, undefined business models and the constantly evolving regulatory framework. It is crucial for those projects which aim to translate their ideas from bench to the bedside, to take into consideration all the challenges placed on the path. Thus, for the success of an idea, the design of biomedical

products have to include from the very beginning a strategic development which contemplates the commercial viability. Considering this, and aside from successful clinical trials, the future of a tissue engineering treatment will also depend on business capacity, financial costs, social acceptance and regulatory issues. And all those issues can be considered during the Phase 0 of a product development; this is, during the research state.

2.1.1. The Regulatory Framework

The understanding of the regulatory requirements involved on the translation of a biomedical product or therapy to the market is paramount for the success. The regulatory framework is complex and the designing of a good strategy can represent a competitive advantage against competitors, or to stay trapped on an unexpected costly regulatory process. The initial decisions done during the Phase 0 will define the product strategy, in which legislation the intended product falls and which regulation route will have to follow. This step is not trivial, and will represent a different time-cost expense depending on the regulatory path. Moreover, considering the scope of the market, different considerations have to be taken, since there are still no harmonized directives around the world, neither inside some parcelled markets like EU. Therefore, market choice and product design can give some competitive advantages or some setbacks.

Concerning the EU market, biomedical products are covered by three different legal frameworks. Depending on the therapy design, it will fall into the legislation for Drugs, Medical Devices or Advanced Medicinal Therapy Products, which in some cases will imply a centralized regulation and in some cases it will not, raising the importance on the individual country policies and regulation bodies. The following sections will provide a comprehensive resource of the different legislations, which can be found on referenced literature [12-15] or in governmental agencies webpage in more detail.

2.1.1.1. Medical Devices

While the regulation for the medical devices in the US began in the mid-1930s, in the EU occurred in the mid-1990s, which is an example of the diphase between both market developments. Before the regulations from 1990s, each country from the EU had its own different legislation. However, on the actuality, medical devices inside the European market are regulated by 3 directives, each one covering different groups: (A) the medical devices directive (European Council Directive 93/42/EEC), which gathers the majority of the medical devices. (B)

The active implantable medical devices directive (European Council Directive 90/385/EEC). And (C) the in vitro diagnostic directive (European Council Directive 98/79/EC).

Medical devices are defined in the EU as "any instrument, appliance, apparatus, material or other article, whether used alone or in combination, including software necessary for its proper application, intended by the manufacturer to be used for human beings for the purpose of: (1) diagnosis, prevention, monitoring, treatment or alleviation of disease; (2) diagnosis, monitoring, alleviation of or compensation of an injury or handicap; (3) investigation, replacement or modification of the anatomy or of physiological processes; and (4) control of conception; and which does not achieve its principal intended action in or on the human body by pharmacological, immunological, or metabolic means, but which may be assisted in its functions by such means" (European Council Directive 93/42/EEC).

The different types of medical devices are classified into four different classes (class I, class IIa, class IIb and class III), using a risk-based system. Medical devices intended for tissue engineering would fall into the class IIb or III (high risk).

In contrast to US, where there is one principal regulatory body (the FDA), the EU presents a more decentralized regulatory system. There are five authorities involved: the European Commission (responsible of the legislation), the competent authorities (authorized body in charge of ensure the translation and application of the European directives to the national law), the notified bodies (private for-profit organization that audit the manufacturer system and the product design for the extension of certificates of compliance) , the authorized representatives (natural or legal person designated by the manufacturer to act on its behalf in compliance matters) and the manufacturers (the natural or legal person with responsibility for the design, manufacturer, packaging and labelling of a device before it is place on the market under his own name, regardless of whether these operations are carried out by that person himself or a third-party).

For the commercialization of medical devices in the EU, the manufacturer must obtain the CE (European Conformity) marking certification and affix the CE marking as part of the device certification efforts (except those devices for clinical investigation). This mark guarantees that device follows the requirements of the directives and accomplishes its intended purposes. It also means that the product can be commercialized freely in the EU without further control, but is not a guarantee of safety or efficacy.

The requirements of the directives include proofs of safety and performance and sometimes technical requirements related to the design and manufacture. When demanded, clinical studies must be offered to fulfil these requirements, but many times data can be supported on bench testing or clinical trials reported on already existing literature, especially if there are equivalent devices already in the market.

Medical Devices are indeed, the less regulated entrance for tissue engineering therapies. Actually, the decentralized system and the intervention of for-profit notified bodies often give place to opaque, non-data supported, uncontrolled market entrance. The post-market surveillance, like the standards of quality and safety, are less strict when compared to Drugs or Advanced Medicinal Therapy Products, which, despite of the problems on health care and the strong controversies that it arises [16], provides the less burdened path and the faster route into the market.

2.1.1.2. Drugs

While drug regulation began in US in 1938 with the creation of the Federal Food, Drug and Cosmetic Act as a respond to the sulphanilamide elixir poisoning of 100 people, mainly children; regulation of Drugs at the European level was legislated in 1965 with the Council Directive 65/65/EEC.

The directive defined Drugs as " Any substance or combination of substances presented for treating or preventing disease in human being or animals", and "Any substance or combination of substances which may be administered to human beings or animals with a view to making a medical diagnosis or to restoring, correcting or modifying physiological functions in human beings or animals".

The regulatory system for drugs at the European level is constituted by the European Commission Directorate General for Health and Consumers Pharmaceutical Unit (in charge for drug regulation) and the European Medicine Agency (responsible for the scientific evaluation of medicines, the overseeing of drugs and pharmacovigilance). For the case of medical devices, there is no analogous agency at the European level, and compared to them, regulatory approval for drugs is far more intensive and expensive.

The free commercialization of drugs in EU needs the marketing authorization, which is only achieved when data supporting their quality, safety and efficacy have been assessed. The acquisition of the marketing authorization can be obtained through three different routes: (A) the

centralized procedure (administered through the European Medicine Agency), (B) the mutual recognition procedure (administered by competent authorities of member states), and (C) the decentralized procedure (administered by one national regulatory agency in agreement with other member states). Alternatively, when product marketing is confined inside only one state, it can be authorized by just national laws.

2.1.1.3. Advanced Therapy Medicinal Products

It was not until 2008 that it was introduced in the European legislation a regulation (EC No. 1394/2007) that provided a centralized and harmonized regulatory framework for the medicine based on regenerative therapeutic products, and tissue-engineered products in particular. This new legislation was framed under the category of Advanced Therapy Medicinal Products (ATMP). The Regulation was designed to allow free movement of the ATMPs within the EU market, better patient access to ATMPs, the highest level of patient health protection, EU competitiveness in the biotechnology area, and the growth of the new regenerative medicine industry. This new regulation established different sub-categories for the ATMPs:

(1) Gene Therapy Medicinal Product (GTMP). Defined as a biological medicinal product which contains an active substance which contains or consists of a recombinant nucleic acid used in or administered to human beings with a view to regulating, repairing, adding or deleting a genetic sequence, and whose therapeutic, prophylactic or diagnostic effect relates directly to the recombinant nucleic acid it contains, or the product of genetic expression of this sequence. GTMP shall not include vaccines against infectious diseases.

(2) Somatic Cell Therapy Product (SCTP). Defined as a biological medicinal product which contains or consists of cells or tissues that have been subject to substantial manipulation so that biological characteristics, physiological functions or structural properties relevant for the intended clinical use have been altered; or which contains or consists of cells or tissues that are not intended to be used for the same essential function(s) in the recipient and the donor; and which is presented as having properties for, or is used in or administered to human beings with a view to treating, preventing or diagnosing a disease through the pharmacological, immunological or metabolic action of its cells or tissues. Manipulations that are not considered as substantial are listed in Annex I to Regulation (EC) No. 1394/2007. Expansion by *ex vivo* culturing is, for instance, currently considered to be a substantial manipulation.

(3) Tissue Engineered Products (TEP). Defined as a product which contains or consists of engineered cells or tissues, and which is presented as having properties for, or is used in or

administered to human beings with a view to regenerating, repairing or replacing a human tissue. A tissue engineered product may contain cells or tissues of human or animal origin, or both. The cells or tissues may be viable or non-viable. It may also contain additional substances, such as cellular products, bio-molecules, biomaterials, chemical substances, scaffolds or matrices. Products containing or consisting exclusively of non-viable human or animal cells and/or tissues, which do not contain any viable cells or tissues, and which do not act principally by pharmacological, immunological or metabolic action, shall be excluded from this definition. Cells or tissues shall be considered 'engineered' if they have been subject to substantial manipulation (Annex I to Regulation EC No. 1394/2007), so that biological characteristics, physiological functions or structural properties relevant for the intended regeneration, repair or replacement are achieved, and if they are not intended to be used for the same essential function or functions in the recipient as in the donor.

Parallel, it was defined a subcategory stated as combined Advanced-Therapy Medicinal Products (CATMP), defined as products that incorporates, as an integral part of the product, one or more medical devices within the meaning of Directive 93/42/EEC or one or more active implantable medical devices within the meaning of Directive 90/385/EEC, and whose cellular or tissue part contains viable cells or tissues, or non-viable cells or tissues that are liable to act upon the human body with action that can be considered as primary to that of the devices referred to.

The regulatory body of ATMPs is headed by the European Medicines Agency (EMA) in a centralized structure. Because of the novelty, complexity and technical specificity of ATMPs, a specialized Committee for Advanced Therapies (CAT) came into force in 2009. The CAT is intended to help developers, by giving scientific advice, protocol assistance, ATMP classification and certification, briefing meetings, incentives and helps to the small and medium-size enterprises, information about the guidelines and regulatory requirements, risk management and so on.

In order to achieve the marketing authorization, ATMPs have to fulfil the Marketing Authorization Application (MAA) to prove their quality, safety and efficacy to the centralized authority (EMA), similarly to drugs pathway. MAA dossier can be prepared using a risk-based approach, which is a concept described in the Directive 2001/83/EC. While optional, it is recommended to follow this path, since the risk-based approach will define the extent and quality of the nonclinical and clinical data to be included in. Despite marketing authorization procedure is centralized in the EMA, and this body has published detailed guidelines and good clinical practice specific to ATMPs, clinical trials are still subjected to regulation by individual member

states. This fact, which is controversial and goes against the globalization and harmonization purpose of the ATMPs legislation, have to be considered when looking competitive advantages between different EU countries.

2.1.2. The Market Panorama

The new regulatory systems (ATMPs regulation) was demanded by and created in accordance to the big industries, which lobbied for business oriented legislation [17]. Academia and public sector, which are traditionally disconnected from this reality, where underrepresented during the policy shaping process, unaware that these policies would apply as well to the spin offs emerged in the context of the new entrepreneurial university models. Later, big pharmas resulted not to be interested on developing and producing new regenerative therapies, because they normally focus on potential best sellers products that can be sold to millions of people [18], and tissue engineering market niches are smaller (while investments needed for market authorization still stays high). Thus, big pharma shifted their interests to the obtaining of research cells and tissues for the clinics, which where a more lucrative market (human tissue can be valued up to 500$/g) [17].

In this context, hospitals and small- and medium-sized enterprises (SME) left on the leading of regenerative medicine products development. Actually, according to Euromed, SMEs (accompanied by academia and Hospitals) did indeed represent the majority of the manufacturers of tissue engineering products, while big industries get only involved as financers and sponsors [19].

However, due to high investments needed for the clinical trials and the strong and thigh regulation of ATMPs regulation, which was created to assure harmonized and the highest standards of quality and safety, hospitals and SME struggle to get their products through the medicinal product accreditation funnel, despite the advantages that the regulatory laws offers to them (like 90% reduction in fees and certification data). Actually, up to now, only four ATMPs products have received approval for marketing authorization; three somatic cell therapy products (ChondroCelect, MACI and Provenge), and one GTMP (Glybera). Many other therapies failed to attempt on the marketing authorization even though some were already on the market in some EU countries. However, these locally authorized products did not meet the current standards of the European regulatory [20].

The inflation of costs associated to the new regulatory regime is problematic and give place to higher product prices compared to established conventional treatments [21], which is

also a problem for the reimbursement of these costs by the governmental health care system. This added problem shows that access to tissue engineering products depends not only on product availability; buy also must be affordable for patients and health care system. One example of this is the case of the first EC authorized ATMP, ChondroCelect (TiGenix 2011), whose reimbursement price of the product is nearly ten times the price of non-ATMP autologous treatments. This provokes that reimbursement of this therapy is restricted, for instance in Belgium, to patients younger than 50 years, going against the "equal access to health care" Belgium *leitmotivs*.

Alternatively, ATMPs developers try hard in order to circumvent the regulatory path. For instance, they try to fit their products inside the classification of not substantially modified cells by using autologous cells. However, the line between substantially and not substantially modified cells or tissues is blurred and controversial [22] and the CAT has already considered several autologous cell therapies to be ATMPs [23], fitting them into the ATMPs regulatory path.

Other manufacturers try to take profit of the Hospital Exemption rule, which dictates that the clinical application of regenerative therapies lacking market authorization is allowed for special individual cases with high-unmet medical needs where there is no other market alternative and if they are produced in a non-routine way. However, there is an overall though that, given the restrictions of the ATMPs regulation, regenerative medicine will shift to the application of off-the-shelf products and devices (acellular scaffolds) that enhances tissue regeneration, or with the implication of cells and tissues that can be processed peri-operatively and applied in a single surgical procedure, thus evading compliance to the ATMP regulation. This new paradigms are putting under revision which is the better model to follow for the regenerative medicine industry, and opening discussions about the advantages of moving towards a service-based model (like Carticel® in US and ChondroCelect® in EU, where the product offered is a procedure) against the off-the-shelf product model.

2.1.3. The Value Proposition

SMEs, which most of them are linked to academia, operate on a high-risk, high-cost and low-investment environment. Thus, it is crucial that in order to attract investments, they are able to manage risk properly and to achieve key milestones. The value proposition (VP), which is defined as 'the benefits offered to the costumer, minus the cost and risks', is one of the most important and key aspects of a business plan, since it addresses the requirements to all the

stakeholders implied on the development and marketing of the product (patient, clinician, regulator, payer and investor) (Figure 2). There are four core elements to a successful VP: quality, safety, efficacy and cost-effectiveness. The assessment of these elements according to the different stakeholders will provide to investors evidences of commercial availability, risk reduction and a satisfactory return on investments (ROI).

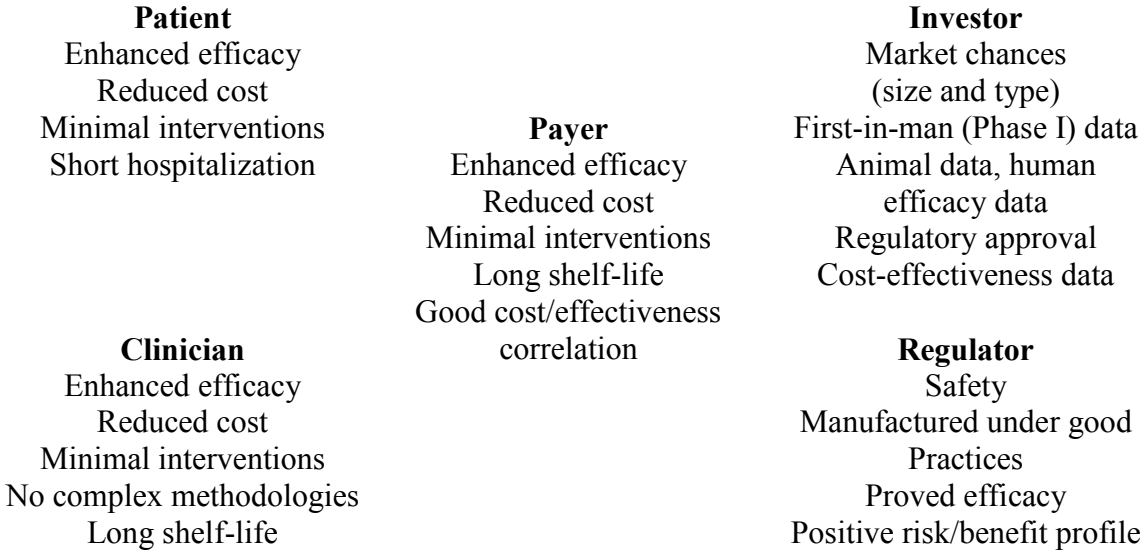

Figure 2. Stakeholder requirements for the construction of the Value Proposition on regenerative medicine products.

All these aspects can be taken into consideration during the Phase 0 of the product development, and most of them will depend on the own product characteristics. On one side, clinical outcome, this is effectiveness, will depend on the added value of the product compared with the already existing therapies. On the other side, product costs will be given by the technical aspects of the manufacturing process on one hand, and the expenses of the regulatory path on the other hand. At the end, both aspects will define the cost-effectiveness, and consequently the acceptable cost of goods sold (COGS), the pricing structure and the resultant ROI.

2.2. Biomaterials for Tissue Engineering

2.2.1. Classification

'A biomaterial is a substance that has been engineered to take a form which, alone or as part of a complex system, is used to direct, by control of interactions with components of living systems, the course of any therapeutic or diagnostic procedure.' [24]

Table 1 Biomaterials classification according to their application. Adapted from [25].

Class 1	**Permanent (long-term) implantable devices…**
Class 1.1	… for the anatomical replacement of removed parts of the body
Class 1.2	… for the correction or restoration of a function as consequence of an injury or disease
Class 1.3	… for cosmetic purposes
Class 2	**Short term implantable devices…**
Class 2.1	… to assist in the repair of hard tissue
Class 2.2	… to assist in the repair of soft tissue
Class 3	**Invasive but removable devices**
Class 3.1	Indwelling catheters and shunts
Class 3.2	Contraceptive devices
Class 4	**External artificial organs/organ assist devices…**
Class 4.1	… that deliver short-term support
Class 4.2	… that act as a bridge to transplant for life-long support
Class 5	**Surgical and clinical accessories**
Class 5.1	Wound dressings
Class 5.2	Short-term catheters and drains
Class 6	**Drug and gene delivery systems**
Class 6.1	Oral drug delivery systems
Class 6.2	Infusion systems
Class 6.3	Systems for delivery across epithelial/ mucosal surfaces
Class 6.4	Monolithic implantable devices
Class 6.5	Microparticulate and nanoparticulate systems
Class 6.6	Prodrugs and polymer therapeutics
Class 6.7	Antimicrobial systems
Class 6.8	Immuno- and chemotherapy hybrids
Class 6.9	Non-viral gene vectors
Class 6.10	Engineered viral vectors
Class 6.11	Vaccine delivery systems
Class 6.12	Theranostic systems
Class 7	**Tissue engineering systems**
Class 7.1	Engineered cell therapy products for regenerative medicine purposes
Class 7.2	Engineered gene therapy products for regenerative medicine purposes
Class 7.3	Ex vivo/bioreactor generated tissue constructs
Class 7.4	Cell seeded implanted scaffolds or templates
Class 7.5	Cell-free implanted scaffolds or templates
Class 7.6	Injectable cell-seeded products
Class 7.7	Injectable cell-free products
Class 7.8	Cell sheet engineered constructs
Class 7.9	Engineered systems for drug discovery and testing
Class 7.10	Engineered tumour models
Class 8	**In vivo diagnostic systems**
Class 8.1	MRI contrast agents
Class 8.2	Ultrasound contrast agents
Class 8.3	Fluorescence and bioluminescence imaging systems
Class 8.4	Contras enhanced CT systems
Class 8.5	Implantable biosensors

Biomaterials are used on many different applications (Table 1) and, in all cases, they need to be designed in order to perform a desired function in an efficient way and for an intended duration, as well as do the patient no harm and be delivered to patient in an efficient cost-effective way. Therefore, requirements regarding its functionality, safety and practical features will vary from situation to situation and, consequently, biomaterial selection will be conditioned to these requirements (Table 2). Biomaterial selection will not only be delimited by final application requirements, but equally important is to consider how this choice will affect and condition the for-coming steps towards the clinics.

Table 2. Generic requirements for biomaterials.
Adapted from [25].

Functionality		**Safety**	
General	Volume, size, shape Surface characteristics	Intrinsic biocompatibility	Appropriate local host response Control of cytotoxicity Absence of remote systemic adverse effects
Mechanical	Elasticity/rigidity Strength/fracture resistance Tribological properties (wear, friction) Stress transfer to cells/tissue	Clinical application	Technique sensitivity Patient sensitivity
Physical	Elastic properties Thermal properties Optical/optoelectronic properties Magnetic properties	**Practical features**	
		Supply	Suitability for quality manufacturing Sterilization and infection control
Chemical	Control of biostability/biodegradation	Economics	Acceptable cost of goods Appropriate business models
Biological and pharmacological	Control of cell phenotype Control of molecular targeting Pharmacokinetics/pharmacodynamics	Regulatory/ Ethical	Absence of insurmountable hurdles

Biomaterials comprise a large variety of types, which depending on their composition can be classified into:

-*metals*: titanium and titanium allows, iron and steels, cobalt-based alloys, nickel-based alloys, tantalum and zirconium alloys, silver, platinum group metals and alloys, gold, magnesium and its alloys.

-*ceramics*: oxides, phosphates, sulphates, silicates, silica-based glasses, nitrides, carbides, titanates.

-*polymers*: thermoplastic polymers, thermosetting resins, synthetic polymers sols and gels, proteins and peptides, polysaccharides, lipids, biodegradable structural polymers, water-soluble polymers, polymers with ionisable or ionic groups, elastomers, fibre, fabrics and textiles, environmentally responsive polymers.

-*composite materials*: fibre reinforced thermoplastic polymers, fibre reinforced resins, ceramic microparticle reinforced biostable polymers, ceramic microparticle reinforced biodegradable polymers, nanocomposites.

-*engineered biological materials*: autologous tissues, allogenic tissues, xenogenic tissues.

-*carbon materials*: diamond and diamond-like materials, graphitic materials, glassy or vitreous carbon, hexagonally bounded carbon nanostructures.

Metals are rarely used as pure metals on practical applications, and alloys are normally used instead. In most cases there are between two and six metallic elements involved and some non-metallic elements like carbon, oxygen and nitrogen, regardless of typical impurities originated during metal refinery or the processing phase. The three main metals and alloys used on surgical implants are 316L stainless steel, cobalt-chromium, titanium and titanium alloys [26,27]. The use of stainless steel is restricted to temporal devices as wires, pins and fracture plates. Despite its adequate physical properties for most of its applications, stainless steel loses its biocompatibility over time due to its corrosion and liberation of toxic elements [28]. In contrast, titanium and titanium alloys form a stable oxide layer, which allows titanium implants to remain chemically inert and stable to corrosion. Moreover titanium has the ability to permit osseointegration when implanted in bone, allowing the intimate growth of the bone around it [29]. Compared to stainless steel and titanium, cobalt-chromium implants present higher wear resistance, reason for which it is used on load-bearing components and the head of femoral joint implants [30].

Ceramics can be described as refractory, polycrystalline compounds. Ceramics are based on the ionic bond, but normally present complex structures involving multiple elements combining ionic and covalent bonds. Depending on the nature, directionality and order of the bonds, ceramics can be crystalline, amorphous (glasses) or a mixture of both. Normally ceramics present high compressive strengths and brittleness, which may limit their use on engineering applications and may raise complications during shaping processes. Therefore, ceramics are often cast or sintered using heat or pressure [31]. Despite ceramics use on the clinics is limited because its poor processability into highly porous structures and its brittleness, they present advantages in front of alloys. Actually, ceramics present lower wear rates at surfaces and release of very low concentrations of inert wear particles compared to other commercial materials [32]. Examples of commonly used ceramics are alumina and zirconia for hip prostheses, artificial femoral heads and tooth implants [33,34]. However, most of ceramics potential uses are found on bioactive ceramics, nanoparticles for contrast agents and semiconductors for imaging [35,36].

Bioceramics are a specific type of ceramics, glasses or glass-ceramics that have specific biological activity, which can be exploited in tissue engineering, especially in bone regeneration [37,38]. Most bioceramics are based on different forms of the compound calcium phosphate (CaP), which is found on the mineral phase of the bone hard tissue. The most famous CaP bioceramic is hydroxyapatite (HA), which has similar chemical composition to the inorganic constituents of living bone. Thus, HA has been extensively used on the clinics to promote

osteogenesis and osseointegration [39-41]. Bioceramics may be also used for other strategies, like the controlled delivery of bioactive signals thanks to their tuneable degradation rates, and their use as tissue-bonding enablers [42].

Polymers (including natural polymers, natural-polymer-derived materials and synthetic polymers) are currently the dominant scaffolding materials in tissue engineering [43]. Their presence on the clinics is extended (Table 3). Their advantages are, in most cases, their biocompatibility, biodegradability and resorbability. Moreover, their mechanical properties cover a wider range of behaviours and magnitudes, being suitable from hard to soft tissue regeneration.

Table 3. Examples of commercial polymeric products for biomedical applications. Adapted from [44].

Polymer	Trade Name	Biomedical application
PGA	DEXON	First synthetic suture in 1969
	Biofix	Bone internal fixation devices
PLLA	Bio-Anchor Meniscal Stringer	Orthopaedic fixation devices
	The Clearfix Meniscal Dart	
	DEXON	High-strength suture
	Dacron	Ligament replacement
		Blood vessel conduits
		Injectable fillers
PLDLA	Resomer	Bioresorbable implant material
PLGA	Vicryl Mesh	Skin graft
	Vicryl Rapid & CRYL	Multifilament suture
	LUPRON DEPOT	Drug delivery vehicle
	PDS	Monofilament suture
PLGA-collagen	CYTOPLAST Resorb	Tissue regeneration membrane
PCL	Capronor	Long-term contraceptive device
PDLLA-CL	MONACRYL	Monofilament suture
PEU	Degrapol	Tissue engineering applications
PGCL, PLCL and PEG	SynBiosys	Drug delivery vehicle
PCLTMC and PGCL	Mazon	Flexible suture material
	Acufex	Orthopaedic tacks and screws
LDI-based PU	Polynova	Orthopaedic application and bone cement
PEAs	CAMEO	Site-specific delivery vehicle
POE	Alzamer	Drug delivery and ocular applications
Polyanhydres	Gliadel	Chemotherapeutic brain cancer
PCA	Dermabond	Tissue adhesives for topical skin application
	Integra Dermal Regeneration Template	Bilayer skin substitute
	Biobrane & Alloderm	Wound dressings
Collagen	Transcyte	Bioengineered skin equivalents
Hyaluronan	HYAFF	Wound dressing application
	OSSIGEL	Synthetic bone graft
HMW viscous Hyaluronan	AMVISC & AMVISC Plus	Corneal transplantation and glaucoma surgery
Viscous Hyaluronan	SYNVISC, ORTHOVISC	Pain relieve and join mobility improvement

Polymers can be classified as synthetic polymers or natural polymers. Natural polymers can come from protein sources (collagen, gelatine, silk, alginate, fibrinogen, elastin, keratin, actin and myosin), polysaccharide sources (cellulose, amylose, dextran, chitin and glycosaminoglycans) or polynucleotide sources (DNA, RNA) [45,46]. Natural polymers tend to match better the biochemical needs of the regenerating tissue, however immunogenicity problems can arise from their natural origin, sources are limited, and batch to batch variations are a serious drawback for good manufacturing [47]. Still, they are very present on the commercial arena. For instant, Apigraf, whose main component is collagen, is a clear and successful example of it. However their mechanical properties are normally under the needs and their use is limited to scaffolds whose supporting function is less relevant, like skin substitutes. Synthetic polymer, on the other hand, can be manufactured in large scales under good manufacturing practices (GMP). Moreover they can be designed to be biocompatible and non-immunogenic, and their mechanical properties are more robust [48,49]. Thus, they are commonly employed for scaffolding. However, synthetic polymers generally lack on bioactivity, which is the most common problem with this kind of materials [50].

Polymers can also be classified into the solid-type polymers, and the hydrogel-type polymers. From solid-type polymers, the major class of synthetic bioresorbable polymers are aliphatic polyesters or poly(α-hydroxy acids), from where the most spread polymers are poly(lactic acid), poly(glycolic) acid and their copolymers [51]. Those polymers degrade by random hydrolysis of their esters bonds and the resulted products are nontoxic natural metabolites that are eliminated from the body through urine excretion or via respiratory route [52]. Due to their multiple ways of being processed, these polymers are widely used. However they present important limitations, like hydrophobicity, lack of bioactivity or rigidity. A commercial example is Dermagraft, which is constituted by a polylactide-co-glycolide polymer mesh with embedded fibroblasts and extracellular matrix (ECM). Despite Dermagraft success, mechanical properties of degradable synthetic polymers are not always suitable for bioengineering due to their inflexibility and tendency to crumble upon degradation [53]. Thus, the mechanical properties decay of rigid polymeric scaffolds under the effect of degradation or ageing has to be seriously considered when mechanical function plays an important role. In response to this, other polymers having better elastic properties like polycaprolactone (PCL), poly(glycerol sebacate) (PGS) or poly(trimethylene carbonate) (PTMC) have been proposed as an alternative, or as integrant part of a copolymer [54].

Hydrogel-type polymers have gained a lot of expectancy as well, and during the last years have been very represented in the scientific scene. Hydrogels usually present a good environment for cells and proteins because of their ECM-like characteristics [55]. Thus, hydrogels can be used to retain and slowly deliver biological factors or cells [56,57]. However, they do not possess a wide range of functional mechanic characteristics. Therefore, they are commonly post-treated or mixed with solid polymers to increase their hardness [58]. Hydrogels are good at promoting cell migration, angiogenesis, water retention and rapid nutrient diffusion. Typical hydrogel-forming polymers are collagen, gelatine, fibrin, hyaluronic acid, alginate, chitosan, PPF-derived copolymers, PEG-derivatives and PVA [59].

Composites are materials made up from the combination of different types of substances, which permits to obtain enhanced properties through the complementation of the pros and cons of different materials. Very common composites are the ceramic-composites, which combine glass materials with other materials like polymers, in order to circumvent the brittleness problem of ceramics and include new properties and features [60]. Examples of glass-polymer composites are HAPEX (high-density polyethylene/HA), Flex Ha (silicone rubber/HA) and Glass Ionomer Cement (basic ion leachable glass/polyacryl acid). These composites are examples of biomaterials that retain the mechanical strength and bioactivity of the ceramic, while the polymeric phase enhance its performance, introducing a more controlled release capacity and allowing them to be cut and shaped according to the needs of the surgery.

2.2.2. Designing Parameters

Regenerative medicine often needs the use of scaffolds during tissue reconstruction, whether with combination of cells or not. Actually, the use of acellular therapies, like active scaffolds, represents an important sector of the regenerative medicinal products due to market characteristics and regulatory handicaps. Therefore, it is very important to be aware of the key aspects that a scaffold must fulfil for a tissue engineering purpose.

As previously stated, most key aspects that will enhance product chances to achieve the commercialization stage relay on satisfying the different requirements of the different stakeholders. Although some requirements are dependent on a good market and commercialization management, most are related to the product design and performance. Thus, it is not only important to have an efficient product, but it is necessary to be aware about how the product can be manufactured in complex shapes and scaled under GMP conditions, as well as to know which aspects will be considered during regulatory inspection, and how to increase

surgeon and patient acceptance by minimizing the complexity of the surgical tasks (using available technology and procedures, reducing surgical intervention and so on). According to this, Hollister [61] stated that scaffolds implied on regenerative medicine, have to satisfy four fundamental needs: Form (complex 3D shape to fit target anatomy), Function (mainly mechanic properties that will temporary support everyday tissue function demands), Formation (aspects that will provide tissue regeneration enhancement through the delivery of biologics and the appropriate mass-transport environment), and Fixation (scaffold consistency so it can be implanted and manipulated by the surgeon with proper tissue-scaffold interface integration).

The four facets of a scaffold design have to be built in an integrated manner. However, 'function' will be normally the first characteristic to take into account and will somehow limit the others. 'Function' will define the mechanical behaviour and properties of the scaffold, which have to match or be close to the mechanical range of target tissue in order to withstand physiological stresses without failure as well as to properly transmit stresses to the surrounding and new-formed tissues [62-64] In tissue engineering, the mechanical properties ranges take several orders of magnitude, since it covers from hard tissues like bone to soft tissues like smooth muscle tissue (arteries, bladder, gastrointestinal tract and so on). Selection of scaffold material will depend on target tissue and needed mechanical properties, and at the same time will limit the available shaping techniques and post-processing modifications.

'Form', and therefore scaffold architecture, will be given by the available techniques that can be applied on selected materials. The architecture, which can have different levels of detail, from the macro- to micro- and nano-size, will have an effect on scaffold mechanical properties, porosity, permeability and diffusivity. Thus, architecture will be limited and guided by desired scaffold properties, and vice versa. This iterative persecution of the best equilibrium between 'form' and 'function' is one of the most difficult parts of the design. However difficulties increase when we take conscience that the shaping technique will impact on the manufacturing costs of the scaffold and the scaling-up, that scaffold properties will affect therapy efficiency and therefore its market competitiveness and that the balance of product efficiency and product complexity will influence surgeon and patient acceptance.

'Fixation' and 'formation' are somehow related and have a close dependence on each other. Fixation of the scaffold, which is an issue that is surprisingly often forgotten during research stage, will be tightly related to scaffold 3D form and type of material used. On the other side, formation, which usually is the most considered issue during research phase, will depend on a large variety of factors like degradation ratio, tissue-scaffold interface, cell-scaffold interaction,

topology, mass transport, factors release, bioactive molecules and a large number of factors affecting cell and tissue behaviour. Here is where research literature is more extended, and sometimes is forgotten that, despite the impressive results of the different designed systems, an increased product complexity is a setback for the commercialization success, whether in regulatory, manufacturing or clinical application terms.

There are no standard guidelines to define which kind of material, mechanical behaviour, surface chemistry or mass transport properties, should have a desired scaffold for a specific purpose. However, for the success translation of the initial concept towards the clinics it is paramount to have an integrated point of view, with a special focus on product design, manufacturing, regulatory constraints, safety, costs, and so on.

2.2.3. Manufacturing Techniques

As it has already been pointed out, it is necessary to know the actual scaffold manufacturing alternatives, with their pros and cons, as well as their feasibility to be scaled on the current state of the industry.

Manufacturing techniques are generally fitted into two different categories. The first one gathers all those methods that have no or weak control on the design, while the second one gathers all those methods based on the solid free-form synthesis (SFF), i.e., the reproduction of a computer-aided design model with the help of an automated machine.

The first group include all the traditional ways of scaffold manufacturing like porogen-leaching, phase separation, solvent-casting, freeze-drying, gas foaming, melt moulding and electrospinning. The advantage of these methods is that they can achieve very fine structural features, high porosities (higher than SFF techniques, see Table 4), and some of them allow shaping by 3D moulding. It is also possible to combine different methods, and they can be used in a large variety of materials. However, they cannot construct complex designs, they are normally subjected to high variations on reproducibility, and it is difficult to work with mechanical and mass-transport anisotropies. Furthermore, some techniques present important drawbacks. For instance, porogen leaching makes difficult the formation of an internal porosity owing to the lack of interconnected porosity, which does not allow the removing of deep porogen particles and gas foaming usually presents a low ratio of interconnected pores (10-30%) [65]. Non-woven fibre meshes obtained by electrospinning present limited 3D shaping possibilities [66]. Other techniques normally use organic solvents that are toxic or harmful for human being, excluding gas foaming and melt moulding. More important, most of the times, the

absence of designed channels does not allow the deep penetration of colonizing cells due to low oxygen and nutrient entrance which frustrate tissue regeneration [67,68]

Thereby, the reproduction of computer-generated models has been used in different manners to create complex shapes [69]. Solid free form (SFF) is a fabrication technique based on the layer-by-layer construction. This working model, however, can be applied using different technologies (Figure 3) fused deposition modelling [70], 3D printing [71,72], stereolithography [73], selective laser sintering [74], wax printing [75] and bioplotter [76].

Alternatively SFF can be applied indirectly by creating a mould that can be filled with a desired material in combination with a traditional scaffolding methodology. An example of this is the use of SFF manufactured moulds for the casting of polymer-ceramic composites materials using conventional procedures (i.e. phase separation, emulsion-solvent diffusion, porogen leaching) in order to fabricate scaffolds with controlled porosity and structure [77]. These computerized techniques are perfect for the construction of user-specific anatomical scaffolds which can serve from Computerized Tomography (CT) scans or Magnetic Resonance Imaging (MRI) to determine the target shape and build a computer model. They also allow a high control on the microstructure, being possible to construct tailored porous and channels, with a high reproducibility. However, limitations on feature size are important. Typically, feature limits of SFF are around 200-500 μm and despite they can be reduced in certain cases, nanometric sizes are out of the SFF range. Moreover, porosities obtained by SFF techniques are lower than traditional techniques (Table 4). Regarding resolution of SFF techniques, it is worthy to point that while they present very good xy resolution, z resolution is normally not so accurate and fine, which implies a non-desired anisotropy that can compromise the function of the scaffold. Also, SFF techniques are limited to materials that can be extruded, UV sintered, chemically printed and so on; and the range of available materials became even narrower when toxicity aspects are considered. Indeed, post-processes are commonly needed in order to remove non-reacted toxic elements or strengthen cross-linking or remove temporary support structures. Also, in many cases, biological molecules cannot be introduced into the process due to the harsh conditions used during the same.

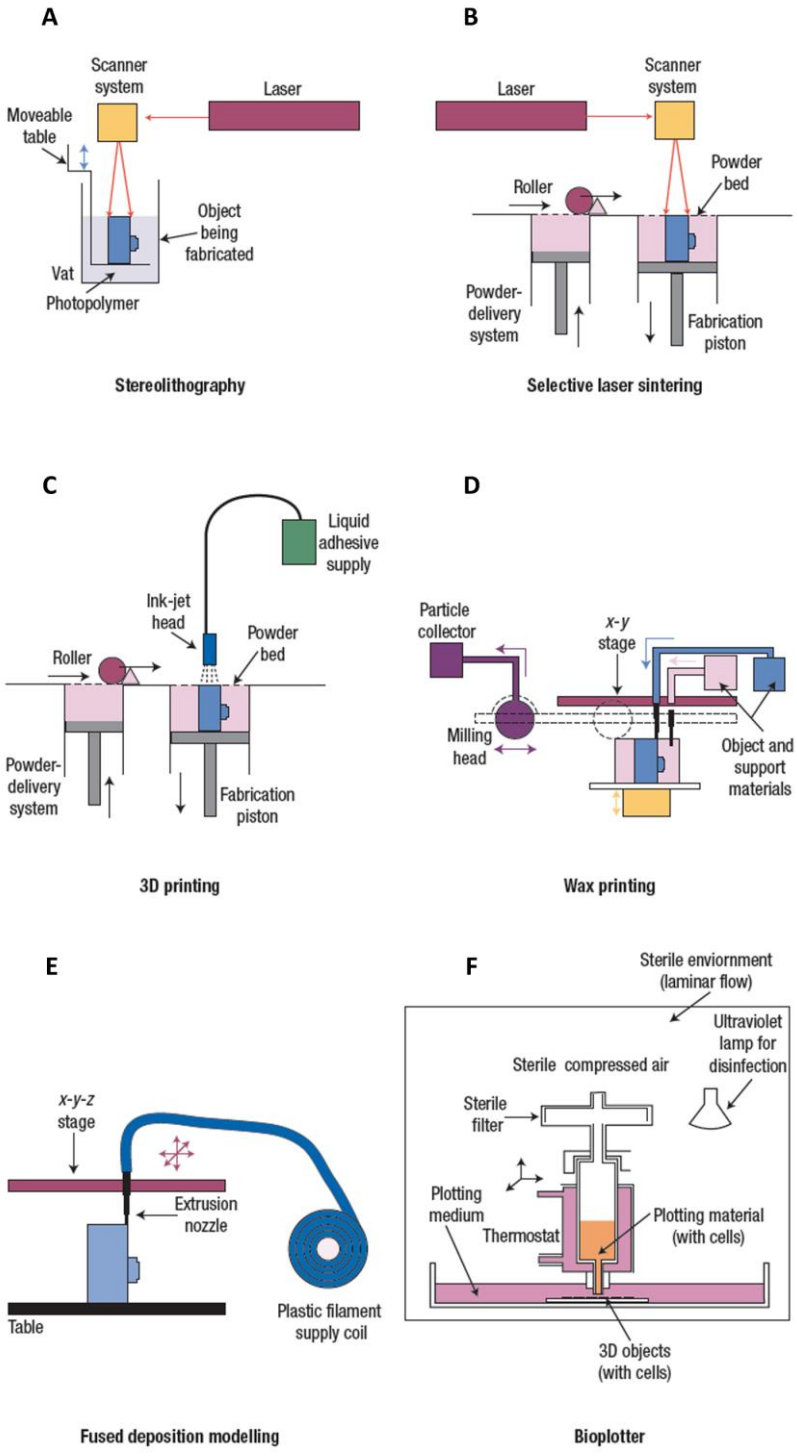

Figure 3. Schematic representation of different SFF techniques. Laser based systems are: (A) the stereolithography system, which photopolymerizes a liquid, and (B) the selective laser sintering system, which sinters a powdered material. Printing based systems are: (C) the 3D printing system, which prints a chemical binder into a powder bed, and (D) the wax printing system, which prints two different types of wax material in different sequences. Nozzle-based systems are: (E) the fuse deposition modelling, which prints a thin filament that is heated through the nozzle, and (F) the bioplotter system, which prints material that is processed either thermally or chemically. Adapted from [78].

Table 4 Porosity ranges for different scaffolding techniques. Adapted from [79,80].

Fabrication Method	Material	Porosity (%)	Fabrication Method	Material	Porosity (%)
Traditional techniques			*SFF Fabrication techniques*		
PL	PLGA	80-92	FDM	PCL	48-77
CM/PL	PLLA	78-97	ND	PLGA/PLLA/TCP	74-81
CM/PL	PLGA	87	ND	HA	41
GF/PL	PLGA	95	ND	PEOT/PBT	29-91
Electrospun	PCL	85	SLS	PCL	37-55
Fibre	PGA	95	Inverse SFF	HA	40
Woven Fibre	PGA	70-74	Inverse SFF	POC	30/50/70
SC	PLLA/PLGA	20-50			
EFD	PLGA	>97			
TIPS	PLDLA	>97			
SCF	PLLA	>97			

PL: Porogen Leaching. CM: Compression Moulding. GF: Gas Foaming. SC: Solvent Casting. FDM: Fused Deposition. EFD: Emulsion Freeze Drying. TIPS: Thermally Induced Phase Separation. SCF: Supercritical-Fluid moulding. ND: Nozzle Deposition. SLS: Selective Laser Sintering. SFF: Solid Free-Form.

All these different techniques present advantages and disadvantages (Table 5), for this reason, it is needed to clearly examine the optimal processing techniques or combination of techniques for a given product. However this is not a trivial point if we try to keep into the limits of what is likely to be scaled up into an industry. For instance, many of the SFF technology is still far to be implemented into the actual industry and market due to their related costs, which substantially increase the COGS.

Table 5. Advantages and disadvantages of the different scaffold fabrication techniques.

Fabrication technique	Advantages	Disadvantages
Solvent evaporation	Simple operation Many materials available	Use of toxic organic solvents Limited featured size around 200 µm Need porogen to introduce porosity Limited 3D shaping
Porogen leaching	Simple operation Close control of the pore size and porosity by selecting porogen particle size and amount	Difficult to obtain homogeneous porogen distribution Difficult to control and obtain good pore interconnectivity Residual porogen Cubic shape pore
Gas foaming	No organic solvents needed Good porosity and pore size control No high temperatures needed Continuous production	Limited materials Non porous surfaces Closed-pore structure
Phase separation	Highly porous structures No harsh conditions Allows bioactive agents incorporation	No control on micro-architecture Residual solvent Limited to small pore size
Thermally induced phase separation	Control on porosity and pore morphology	Pore size limited at 10 to 2000 µm
Electrospinning	High porosity Easy process Scalable High surface to volume ratio	Limited range of polymers Lack mechanical strength Residual solvents No complex and large 3D shapes
Emulsion/Freeze-Drying	Highly porous structures	Low control on pore size distribution and porosity homogeneity
Solid free-form fabrication	Customized designs Compute controlled fabrication Anisotropic and complex structures Highly reproducible and scalable	Limited pore size at 70-500 µm Limited polymers Harsh processing conditions

2.2.4. Mimicking Tissues

Neo-tissue formation in tissue engineering processes does not follow the same biological processes than tissue development or wound healing processes. For instance, mature ECM often does not possess the highly interconnected pore structure needed for a quick cell homing and a fast regeneration process. Then, in order to promote an accelerated regeneration, the designed scaffolds should mimic the advantageous properties of natural tissues in order to obtain the best healing performance and do not entirely replicate the ECM.

As previously mentioned, we should mimic the ECM in order to create the proper environment for tissue regeneration. Mimicry can be considered on the macros-scale, the micro-scale, the nano-scale and even the pico-scale. Each level will attain different key aspects of

scaffold integration, like shape and geometry on the macro-scale and topological features at the micro-scale, but all of them will work in an integrative manner for the good performance of the scaffold. Mimicry on tissue engineering has proven importance since it was observed that scaffolds does not only act as supportive structures, but also can guide cell behaviour and cell response in a controlled manner, both in space and time [81,82]. Such attention on the design of the different topographic properties on the different scales has evolved parallel to the development of new fabrication techniques, which have incredibly improved the range of working parameters during scaffold fabrication.

2.2.4.1. The Macro-scale

The vast majority of body tissues present different degrees of anisotropy and organization at the macro-scale level, which need to be addressed during scaffold fabrication. Normally, the factors and properties implied at the macro-scale level are related to the tissue organization, the biomechanical properties, the scaffold shape, the scaffold integration, the blood supply and cell homing.

Special attention on the macro-scale tissue organization must be taken when designing scaffolds for interface systems, like orthopaedic interfaces (bone-ligament/tendon, muscle/tendon or osteochondral interface). These systems usually exhibit gradients of structural properties, mechanics, biomolecules and cell types [83]. The absence of this anisotropy on the scaffold surrogate would make it fail at regenerating such interfaces. This is because the gradated structure and organization, which can be either continuous or multiphasic (layered), offers the possibility to growth a multitissue organization on a single scaffold system that improves biological integration and fixation at the point of injury [84].

Scaffold gradation can be compositional, molecular or structural. These gradients play important roles on biology and mechanical properties, creating niches for specific cell types or helping to spatially distribute a mixture of different cell types. Examples of compositional gradients are found on collagen matrices, in which minerals have been distributed along the scaffold to mimic the osteochondral region [85]. Indeed, multiphasic scaffolds for bone-soft tissue interfaces are widely studied. For instance, it is possible to find scaffolds for the restoration of the bone-cartilage interface whose macro-scale organization has been designed using a triphasic scheme (Figure 4).

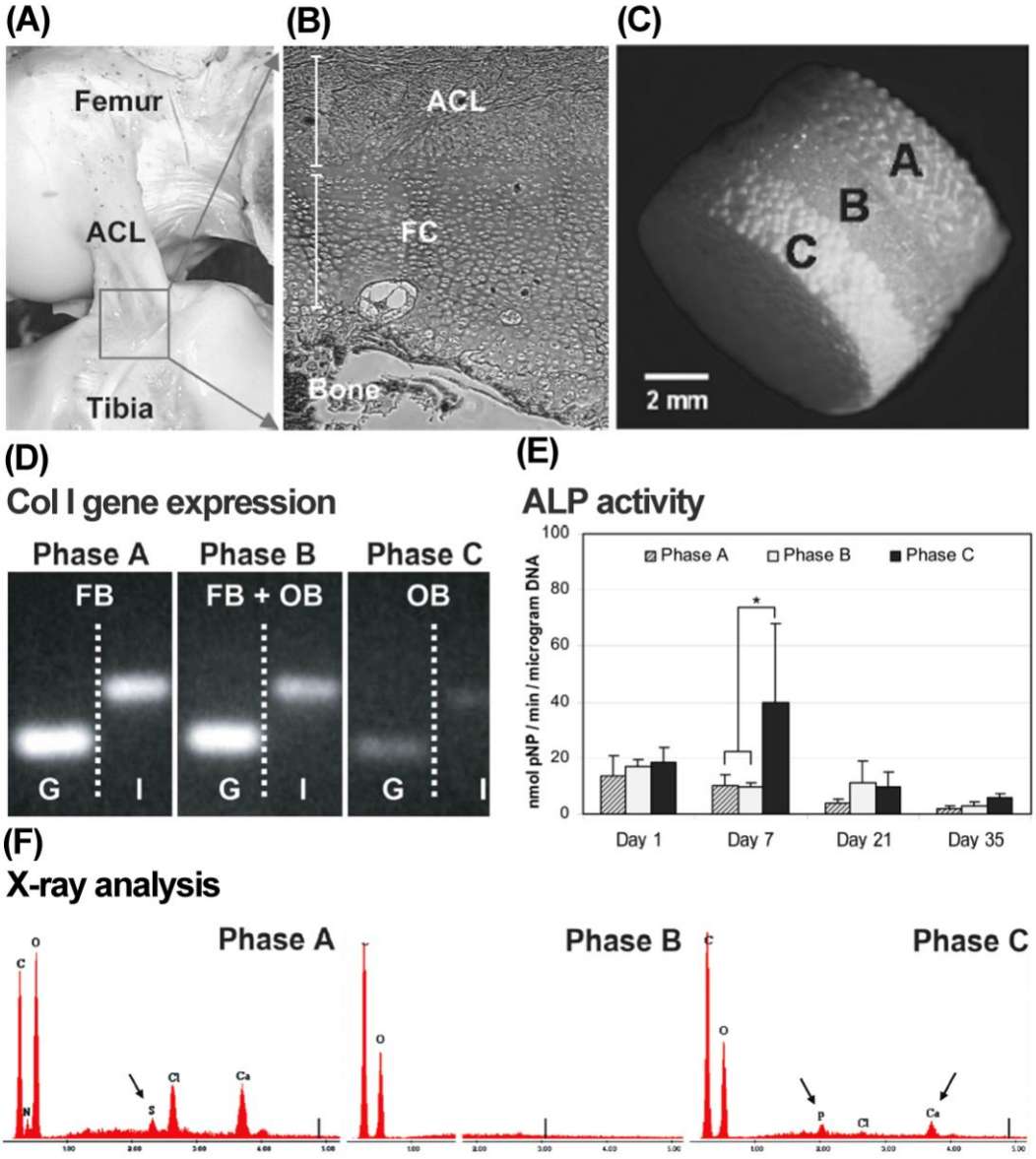

Figure 4. Example of a triphasic scaffold with controlled matrix heterogeneity. (A) Posterior view of an anterior cruciate ligament (ACL) inserted into the bone. (B) Histology of the three main tissues found on the interface: ligament (ACL, phase A), fibrocartilage (FC, phase B) and bone (OB, phase C). (C) Designed triphasic mimicking scaffold. (D) Protein expression study: after 42 days of cell culture on the scaffold it is observed an increased collagen I gene expression (I column) on phase A and B. (E) Alkaline phosphatase (ALP) activity study: after 7 of cell culture it can be found an ALP activity peak on phase C. (F) Mineralization study: after 35 days of culture, X-ray analysis performed on new formed ECM showed the formation of sulphated ECM on ligament phase, and matrix mineralization (Ca-P deposition) on bone phase. Adapted from [86].

The first phase (phase A, Figure 4C), formed from a polylactide knitted mesh sheet, hosts the ligament soft tissue. The second phase (phase B, Figure 4C), formed from sintered PLGA-based microspheres, hosts the fibrocartilage tissue. And the third phase (phase C, Figure 4C), formed of sintered PLGA-based microspheres and bioactive glass, hosts the bone tissue. In a scaffold of such characteristics, each different layer triggers different cell responses during new tissue development. For instance, cells cultured on the first layer show high levels of collagen I and III, while cells cultured on the second phase show high levels of collagen I and II and cells cultured on the third phase show high levels of mineralization. This study exemplifies how macro-scale organization of the scaffold composition can guide cell behaviour in an anisotropic gradated fashion.

Structural gradation is also used to create different mechanical regions. Mechanical anisotropies that mimic natural tissues can be created with the gradations of porosity or stiffness and fibre or structure orientation [84]. On hydrogels, polymers and ceramics, porosity gradients can be created with controlled distribution of porogen agents or SFF techniques. Also, stiffness anisotropies can be obtained applying different cross-linking gradients, mineral contents and microstructures gradients (such as microparticle gradients) [87]. As a result of tailoring the macro-scale structural gradients and organization, it is possible to control and trigger effects on cell behaviour like migration towards regions of increased stiffness [88].

2.2.4.2. The Micro- and Nano-scale

Within tissues, cells are surrounded by ECM, which is characterized by a natural web of hierarchically organized nanofibres that regulates cellular functions such as morphogenesis, differentiation, proliferation, adhesion and migration [89]. The ECM is composed of an intricate weaving system of protein fibres such as fibrillary collagens and elastins, ranging from 10 to several hundreds of nanometres (Figure 5). The mesh is covered with nanoscale adhesive proteins such as laminin and fibronectin that provide specific binding sites for cell adhesion, growth, migration and differentiation. Polysaccharides such as hyaluronic acid and heparan sulphate occupy the interstitial space between the fibres and act as a compression buffer against stresses as well as a growth factor reservoir. Actually, ECM plays a vital role in storing, releasing and activating a wide range of biological factors, along with aiding cell-cell and cell-soluble factor interactions [89].

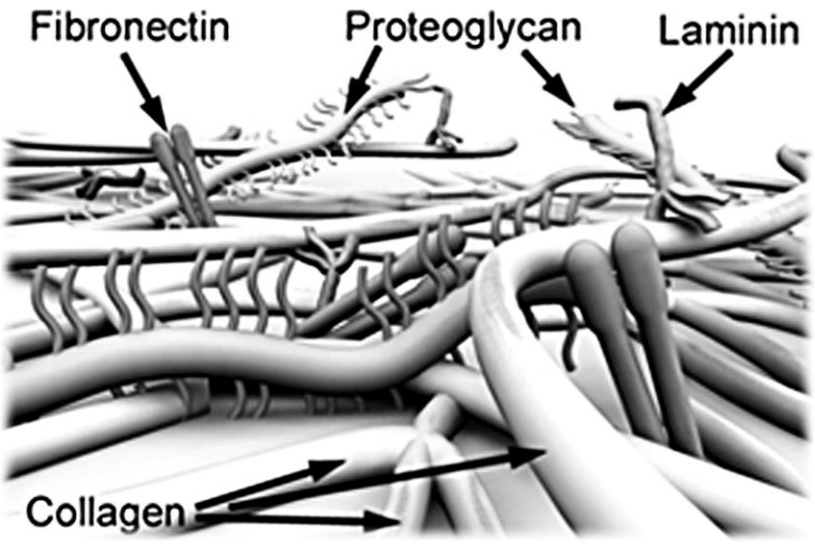

Figure 5. Schematic representation of the ECM showing the interaction between the different entangled structural fibres and the adhesive molecules.

In the natural cell environment, micro- and nano-architecture are very important because they provide cell support and direct cell behaviour via cell-ECM interactions. Indeed, there is growing evidence that topographical clues can direct cell fate in the same manner than chemical induction [90]. Actually, nanotextured materials can interact with certain types of proteins like fibronectin, vitronectin and laminin, which stimulate cell adherence and tissue growth [91,92]. Thus, nanodesigned devices can direct cellular behaviour from cell adhesion to gene expression.

Nanotopographies and nanotopographic features can be created by lithography, anodization, electrospinning, polymer demixing, chemical etching, self-assembly and phase separation [93-97]. The different micro- and nano-scale topographical features and structures have been investigated for their role on cell fate [97]. It has been observed that different aspects of topographical features such as scale (micro- or nano-), geometry (ridges, pillars, pits or grooves) and distribution (random or organized) can trigger different cell responses [98-100]. Indeed, the spatial information can govern stem cell growth, apoptosis and differentiation since it defines the cell shape, size, and elongation, as well as the clustering of focal adhesion points [101-105]. For instance, space availability may decide whether a stem cell differentiates into adipocyte/osteoblastic lineage [106], or chondrogenic/myogenic lineage [107]. Other studies have shown that surface topography have an important impact on cell behaviour by means of nuclei shape modification. Actually, when a cell spreads his area onto a surface or stretches himself, his nuclei is also mechanically stretched as an effect of nuclei integration within the cytoskeleton filaments. This nuclear elongation and stretching has shown to influence

osteoblastic stem cell differentiation [108]. Other studies have shown that disordered nanotopographic features present a strong induction of stem cells towards osteogenic differentiation, while ordered features present lower potential [109]. In this case, the precise mechanism responsible for the response against the different states of nanotopographical order is still debated, although there is some consensus pointing towards the generation of anisotropic stresses [110]. Relating to topographic cues size-effect, a comparative study between patterned surfaces with 10 nm and 100 nm features have shown that the induction of focal adhesion points occurs on 100 nm but not on 10 nm features, which generates a stress by means of actin filaments, triggering through this tension the osteogenic differentiation of stem cells [111]. On the same line, it has been widely observed that stem cells may respond to the mechanical properties of the substrate material like stiffness and elasticity [112-114]. Indeed, it is believed that integrins are the starting point for cells to sense the mechanical stimuli of the biomaterial to which they are adhered, so they can sense and respond to the substrate elasticity and trigger different cell responses [115,116]. Regarding cell growth guiding, it has been proved that the creation of nanogrooves is a useful tool for the control of cellular orientation and migration by means of contact guidance mechanism [117]. In a parallel manner, similar results have been obtained with cells cultured on fibrous matrices [117].

Equally important is the control of porosity during scaffold development. The control of pore size, distribution, pore volume, shape and interconnectivity are very important issues. If the pores employed are too small, pore occlusion by the cells will happen, preventing cellular penetration, ECM production and neovascularisation of the inner areas. Also, it has been proved that different applications may have different optimal pore size ranges. For instance, optimum pore sizes for neovascularisation have been observed at 5 μm [118], fibroblast ingrowths at 5-15 μm [119], hepatocytes ingrowths at 20μm [120], osteoconduction at 200-350 μm [121] and regeneration of adult mammalian skin at 20-125 μm [122]. Pore interconnectivity is also critical to ensure that cells keep a distance below the 200 μm far from the nearest blood stream that provides nutrients and oxygen supply [120,123].

Beyond nanotechnology there is picotechnology, which is a field that has been explored very recently on the tissue engineering field. Picotechnology aims to control the electron distribution around atoms of a biomaterial to provide desirable properties. In such a way, atoms of a nanomaterial can be stimulated to increase surface energy and thus, increase absorbed proteins on a desired material [124,125]. Picotechnology has been little investigated. However it

is a technique that present potentially less toxic effects compared to nanotechnology and could be of interest when combined with other techniques.

2.2.4.3. Nano-fibrous Materials

Many extracellular proteins have a fibrous structure with diameters on the nanometre or sub-micrometre range. Collagen, the most abundant ECM protein in the human body, is a fibrous protein with a diameter ranging from 50 to 500 nm [126,127]. Mimicking these structures has been pursued because of their biological benefits [128]. For instance, nano-fibrous scaffolds are found to adsorb 4.2-fold more human serum proteins than solid-walled scaffolds (scaffolds with smooth pore wall morphology) [129]. Moreover, the profile of adsorbed serum proteins has shown to be different from that one adsorbed to the solid-walled scaffolds. Indeed, nano-fibrous scaffolds have shown to adsorb significantly higher levels of fibronectin and vitronectin from serum, while cell-adhesion proteins are barely detected on solid walled scaffolds [129]. Also, it has been observed that nano-fibrous architecture enhance cell attachment and osteoblastic marker gene expression on osteoblastic lines [130]. It is thought that nano-fibrous structure may trigger and maintain the expression of α2 integrin (associated to the expression of osteocalcin and bone sialoprotein genes) [131,132] in a similar manner than collagen, promoting in such a way an enhanced mineral deposition on nano-fibrous scaffolds [130,133]. Because of these observed benefits, nano-fibrous structures have been produced through different techniques.

Electrospinning is very well-known for its good performing on creating meshes of nano-fibrous matrices from either natural macromolecules or synthetic polymers. Electrospinning was already reported in the literature more than 100 years ago [134], and has evolved from the fabrication of nonwoven fabric products in the early 1930s [135] to the high-tech sub-micron fibrous mats nowadays. Despite the simplicity of creating fibrous scaffolds by electrospinning, obtained fibres are usually at the upper limits of the 50-500 nm range found in natural ECM [136]. Moreover, problems for the fabrication of complex three-dimensional scaffolds with designed internal pore structures are still a limitation. Compared to fibrous scaffolds created by electrospinning, structures created by self-assembly processes can have fibrous structures with lower diameter ranges (5-8 nm) [137]. However, scaling up of this processes, as well as the inability to control the formation of macro-sized pores, the limitation on the creation of complex 3D geometric structures, the degradation problems and the poor mechanical properties, are some of the major drawbacks of self-assembled fibrous scaffolds. On the other hand, phase separation is a process that can produce nano-fibrous matrices at larger scales. Phase separation occurs when a polymer solution separates into two phases, a polymer-rich phase, and a polymer-lean

phase. Indeed, phase separation starts with a homogeneous multi-component system that becomes thermodynamically unstable under certain conditions and tends to separate into a multiphase system in order to lower the system free energy [138]. Once phase separation has occurred, solvent can be removed so the polymer-rich phase solidifies and, depending on system conditions and materials used, different forms may be obtained (powder, closed-pore foam or open-pore foam). Phase separation can build complex 3D structures with nano-fibrous structures, but still some limitations like lacking of inter-connected macro-pores. However, phase separation technique can be easily combined with SFF processing or porogens to obtain designed macro-porosities [129,139,140].

2.2.4.4. Chemical Cues Functionalization

Aside from mimicking the structure and mechanical properties of tissues, it is important as well to consider the chemical modifications that biomaterials can be subjected to, in order to enhance cell response or/and resemble the natural ECM. Surface chemistry has shown to control cell behaviour on many levels, from adhesion to transcription, differentiation and morphogenesis. Strategies based on surface chemical modification comprise from the use of functional groups, to peptides, proteins, carbohydrates and DNA/RNA molecules (Figure 6).

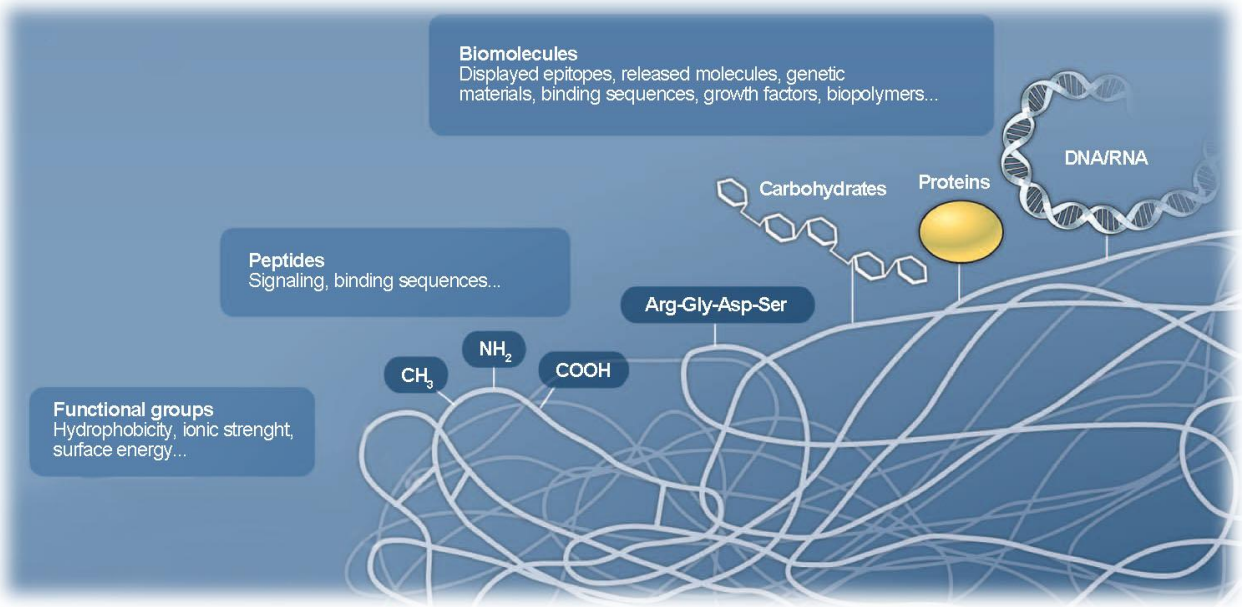

Figure 6. Scaffold functionalities that can be added to enhance and improve bioactivity. Functional groups improve cell response through physical properties such as hydrophobicity, ionic strength and surface energy. Peptides and biomolecules enhance cell response through biochemical and biological pathways. Adapted from [141].

Due to the nature of the scaffold-tissue interface, processes that take place on it are extremely complex. It is well known that cells interact with their environment through bio-

recognition processes, in which cell surface receptors play an important role [142,143]. However, cells are not the first element to interact with the scaffold surface, but proteins from the physiological fluids do. In this sense, protein adsorption will depend on surface properties like hydrophobicity, surface energy or surface charge, and will influence cell behaviour and, therefore, scaffold biocompatibility [144,145].

Hydrophilicity/hydrophobicity, ionic charge and surface energy are important factors regulated by the chemistry of the added functional groups, peptides and other molecules. The importance of these factors relies on the adsorption processes that proteins from the body fluids will have towards the scaffold surface, which will determine the subsequent cell response [146]. Indeed, hydrophobic surface favours the adsorption of proteins from aqueous solution from a thermodynamically point of view. However, hydrophobic surfaces induce the denaturalization of adsorbed proteins. Opposite to this, highly hydrophilic surfaces prevent protein adsorption [147]. This effect is explained by the 'Molecular self-association theory', which exposes that different water structures can be organized on the interface between the material and the water bulk [147]. For instance, a hydrophobic material will have an interface with a relatively less dense water region and a more open hydrogen-bonded network, which allows proteins to interact. Instead a hydrophilic material will have an interface with a relatively more dense water region with a collapsed hydrogen-bonded network, which prevents protein interaction. According to this, surfaces with moderate wettability are considered to be optimal for protein adsorption and have shown to present best cell response [148,149].

As previously mentioned, energetic properties can be modified by introducing functional groups on surface like the methyl ($–CH_3$), hydroxyl (-OH), carboxyl (-COOH) amino ($-NH_2$) groups, and so on. These functional groups have been extensively studied because they can control the extension of cell adhesion as well as the level of protein adsorption. For instance, it has been observed that surfaces functionalized with CH_3/OH, CH_3/COOH or CH_3/NH_2 functional group blends presented optimal moderate wettability conditions for cell adhesion [150]. The study also noticed that not only wettability, but also functional group type and density, as well as cell type, affected the adhesion behaviour. In the same study, it was observed that, on hydrophobic surfaces with high levels of methyl groups, albumin strongly adsorbed and resisted replacement by cell adhesive proteins. However, in hydrophilic surfaces, albumin was easily displaced, allowing cell attachment.

The introduction of functional groups has also been used to mimic the environment of different tissues. For instance, carboxylic groups presented on biomaterials surface have been

used to mimic the glycosaminoglycans (GAGs) environment in cartilage, phosphate groups for their role in bone mineralization and tert-butyl to mimic the lipid rich environment in adipose tissue [151]. Also, the addition of different functional groups such as ($–CH_3$), (-OH), (-COOH) and ($-NH_2$) have shown to induce stem cell differentiation towards different lines. For instance, amino groups have shown to promote mesenchymal stroma cell (MSC) osteoblastic differentiation due to increased fibronectin adsorption [152], while hydroxyl and carboxyl groups have shown to promote MSC chondrogenesis, and methyl groups to maintain MSC phenotype [153].

Moving towards complexity, the use of peptides, proteins and other biomolecules are used to introduce all form of bioactivity (biosignalling, adhesive sequences, gene transcription, chemotactic effects, and so on). First used biomolecules were natural ECM proteins and biopolymers such as collagen, laminin, fibronectin or elastin [154]. However, natural proteins present important drawbacks on their implementation. For instance, they are more susceptible to proteolytic degradation effects [155], their functionalization may present conformation and orientation problems [156,157], and their origin can be a source of immunogenic problems and batch-to-batch variation [155,158]. Therefore, alternatives like simplified sequences based on natural proteins are commonly used. Indeed short peptides are simpler, easier to produce, easier to functionalize, well-defined and non-immunogenic [159,160].

The first studied short peptide was RGD (Arg-Gly-Asp) sequence, which was identified from fibronectin [161]. Actually, the RGD amino acid sequence is found on many ECM proteins like collagen, laminin and vitronectin [155], and is the shortest sequence that interacts with cell integrins to allow cell adhesion. However RGD sequence lacks on cell-type specificity. Indeed, this limitation is a shared problem between most short peptides due to the oversimplification [162]. Thus, despite some peptides are preferentially recognized by some cell types, normally it is necessary to combine at least two different peptide types to present cell selectivity [163].

Short peptides have been studied for long time, and many adhesive sequences have been defined (Table 6). However, short peptides cannot perform the complex tasks of natural ECM proteins. ECM matrix is a complex integrated system with multivalent signals regulated spatially and timely [164]. Indeed, full proteins often contain cryptic cell-adhesive or bioactive regions that are exposed to cells after selective enzymatic proteolysis or mechanical forces [165,166].

Table 6. List of short peptide sequences and targeted cell types.

Amino acid sequence	Function
RGD	Cell adhesion
YGISR	Cell adhesion
IKVAV	Neurite extension
KRSR	Osteoblast adhesion
REDV	Endothelial cells adhesion
DGEA	Neuronal cells adhesion
PDSGR	Neuronal cells adhesion
KQAGDV	Smooth muscle cell adhesion
KHIFSDDS	Astrocyte adhesion
FHRRIKA	Induction of osteoblast mineralization
PHSRN	Human corneal epithelial cells, Osteoblasts cell adhesion

For an exhaustive analysis of cell recognition motifs, review [167], [168] and [169] are referred.

Because complex properties are desired for the design of intelligent scaffolds (see section 2.2.5), but natural proteins present immunogenic problems and batch-to-batch variations, genetically modified proteins are presented as an alternative [170]. Genetically modified proteins are produced by recombinant expression on bioreactor cultures, which allows the scaling up in a reproducible and cost-effective manner [171]. Examples of tailored biomolecules are elastin-like recombinamers (ELRs), which are based on the structure of natural protein elastin [172]. Because ELRs are genetically modified proteins, they can include tailored sequences with specific properties like cross-linking sites, HA nucleation sites or cleavage sites for matrix remodelling [173-175].

Beyond peptides and ECM proteins, other biomolecules are available to introduce bioactivity on surface scaffolds. For instance, growth factors are commonly used to attract specific cell types and stimulate cell growth [176]. Indeed, it has been observed that immobilization of growth factors can strongly stimulate cell homing and proliferation locally, reducing the required systemic dose [175,177]. However, the use of growth factors is correlated with tissue hyperplasia and tumorigenesis [178]. Another example is the immobilization of carbohydrates like galactose on polymeric to enhance surface wettability and MSC viability [179]. Oligonucleotide sequences are also immobilized on scaffold surfaces as adhesive agents. For instance, DNA aptamers are used to capture circulating endothelial progenitor cells [180].

Because options are multiple, depending on selected molecule, the ligation strategy will vary. Biomolecules can be graft onto surface by means of chemical grafting, physical adsorption,

plasma etching, ionic interaction, surface entrapment and so on. Strategies are multiple and each case present unique complex characteristics. Thus, for further information, other reviews and books with more comprehensive view are referred [181,182]. However it is important to consider some key aspects during biomolecule functionalization. The first factor is the peptide density and distribution, which has proved to affect cell adhesion and proliferation [169,183]. Indeed, it has been observed that, for instance, an intermolecular spacing of 36 nm between RGD sequences is sufficient to promote cell adhesion, but a spacing of 11 nm is necessary for integrin clustering and the formation of focal adhesion points [184]. Similarly, the spacer used to link the biomolecule to the substrate affects accessibility and recognition, and therefore must be taken into account [182]. In this sense, some studies have pointed out that RGD binding sites can be reached by grafted peptides that go as far as approximately 11-32 Å from surface [185].

2.2.4.5. Degradability

Biodegradability is a common requirement for tissue engineering scaffolds that helps scaffold assimilation and integration into the body. Depending on the application and the purpose to which the scaffold serves, degradation process will have to match specific kinetics [186]. Generally, most scaffolds act as simple supportive template in which cells growth and neo-tissue expands. In such cases the scaffold must disappear at similar rate than the speed of new tissue growth. This is the case of most synthetic and natural used polymers, like aliphatic polyesters, or collagen matrices. Special consideration has to be taken when the scaffold has a mechanical supportive function. In these cases, the degradation and the consequent loss of mechanical properties must be considered in order to match the gained mechanical properties from the new tissue so the mechanical function of regenerated tissue is not compromised [187]. Biodegradation also play an important role on biomaterials that act as mechanism to deliver bioactive factors such as molecules, ions or proteins [188]. Such kind of biomaterials, whether they are scaffolds or not, have to consider if they want a maintained, increasing or decreasing patron release, as well as they need to define the duration of the delivering [189,190].

Degradation processes have to mimic the timings of regeneration processes in order to ensure the correct performance of biomaterials. But beyond this, biodegradation can be used to design smart biomaterials. On this line, some biomaterials include active regions that can be recognized and cut by enzymes like matrix metalloproteases (MMPs) [191], or that degrade under specific circumstances (pH, ionic strength and so on). The control of degradation along time as a response to an external stimulus is an example of how intelligent biomaterials can be

designed to trigger different cellular responses depending on the regeneration stage and tissue inputs (see section 2.2.5).

2.2.4.6. Mechanical Properties

Each body tissue has distinct mechanical properties that withstand different functionalities (Figure 7). Scaffold mechanical properties have to present enough similitude to the aimed tissue in order to perform properly. Thus, biomaterial choice will depend on the mechanical properties to mimic. For instance, hard tissues like bones are commonly treated with composites [192,193], because they can withstand high compressive forces. Instead, tissues like cardiac muscle and blood vessels are treated with elastomeric polymers like TCM, PCL and PU [194,195], because elastic behaviour is necessary to mimic these compliant tissues. And soft connective tissues are usually treated with hydrogels as space-fillers or cell carriers [196].

Mechanical properties are not only important to resemble as much as possible the tissue properties, but they also offer to cells an environment that can be perceived as their natural niche. This is extremely important because it has been observed that properties like stiffness and viscoelasticity may have an important effect on cell behaviour, controlling cell growth, proliferation and differentiation [197,198].

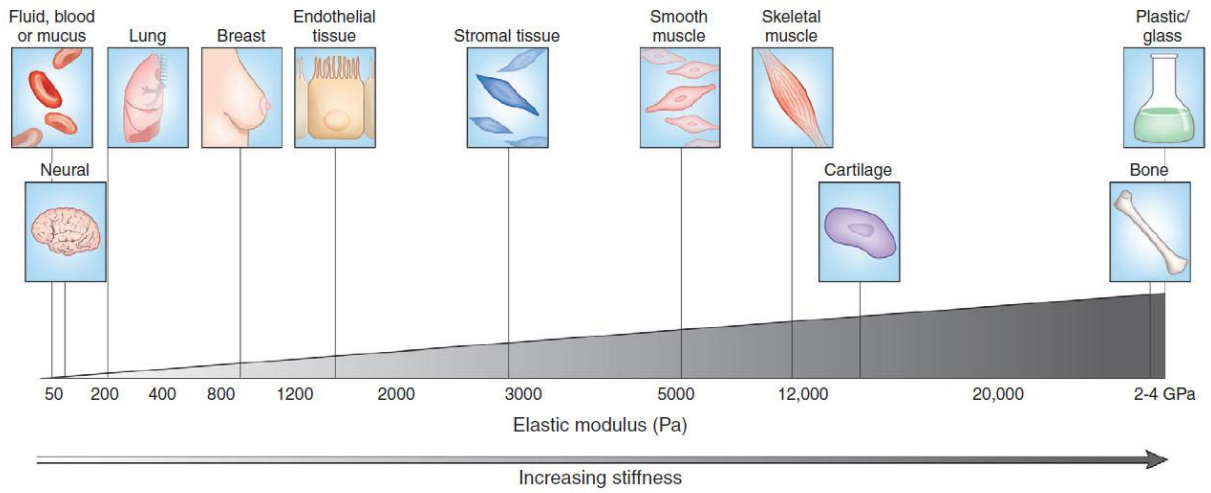

Figure 7. Mechanical properties of the different body tissues occupy a wide range of magnitudes and are tightly related to tissue function. On the lower range, static tissues like brain or soft compliant tissues like lung exhibit low stiffness. On the higher range, tissues that must stand high mechanical loads like skeletal muscle, cartilage or bone, exhibit several orders of magnitude higher stiffness values. Adapted from [199].

2.2.5. Intelligent Biomaterials

An emerging trend in tissue engineering is that rather than attempting to recreate the complexity of living tissues, we should aim to develop synthetic materials that establish key interactions with cells in ways that unlock the body's innate powers of organization and self-repair. Thus, it is important to develop smart biomaterials that can trigger own body's capabilities in an ordered and structured way.

Intelligent properties represent the complex behaviour of natural, artificial and hybrid systems. Intelligent properties can be thought of as subproperties of complex adaptive systems that possess self-maintenance, adaptability, information preservation and/or spontaneous increase in complexity. The intelligent subproperties include self-assembly, self-organization, self-repair, self-replication, self-maintenance, redundancy, self-diagnosis, recognition, learning, adaptability, information storage, signalling and evolution, to name a few [200].

On tissue engineering, intelligent biomaterials are those capable of trigger some action in a designed and complex manner, as a response of external output like environmental conditions or signals [201]. Examples of smart biomaterials can be found on devices with a controlled release mechanism that deliver a drug or a bioactive molecule with very accurate dosing, locally, with complex release patterns and in a stable manner (Figure 8). Other examples of intelligent scaffolds are those including oligopeptide with specific bioactivity like cleaving sequences for matrix MMPs, integrin binding domains, growth factors, anti-thrombin sequences, plasmin degradation sites and morphogenetic proteins [202]. These scaffolds can be designed to show the bioactive signals whether spatially organized or timely organized, in a way that can guide tissue regeneration in an orchestrated manner.

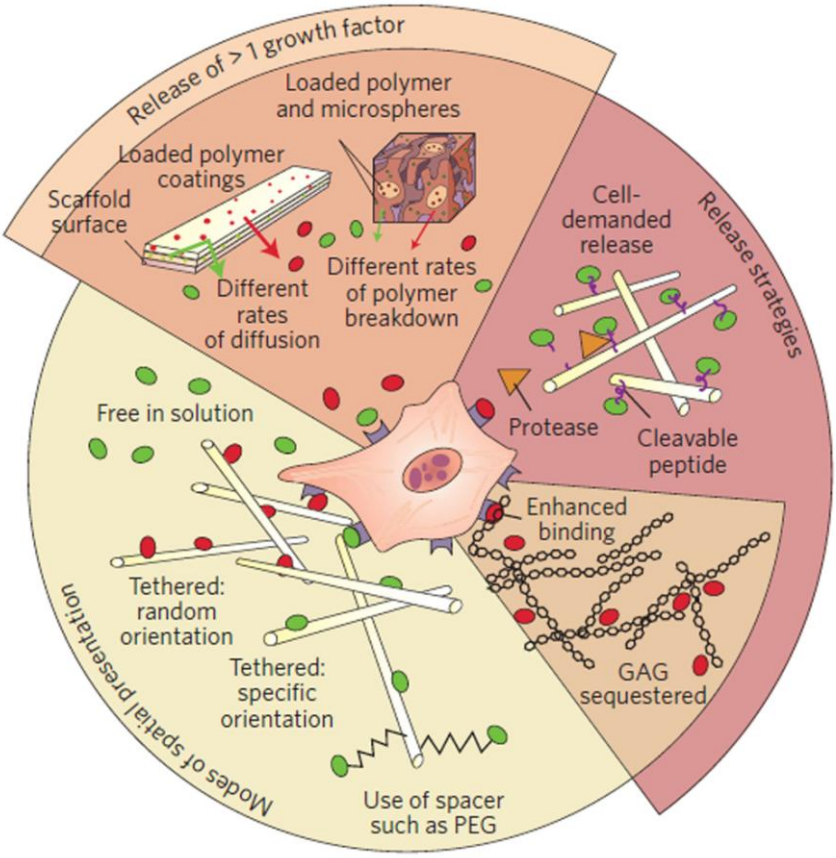

Figure 8. Scheme of different strategies used on intelligent biomedical systems for the controlled delivery of active molecules. Clockwise, from top : Bioactive molecules loaded into polymeric scaffolds are release by means of modulated polymer degradation rates or modulated diffusive properties. Bioactive molecules are released from the scaffold by the cleavage of a protease-sensitive peptide spacer. Bioactive molecules are entrapped by non-covalent associations within matrix components like GAGs, and slowly released by diffusion. Exposure of cells to different growth factors with time may imitate developmental pathways and healing responses. Adapted from [203]

For instance, these scaffolds can recruit different cell types around defined spaces during scaffold cell homing, or trigger different specific cell response along time in a designed manner. Particularly interesting are those scaffolds that, by cleavage of peptidic sequences, can release bioactive factors or uncover cryptic sites contained within the amino acid sequences [204]. Such strategies are useful to trigger cell responses at specific times, or under specific circumstances. For instance, cells can exert physical manipulation on ECM proteins by integrin interaction, inducing in such a way conformational changes that expose cryptic sites that allow it to self-assemble [205,206]. Another example is the release of stored soluble factors that induce tissue formation when ECM proteins are enzymatically degraded during remodelling (Figure 9).

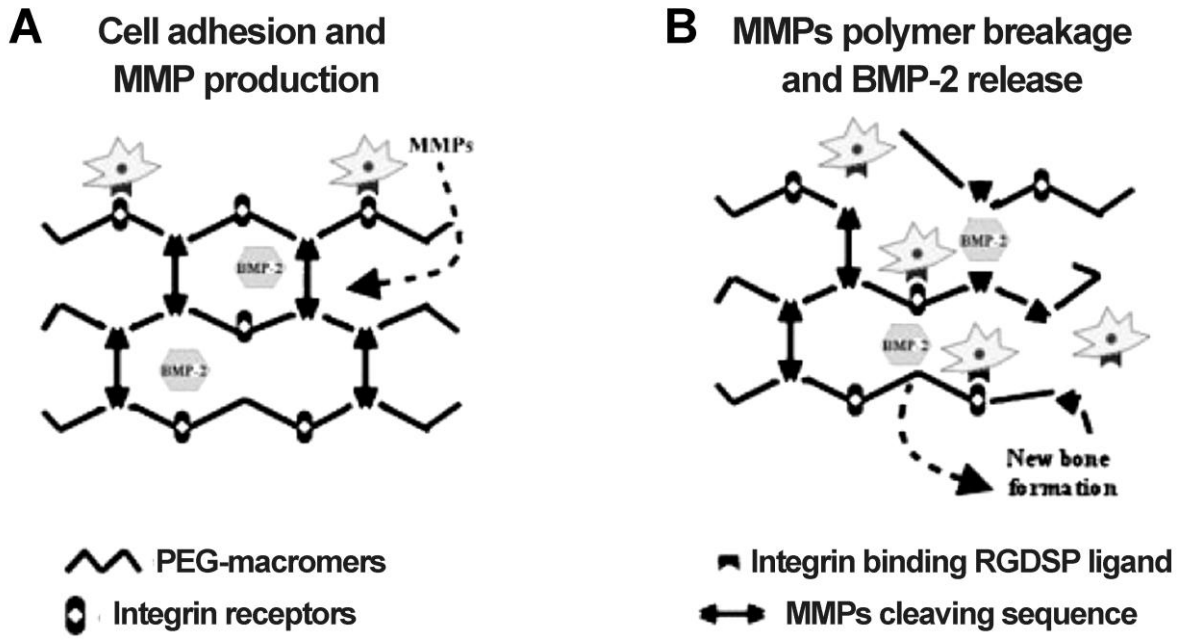

Figure 9. Sequential diagram of modified PEG hydrogel-cells interactions and new bone formation. (A) Cells adhere on modified PEG hydrogel via integrin receptors and produce matrix MMPs. (B) Produced MMPs remodel the PEG modified hydrogel, which induce bone morphogenetic protein-2 (BMP-2) local release and new bone formation. Adapted from [207]

Attachment of growth factors and controlled delivery by proteolytic release have shown as well to be an important technique to develop smart biomaterials that offer better performance than soluble bioactive agents [208,209]. An example of the enhanced effect of controlled delivery has been observed on new blood vessel formation (Figure 10). In this case, it has been observed that, normally, a rapid burst leads to the formation of unstable leaky vessels. Instead, using alginate hydrogels scaffolds with different molecular weights, which act as growth factors reservoirs, it is possible to obtain a slower low-level sequential release that allows the formation of stabilized vessels [210,211].

The slow release of factors can be controlled by either the attachment of active factors on substrate or by sequestering them on hydrogels like GAGs hydrogels. GAGs (like heparin) can have regulated regiospecific sulphating patterns that determine their specific interactions with proteins [212]. For example, fibrin hydrogels scaffolds have been modified to include attached heparin on the matrix. Thus, heparin binding affinity to heparin-binding growth factors can be used to transform fibrin hydrogels into a reservoir, which can act as a delivery system through the active released controlled by cell-mediated degradation of the hydrogel reservoir. In such a way, it is possible to obtain a slow release mechanism for the controlled modulation of cell signalling [213,214].

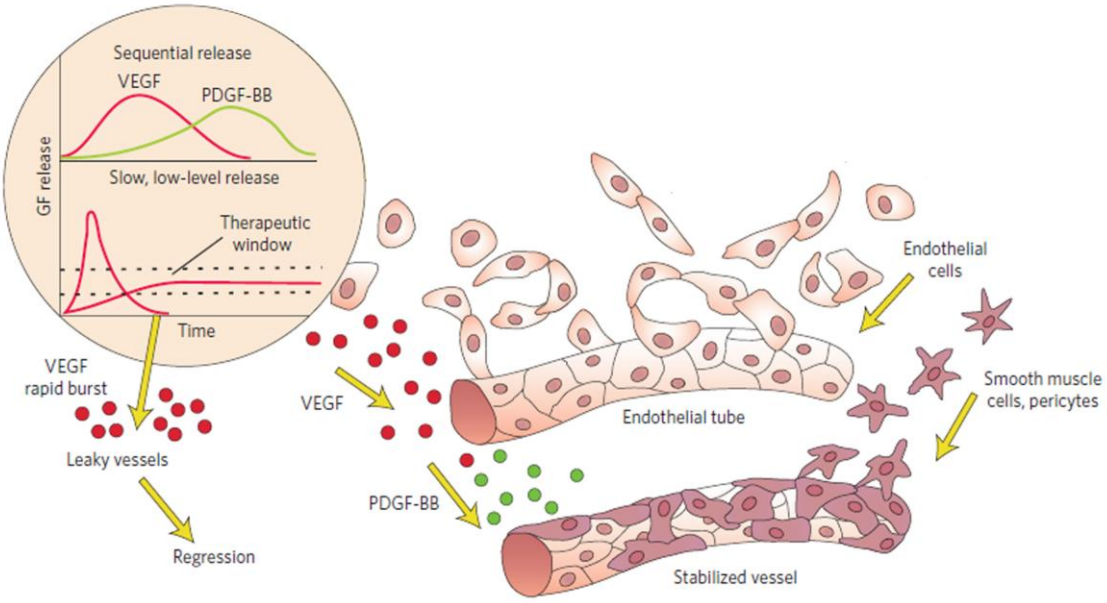

Figure 10. Controlled slow delivery of different growth factors in time, by means of intelligent systems, favours the maturation and stabilization of blood vessels. Adapted from [203]

Special interest is found on the development of smart scaffolds free from biological factors or cells that may trigger or enhance collateral non-desired responses. For these reason, smart scaffolds are also designed from a structural point of view, since it is know that 3D organization, topographical patterns and available space may direct cell behaviour and morphogenesis. Examples of these smart scaffolds are found on biomimetic matrices that self-initiate the induction of bone formation without the use of exogenous applications of osteogenic-soluble molecular signals. These scaffolds use the pits and concavities to induce angiogenesis and bone formation through geometric signals, because these concavities per se are geometric regulators that participate during the remodelling processes of the corticocancellous bone [215]. Other smart scaffolds that work with non-biological compounds are bioglass-polymer composites nanoparticles with designed ion release that enhance angiogenesis through the calcium ion activity, thus avoiding the use of growth factors or cells [216].

Other intelligent biomaterials are those that can retain shape memory. These materials are of particular interest for the design of systems with a minimally invasive delivery. These materials can be injected and can regain their original form by gelation or recovering their original form in response to stimuli such as ultraviolet illumination or physiological conditions (temperature, pH, electromagnetic radiation or ionic strength) [151,217-219]. Biodegradable stimuli-responsive hydrogels are typical materials that exhibit large and sharp physical-chemical changes in response to small physical or chemical stimuli like pH, temperature, magnetic field,

ionic strength and so on. Moreover, these hydrogels can be single stimulus-responsive or multi-stimuli-responsive materials. An example of these systems is a polypeptide hydrogel synthesized from the cross-linking of poly(L-glutamic acid) and PEG polymers [220]. Obtained hydrogel can achieve high extents of swelling through the high ionization of PLG, which is regulated by means of pH changes. Thus, due to the ion-ion repulsion and the internal ion osmotic pressure, this pH-sensitive hydrogels can swell and store molecules such as growth factors, which can be released in a controlled manner. These kinds of biomaterials may be useful in tissue engineering for the neovascularisation treatment of ischemia or the inflammation regulation through the controlled delivery of factors by means of pH-sensitive swelling/deswelling behaviours [221,222].

Intelligent biomaterials are fabricated to respond to changes in the immediate environment and to stimulate specific cellular response at the molecular level. Micro-and nano-scale design are a key aspect for the construction of intelligent scaffolds, as well as innovative materials development. New generations of synthetic polymers are being developed, which can change their molecular conformation in response to changes in temperature, pH, electrical stimuli, ionic strength, forces, or energetic status. Conducting polymers, photoresponsive polymers, temperature responsive polymers and so on are examples of currently investigated materials that will be used to create the forth-coming resorbable systems that can elicit specific interactions in a controlled manner.

2.3. Conclusions and Outlook

We have seen that owing to market characteristics, current clinical technology and regulatory difficulties; regenerative medicinal therapies based on scaffolds, whether with the use of cells (mainly autologous, treated peri-operatively) or as acellular materials, are gaining interest on tissue engineering industry. These scaffolds, in general, are demanded to be composed by biocompatible materials, to be easily manufactured and to biodegrade into non-toxic products. Additionally, scaffolds should have a macrostructure that is designed to fit the shape for the intended target tissue, with a good porosity and interconnected channels for proper mass transport properties, presenting a macro-scale organization and yet be mechanically satisfactory and stable. Moreover, it should also have a microstructure to enhance cell interaction, to resemble ECM and to induce specific and desired cell response towards tissue regeneration. When possible, the mode of action of the medical device should be based on physical signals, molecular cues or factors, thus avoiding the legal status of drugs and ATMP, which implies an expensive route through the clinics. Moreover, the scaffold should resorb or degrade once it has served its purpose, and degradation should be adjustable to match the rate of tissue regeneration and tissue function recovery.

Furthermore, the integration of all these factors should be achieved by means of easy, cheap, reproducible and safe techniques, in order to satisfy the requirements of the different stakeholders (patient, investors, regulatory agencies, surgeons…) found during the path through the product commercialization.

Thus, it is clear that product commercialization success is not an easy task, and proof of it is the number of therapies found on the market regarding to the amount of money invested on research and development, as well as the number of products that fail on clinical trials. Therefore, the scope of this Thesis is to expose, characterize and show the potential of two different techniques, that used alone or in combination, permit to obtain scaffolds, with tailored mechanical properties, porosity, diffusivity, shape and bioactivity by means of easy, cheap, safe and reliable protocols; thus, providing tools for a better penetration of scaffolding technology into clinics.

The next chapters will expose separately these two strategies. The first technique will expose and characterize a scaffold fabrication methodology for the obtaining of nanofibrous scaffolds, which is based on the interaction of poly(lactic) acid polymer and ethyl lactate solvent. And the second technique will expose and characterize a scaffold surface modification technique

for the improvement of cell-material interaction, which is based on the functionalization of surface materials with ELRs.

2.4. References

1. Viola J, Lal B, Grad O. The Emergence of Tissue Engineering as a Research Field. The National Science Foundation. 2003. Available from URL: http://www.nsf.gov/pubs/2004/nsf0450/start.htm.
2. Wolter JR, Meyer RF. Sessile macrophages forming clear endothelium-like membrane on inside of successful keratoprosthesis. Trans Am Ophthalmol Soc 1984;82:187-202.
3. Langer R, Vacanti JP. Tissue engineering. Science 1993;260:920926.
4. Carrel A, Lindbergh C. The culture of organs. New York: PB Hoeber, Inc., 1938.
5. Ayers T. Science and technology leaders discuss innovations for the future. Science 1999;286:1753-54.
6. Lysaght MJ, Hazlehurst AL. Tissue Engineering: The End of the Beginning. Tissue Eng 2004;10:309-20.
7. Lysaght MJ, Jaklenec A, Deweerd E. Great Expectations: Private Sector Activity in Tissue Engineering, Regenerative Medicine, and Stem Cell Therapeutics. Tissue Eng Part A 2008;14(2):305-U57.
8. Nerem RM. Regenerative medicine: the emergence of an industry. J R Soc Interface 2010;7(6): S771-75.
9. Zandonella C. Tissue engineering: The beat goes on. Nature 2003;421:884-86.
10. Gillian M. Good Morning America. April 29, 1999.
11. Special Report. The hottest jobs of the future. Time, May 22, 2000.
12. Masterson F, Cormican K. Overview of the Regulation of Medical Devices and Drugs in the European Union and United States. Ther Innov Regul Sci 2013; 47(6):715-22.
13. Kellathur SN, Lou HX. Cell and tissue therapy regulation: Worldwide status and harmonization. 7th International-Association-of-Biological-Standardization Symposium on Advances in Transfusion Safety. Singapore 2011.
14. Cohen-Haguenauer O. A Comprehensive Resource on EU Regulatory Information for Investigators in Gene Therapy Clinical Research and Advanced Therapy Medicinal Products. Hum Gene Ther 2013;24(1):12-18.
15. Voltz-Girolt C, Celis P, Boucaumont M, D'Apote L, Pinheiro MH, Papaluca-Amati M. The advanced therapy classification procedure Overview of experience gained so far. Bundesgesundheitsbla 2011;54(7):811-15.
16. Campillo-Artero C. A full-fledged overhaul is needed for a risk and value-based regulation of medical devices in Europe. Health Policy 2013;113(1-2): 38-44.
17. Pirnay JP, Vanderkelen A, De Vos D, Draye JP, Rose T, Ceulemans C, et ál. Business oriented EU human cell and tissue product legislation will adversely impact Member States' health care systems. Cell Tissue Bank 2013;14(4):525-60.
18. European Union (2001b). Communication from the Commission: Towards a strategic vision of life sciences and biotechnology: consultation document. (COM(2001) 454 final). Available from URL: http://ec.europa.eu/biotechnology/docs/doc_en.pdf. 2012.
19. Hildebrandt M, Sethe S. Caught in the gap: ATMP manufacture in academia. Telegraft 2012;19(1):1–10. Available from URL: http://mediatum.ub.tum.de/doc/1100606/document.pdf.
20. Ruiz S, Timon M, de Felipe P, Rojo S, Moreno S. ATMP in the EU: the long and winding road. Hum Gene Ther 2013;24(12):A6-A6.
21. Bock AK, Rodriguez-Cerezo E, Hu¨sing B, Bu¨hrlen B, NusserM (2005) Human tissue engineered products: potential socioeconomic impacts of a new European regulatory framework for authorisation, supervision and vigilance (report EUR 21 838 EN). European Commission Joint Research Centre (DG JRC) Institute for Prospective Technological Studies (IPTS). http://ftp.jrc.es/EURdoc/eur21838en.pdf. Accessed 2 Nov 2012
22. Kent J. Making connections—linking ethics and regulation in the social world of tissue engineering. Regulatory Affairs Focus 2005. Available from URL: http://www.esrc.ac.uk/my-esrc/grants/L218252058/outputs/Read/22633975-affb-47e4-9430-da93a1a692a6.

23. EMA/CAT (2012a). Summaries of scientific recommendations on classification of advanced-therapymedicinal products. Available from URL:

http://www.ema.europa.eu/ema/index.jsp?curl=pages/regulation/general/general_content_000301.jsp&mid=WC0b01ac05800862c0. 2012.

24. Williams DF. On the nature of biomaterials. Biomaterials 2009;30:5897-909.

25. Williams DF. Essential Biomaterials Science. Cambridge University Press, 2014.

26. Park JB, Lakes RS. Biomaterials: An introduction, 3rd ed. Springer 2010.

27. Black J. Biological performance of materials–fundamentals of biocompatibility, 2nd ed. New York: Marcel Dekker Inc., 1992

28. McGregor DB, Baan RA, Partensky C, Rice JM, Wilbourn JD. Evaluation of the carcinogenic risks to humans associated with surgical implants and other foreign bodies: a report of an IARC Monographs Programme Meeting. International. Agency for Research on Cancer, Eur J Cancer 2000;36: 307-13

29. Le Guehennec L, Soueida, A, Layrolle P, Amouriq Y. Surface treatments of titanium dental implants for rapid osseointegration. Dent Mater 2007;23(7):844-54.

30. Long, M; Rack, HJ. Titanium alloys in total joint replacement - a materials science perspective. Biomaterials 1998;19:1621–39.

31. Gmeiner R, Deisinger U, Schonherr J, Lechner B, Detsch R, Boccaccini AR, Stampfl J. Additive Manufacturing of Bioactive Glasses and Silicate Bioceramics. J Ceram Sci Tech 2015;6(2):75-86.

32. Jazrawi LM, Bogner E, Della Valle CJ, Chen, FS, Pak KI, Stuchin SA. Wear rates of ceramic-on-ceramic bearing surfaces in total hip implants: A 12-year follow-up study. J Arthoplasty 1999;14(7):781-87.

33. KamitakaharaM, Ohtsuki C, Miyazaki T. Review paper: behavior of ceramic biomaterials derived from tricalcium phosphate in physiological condition. J Biomater Appl 2208;23:197–212.

34. Heimke G. Safety Aspects of Alumina and Zirconia Ceramics in Hip Surgery. In: Yaszemski MJ. Biomaterials in Orthopedics. CRC Press, 2003. p. 381–399

35. Jones JR. Review of bioactive glass: From Hench to hybrids. Acta Biomater 2013;9(1):4457-86.

36. Mohn D, Zehnder M, Imfeld T, Stark WJ. Radio-opaque nanosized bioactive glass for potential root canal application: evaluation of radiopacity, bioactivity and alkaline capacity. Int Endodont J 2010;43:210–7.

37. Ioannou AL, Kotsakis GA, Kumar T, Hinrichs JE, Romanos G. Evaluation of the bone regeneration potential of bioactive glass in implant site development surgeries: a systematic review of the literature. Clin Oral Invest 2015;19(2):181-191.

38. Hench LL. Bioceramics. J Am Ceram Soc 1998;81(7): 1705-28.

39. Paul W, Sharma CP. Ceramic drug delivery: a perspective. J Biomater Appl 2003;17:253–64.

40. Murshed M, Harmey D, Millan JL, McKee MD, Karsenty G. Unique coexpression in osteoblasts of broadly expressed genes accounts for the spatial restriction of ECM mineralization to bone. Genes Dev 2005;19:1093-104.

41. Boyan BD, Schwartz Z. Regenerative medicine: are calcium phosphate ceramics ‘smart’ biomaterials? Nat Rev Rheumatol 2011;7:8-9.

42. Radin S, El-Bassyouni G, Vresilovic EJ, Schepers E, Ducheyne P. In vivo tissue response to resorbable silica xerogels as controlled-release materials. Biomaterials 2005;26:1043-52.

43. Tian HY, Tang ZH, Zhuang XL, Chen XS, Jing XB. Biodegradable synthetic polymers: preparation, functionalization and biomedical application. Prog Polym Sci 2012;37:237-80.

44. Dhandayuthapani B, Yoshida Y, Maekawa T, Kumar DS. Polymeric Scaffolds in Tissue Engineering Application: A Review. Int J Polym Sci 2011;290602.

45. Mano JF, Silva GA, Azevedo HS, et ál. Natural origin biodegradable systems in tissue engineering and regenerative medicine: present status and some moving trends. J R Soc Interface 2007;4(17):999-1030.

46. Gomes S, Leonor IB, Mano JF, Reis RL, Kaplan DL. Natural and Genetically Engineered Proteins for Tissue Engineering. Prog Polym Sci 2012;37(1):1–17.

47. Williams DF. The role of short synthetic adhesion peptides in regenerative medicine; The debate. Biomaterials 2011;32:4195-97.

48. Van de Velde K, Kiekens P. Biopolymers: overview of several properties and consequences on their applications. Polym Test 2002;21:433-42.

49. Guo BL, Ma PX. Synthetic biodegradable functional polymers for tissue engineering: a brief review. Sci China Chem 2014; 57(4):490-500.

50. Ma Z, Mao Z, Gao C. Surface modification and property analysis of biomedical polymers used for tissue engineering. Colloid Surfaces B 2007;60:137-157.

51. Nair LS, Laurencin CT. Biodegradable polymers as biomaterials. Prog Polym Sci 2007;32(8-9):762-98.

52. Maurus PB, Kaeding CC. Bioabsorbable implant material review. Oper Tech Sport Med 2004;12:158–60.

53. Griffith LG. Emerging Design Principles in Biomaterials and Scaffolds for Tissue Engineering. Ann NY Acad Sci 2001;961:83-95.

54. Serrano MC, Chung EJ, Ameer GA. Advances and Applications of Biodegradable Elastomers in Regenerative Medicine. Adv Funct Mater 2010;20(2):192-208.

55. Drury JL, Mooney DJ. Hydrogels for tissue engineering: scaffold design variables and applications. Biomaterials 2003;24:4337-51.

56. Tabata Y, Miyao M, Ozeki M, Ikada Y. Controlled release of vascular endothelial growth factor by use of collagen hydrogels. J Biomater Sci: Polym Ed 2000;11:915-30.

57. Burdick JA, Anseth KS. Photoencapsulation of osteoblasts in in-jectable RGD-modified PEG hydrogels for bone tissue engineering. Biomaterials 2002;23:4315-23.

58. Billie T. A review of trends and limitations in hydrogel-rapid prototyping for tissue engineering. Biomaterials 2012;33(26):6020-41.

59. Lee KY, Mooney DJ. Hydrogels for tissue engineering. Chem Rev 2001;101(7):1869-79.

60. Zeimaran E, Pourshahrestani S, Djordjevic I, Pingguan-Murphy B, Kadri NA, Towler MR. Bioactive glass reinforced elastomer composites for skeletal regeneration: A review. Mater Sci Eng C Mater Biol Appl 2015;53:175-88.

61. Hollister SJ. Scaffold Design and Manufacturing: From Concept to Clinic. Adv Mater 2009;21(32-33):3330-42.

62. Brekke JH, Toth JM. Principles of tissue engineering applied to programmable osteogenesis. J Biomed Mater Res 1998;43(4):380-98.

63. Hutmacher DW. Scaffold design and fabrication technologies for engineering tissues--state of the art and future perspectives. J Biomater Sci Polym Ed 2001;12(1):107-24.

64. Thomson RC, Yaszemski MJ, Powers JM, Mikos AG. Fabrication of biodegradable polymer scaffolds to engineer trabecular bone. J Biomater Sci Polym Ed. 1995;7(1):23-38.

65. Mooney DJ, Baldwin DF, Suh NP, Vacanti JP, Langer R. Novel approach to fabricate porous sponges of poly(D,L-lactic co-glycolic acid) without the use of organic solvents. Biomaterials 1996;17:1417-22.

66. Teo WE, Ramakrishna S. A review on electrospinning design and nanofibre assemblies. Nanotechnology 2006;17(14):R89-R106.

67. Ishaug-Riley SL, Crane GM, Gurlek A, Miller MJ, Yasko AW, Yaszemski MJ, Mikos AG. Ectopic bone formation by marrow stromal osteoblast transplantation using poly(DL-lactic-co-glycolic acid) foams implanted into the rat mesentery. J Biomed Mater Res 1997;36:1-8.

68. Freed LE, Vunjak-Novakovic G. Culture of organized cell communities. Adv Drug Deliver Rev 1998;33:15-30.

69. Tsang VL, Bhatia SN. Three-dimensional tissue fabrication. Adv Drug Deliv Rev 2004;56(11):1635-47.

70. Scott CS. Apparatus and method for creating three-dimensional objects. US Patent No. 5121329, 1991.

71. Landers R, Mulhaupt R. Desktop manufacturing of complex objects, prototypes and biomedical scaffolds by means of computer-assisted design combined with computer-guided 3D plotting of polymers and reactive oligomers. Macromol Mater Eng 2000;282:17-21.

72. Bredt JF, Sach E, Brancazio D, Cima M, Curodeau A, Fan T. Three dimensional printing system. US Patent No. 5807437, 1998.

73. Hull C. Method for production of three-dimensional objects by stereolithography. US Patent No. 4929402, 1990.

74. Williams JM, Adewunmi A, Schek RM, Flanagan CL, Krebsbach PH, Feinberg SE, Hollister SJ, Das S. Bone tissue engineering using polycaprolactone scaff olds fabricated via selective laser sintering. Biomaterials 2005;26:4817-4827.

75. Chu TM., Orton DG, Hollister SJ, Feinberg SE, Halloran JW. Mechanical and in vivo performance of hydroxyapatite implants with controlled architectures. Biomaterials 2002;23:1283-93.

76. Woodfield TB, Malda J, de Wijn J, Péters F, Riesle J, van Blitterswijk CA. Design of porous scaffolds for cartilage tissue engineering using a three-dimensional fiber-deposition technique. Biomaterials 2004; 25:4149-61.

77. Taboas JM, Maddox RD, Krebsbach PH, Hollister SJ. Indirect solid free form fabrication of local and global porous, biomimetic and composite 3D polymer-ceramic scaffolds. Biomaterials 2003;24(1):181-94.

78. Hollister SJ. Porous scaffold design for tissue engineering. Nat Mater 2005;4(7):518-24.

79. Hutmacher DW. Scaffolds in tissue engineering bone and cartilage. Biomaterials 2000;21(24):2529-43.

80. Hollister SJ. Scaffold Design and Manufacturing: From Concept to Clinic. Adv Mater 2009;21(32-33):3330-42.

81. Place ES, Evans ND, Stevens MM. Complexity in biomaterials for tissue engineering. Nat Mater 2009;8(6):457-70.

82. Edalat F, Sheu I, Manoucheri S, Khademhosseini A. Material strategies for creating artificial cell-instructive niches. Curr Opin Biotechnol 2012;23(5):820-5.

83. Mikos AG, Herring SW, Ochareon P, Elisseeff J, Lu HH, Kandel R, Schoen FJ, Toner M, Mooney D, Atala A, Van Dyke ME, Kaplan D, Vunjak-Novakovic G. Engineering Complex tissues. Tissue Eng 2006;12(12):3307-39.

84. Dormer NH, Berkland CJ, Detamore MS. Emerging Techniques in Stratified Designs and Continuous Gradients for Tissue Engineering of Interfaces. Ann Biomed Eng 2010;38(6):2121-41.

85. Liu C, Han Z, Czernuszka JT. Gradient collagen/nanohydroxyapatite composite scaffold: Development and characterization. Acta Biomater 2009;5(2):661-9.

86. Spalazzi JP, Doty SB, Moffat KL, Levine WN, Lu HH. Development of Controlled Matrix Heterogeneity on a Triphasic Scaffold for Orthopedic Interface Tissue Engineering. Tissue Eng 2006;12(12):3497-508.

87. Singh M, Dormer N, Salash JR, Christian JM, Moore DS, Berkland C, Detamore MS. Three-dimensional Macroscopic Scaffolds With a Gradient in Stiffness for Functional Regeneration of Interfacial Tissues. J Biomed Mater Res A 2010;94(3):870-6.

88. Hadjipanayi E, Mudera V, Brown RA. Guiding Cell Migration in 3D: A Collagen Matrix with Graded Directional Stiffness. Cell Motil Cytoskeleton 2009;66(3):121-8.

89. Hynes RO. The extracellular matrix: not just pretty fibrils. Science 2009;326(5957):1216-9.

90. Seidlits SK, Lee JY, Schmidt CE. Nanostructured scaffoldsfor neural applications. Nanomedicine (Lond) 2008;3(2):183-99.

91. Webster TJ, Nanophase ceramics: The future Orthopedic and Dental Implant Material. In: Advances in Chemical Engineering. Vol. 27; Ying JY. Ed. Academic Press: NY; 2001:125-166.

92. Colon G, Ward BC, Webster TJ. Increased osteoblast and decreased Staphylococcus epidermidis functions on nanophase ZnO and TiO2. J Biomed Mater Res A 2006;78(3):595–604.

93. Liu X, Ma PX. Phase separation, pore structure, and properties of nanofibrous gelatin scaffolds. Biomaterials 2009;30(25):4094-103.

94. Zhang S. Fabrication of novel biomaterials through molecular self-assembly. Nature Biotechnol 2003;21:1171-8.

95. Kim HN, Jiao A, Hwang NS, Kim MS, Kang do H, Kim DH, Suh KY. Nanotopography-guided tissue engineering and regenerative medicine. Adv Drug Deliv Rev 2013;65(4):536-58.

96. Shi J, Votruba AR, Farokhzad OC, Langer R. Nanotechnology in drug delivery and tissue engineering: from discovery to applications. Nano Lett 2010;10(9):3223-30.

97. Bettinger CJ, Langer R, Borenstein JT. Engineering Substrate Topography at the Micro- and Nanoscale to Control Cell Function. Angew Chem Int Ed Engl 2009;48(30):5406-15.

98. Yim EK, Pang SW, Leong KW. Synthetic nanostructures inducing differentiation of human mesenchymal stem cells into neuronal lineage. Exp Cell Res 2007;313(9):1820-9.

99. Dalby MJ, Gadegaard N, Tare R, Andar A, Riehle MO, Herzyk P, Wilkinson CD, Oreffo RO. The control of human mesenchymal cell differentiation using nanoscale symmetry and disorder. Nat Mater 2007;6(12):997-1003.

100. Oh S, Brammer KS, Li YS, Teng D, Engler AJ, Chien S, Jin S. Stem cell fate dictated solely by altered nanotube dimension. Proc Natl Acad Sci U S A 2009;106(7):2130-5.

101. Dalby MJ, McCloy D, Robertson M, Wilkinson CD, Oreffo RO. Osteoprogenitor response to defined topographies with nanoscale depths. Biomaterials 2006;27(8):1306-15.

102. Huang J, Grater SV, Corbellini F, Rinck S, Bock E, Kemkemer R, Kessler H, Ding J, Spatz JP. Impact of order and disorder in RGD nanopatterns on cell adhesion. Nano Lett 2009;9:1111–6.

103. Ranzinger J, Krippner-Heidenreich A, Haraszti T, Bock E, Tepperink J, Spatz JP, Scheurich P. Nanoscale arrangement of apoptotic ligands reveals a demand for a minimal lateral distance for efficient death receptor activation. Nano Lett 2009;9:4240-5.

104. Janmey PA, McCulloch CA. Cell mechanics: integrating cell responses to mechanical stimuli. Annu Rev Biomed Eng 2007;9:1-34.

105. Chen W, Villa-Diaz LG, Sun Y, Weng S, Kim JK, Lam RH, Han L, Fan R, Krebsbach PH, Fu J. Nanotopography influences adhesion, spreading, and self-renewal of human embryonic stem cells. ACS Nano 2012;6(5):4094-103.

106. McBeath R, Pirone DM, Nelson CM, Bhadriraju K, Chen CS. Cell shape, cytoskeletal tension, and RhoA regulate stem cell lineage commitment. Dev Cell 2004;6(4):483-95.

107. Gao L, McBeath R, Chen CS. Stem cell shape regulates a chondrogenic versus myogenic fate through Rac1 and N-cadherin. Stem Cells 2010;28(3):564-72.

108. Brammer KS, Oh S, Cobb CJ, Bjursten LM, van der Heyde H, Jin S. Improved bone-forming functionality on diameter-controlled TiO(2) nanotube surface. Acta Biomater 2009;5(8):3215-23.

109. Dalby MJ, Gadegaard N, Tare R, Andar A, Riehle MO, Herzyk P, Wilkinson CD, Oreffo RO. The control of human mesenchymal cell differentiation using nanoscale symmetry and disorder. Nat Mater 2007;6(12):997-1003.

110. Kurpinski K, Chu J, Hashi C, Li S. Anisotropic mechanosensing by mesenchymal stem cells. Proc Natl Acad Sci U S A 2006;103(44):16095-100.

111. Zouani OF, Chanseau C, Brouillaud B, Bareille R, Deliane F, Foulc MP, Mehdi A, Durrieu MC. Altered nanofeature size dictates stem cell differentiation. J Cell Sci 2012;125(Pt 5):1217-24.

112. Engler AJ, Sen S, Sweeney HL, Discher DE. Matrix elasticity directs stem cell lineage specification. Cell 2006;126(4):677-89.

113. Murphy CM, Matsiko A, Haugh MG, Gleeson JP, O'Brien FJ. Mesenchymal stem cell fate is regulated by the composition and mechanical properties of collagen-glycosaminoglycan scaffolds. J Mech Behav Biomed Mater 2012;11:53-62.

114. Banerjee A, Arha M, Choudhary S, Ashton RS, Bhatia SR, Schaffer DV, Kane RS. The influence of hydrogel modulus on the proliferation and differentiation of encapsulated neural stem cells. Biomaterials 2009;30(27):4695-9.

115. Janmey PA, McCulloch CA. Cell mechanics: integrating cell responses to mechanical stimuli. Annu Rev Biomed Eng 2007;9:1-34.

116. Chen W, Villa-Diaz LG, Sun Y, Weng S, Kim JK, Lam RH, Han L, Fan R, Krebsbach PH, Fu J. Nanotopography influences adhesion, spreading, and self-renewal of human embryonic stem cells. ACS Nano 2012;6(5):4094-103.

117. Harrison RG. On the Stereotropism of Embryonic Cells. Science 1911;34(870):279-81.

118. Brauker JH, Carr-Brendel VE, Martinson LA, Crudele J, Johnston WD, Johnson RC. Neovascularization of synthetic membranes directed by membrane microarchitecture. J Biomed Mater Res 1995;29(12):1517-24.

119. Klawitter JJ, Hulbert SF. Application of porous ceramics for the attachment of load-bearing internal orthopedic. Applications. J Biomed Mate Res A Symposium 1971;(2):161-8.

120. Yang S, Leong KF, Du Z, Chua CK. The design of scaffolds for use in tissue engineering. Part I. Traditional factors. Tissue Eng 2001;7(6):679-89.

121. Whang K, Healy KE, Elenz DR, Nam EK, Tsai DC, Thomas CH, Nuber GW, Glorieux FH, Travers R, Sprague SM. Engineering bone regeneration with bioabsorbable scaffolds with novel microarchitecture. Tissue Eng 1999;5(1):35-51.

122. Yannas IV, Lee E, Orgill DP, Skrabut EM, Murphy GF. Synthesis and characterization of a model extracellular matrix that induces partial regeneration of adult mammalian skin. Proc Natl Acad Sci U S A 1989;86(3):933-7.

123. Salgado AJ, Coutinho OP, Reis RL. Bone tissue engineering: state of the art and future trends. Macromol Biosci 2004;4(8):743-65.

124. Webster TJ. Transitioning from Nanomedicine to Picomedicine: What's on the Horizon? Annual meeting; 38th, Society for Biomaterials; annual meeting and exposition 2014: pioneering the future of biomaterials 2014;36:101.

125. Alpaslan E, Webster TJ. Nanotechnology and picotechnology to increase tissue growth: a summary of in vivo studies. Int J Nanomedicine 2014;9(Suppl 1):7-12.

126. Linsenmayer TF. What is extracellular matrix? In: Hay ED. Cell biology of extracellular matrix 2nd ed. New York: Plenum Press, 1991. p. 7-40.

127. Elsdale T, Bard J. Collagen substrata for studies on cell behavior. J Cell Biol 1972;54:626-37.

128. Ma Z, Kotaki M, Inai R, Ramakrishna S. Potential of nanofiber matrix as tissue-engineering scaffolds. Tissue Eng 2005;11(1-2):101-9.

129. Woo KM, Chen VJ, Ma PX. Nano-fibrous scaffolding architecture selectively enhances protein adsorption contributing to cell attachment. J Biomed Mater Res A 2003;67(2):531-7.

130. Chen VJ, Smith LA, Ma PX. Bone regeneration on computer-designed nano-fibrous scaffolds. Biomaterials 2006;27(21):3973-9.

131. Xiao G, Wang D, Benson MD, Karsenty G, Franceschi RT. Role of the alpha2-integrin in osteoblast-specific gene expression and activation of the Osf2 transcription factor. J Biol Chem 1998;273(49):32988-94.

132. Mizuno M, Fujisawa R, Kuboki Y. Type I collagen-induced osteoblastic differentiation of bone-marrow cells mediated by collagen-alpha2beta1 integrin interaction. J Cell Physiol 2000;184(2):207-13.

133. Woo KM, Jun JH, Chen VJ, Seo J, Baek JH, Ryoo HM, Kim GS, Somerman MJ, Ma PX. Nano-fibrous scaffolding promotes osteoblast differentiation and biomineralization. Biomaterials 2007;28(2):335-43.

134. Morton, WJ. Method of Dispersing Fluids. US patent No. 705691, 1902.

135. Formhals, A. Process and apparatus for preparing artificial threads. US Patent No. 1975504, 1934.

136. Dvir T, Timko BP, Kohane DS, Langer R. Nanotechnological strategies for engineering complex tissues. Nat Nanotechnol 2011;6(1):13-22.

137. Hartgerink JD, Beniash E, Stupp SI. Peptide-amphiphile nanofibers: a versatile scaffold for the preparation of self-assembling materials. Proc Natl Acad Sci U S A 2002;99(8):5133-8.

138. Ma PX. Tissue Engineering. In: Mark HF, Kroschwitz JI. Encyclopedia of Polymer Science and Technology 3rd ed. John Wiley & Sons, Inc., 2005. p. 261-291.

139. Zhang R, Ma PX. Synthetic nano-fibrillar extracellular matrices with predesigned macroporous architectures. J Biomed Mater Res 2000;52:430-8.

140. Ma PX, Choi JW. Biodegradable polymer scaffolds with well-defined interconnected spherical pore network. Tissue Eng 2001;7:23-33.

141. Pashuck ET, Stevens MM. Designing Regenerative Biomaterial Therapies for the Clinic. Sci Transl Med 2012;4(160):160sr4.

142. Ruoslahti E, Pierschbacher MD. Arg-Gly-Asp: a versatile cell recognition signal. Cell 1986;44(4):517-8.

143. Kasemo B. Biological surface science. Surf Sci 2002;500:656-77.

144. Vogler EA. Structure and reactivity of water at biomaterial surfaces. Adv Colloid Interface Sci 1998;74:69-117.

145. Lee JH, Khang G, Lee JW, Lee HB. Platelet adhesion onto chargeable functional group gradient surfaces. J Biomed Mater Res 1998;40(2):180-6.

146. Elbert DL, Hubbell JA. Surface treatments of polymers for biocompatibility. Annu Rev Mater Sci 1996;26:365-94.

147. Ma Z, Mao Z, Gao C. Surface modification and property analysis of biomedical polymers used for tissue engineering. Colloids Surf B Biointerfaces 2007;60(2):137-57.

148. van Wachem PB, Beugeling T, Feijen J, Bantjes A, Detmers JP, van Aken WG. Interaction of cultured human endothelial cells with polymeric surfaces of different wettabilities. Biomaterials 1985;6(6):403-8.

149. van Wachem PB, Hogt AH, Beugeling T, Feijen J, Bantjes A, Detmers JP, van Aken WG. Adhesion of cultured human endothelial cells onto methacrylate polymers with varying surface wettability and charge. Biomaterials 1987;8(5):323-8.

150. Arima Y, Iwata H. Effect of wettability and surface functional groups on protein adsorption and cell adhesion using well-defined mixed self-assembled monolayers. Biomaterials 2007;28(20):3074-82.

151. Benoit DS, Schwartz MP, Durney AR, Anseth KS. Small functional groups for controlled differentiation of hydrogel-encapsulated human mesenchymal stem cells. Nat Mater 2008;7(10):816-23.

152. Phillips JE, Petrie TA, Creighton FP, García AJ. Human mesenchymal stem cell differentiation on self-assembled monolayers presenting different surface chemistries. Acta Biomater 2010;6(1):12-20.

153. Curran JM, Chen R, Hunt JA. The guidance of human mesenchymal stem cell differentiation in vitro by controlled modifications to the cell substrate. Biomaterials 2006;27(27):4783-93.

154. Fernandes H, Moroni L, van Blitterswijka C, de Boer J. Extracellular matrix and tissue engineering applications. J Mater Chem 2009;19:5474-84.

155. Hersel U, Dahmen C, Kessler H. RGD modified polymers: biomaterials for stimulated cell adhesion and beyond. Biomaterials 2003;24:4385-415.

156. Iuliano DJ, Saavedra SS, Truskey GA. Effect of the conformation and orientation of adsorbed fibronectin on endothelial cell spreading and the strength of adhesion. J Biomed Mater Res 1993;27(8):1103-13.

157. Hlady VV, Buijs J. Protein adsorption on solid surfaces. Curr Opin Biotechnol 1996;7(1):72-7.

158. Langer R, Tirrell DA. Designing materials for biology and medicine. Nature 2004;428(6982):487-92.

159. Collier JH, Segura T. Evolving the use of peptides as components of biomaterials. Biomaterials 2011;32(18):4205-10.

160. Bellis SL. Advantages of RGD peptides for directing cell association with biomaterials. Biomaterials 2011;32:4205-10.

161. Pierschbacher MD, Ruoslahti E. Cell attachment activity of fibronectin can be duplicated by small synthetic fragments of the molecule. Nature 1984;309(5963):30-3.

162. Delaittre G, Greiner AM, Pauloehrl T, Bastmeyer M, Barner-Kowollik C. Chemical approaches to synthetic polymer surface biofunctionalization for targeted cell adhesion using small binding motifs. Soft Matter 2012;8:7323-47.

163. Aucoin L, Griffith CM, Pleizier G, Deslandes Y, Sheardown H. Interactions of corneal epithelial cells and surfaces modified with cell adhesion peptide combinations. J Biomater Sci Polym Ed 2002;13(4):447-62.

164. Hynes RO. The extracellular matrix: not just pretty fibrils. Science 2009;326(5957):1216-9.

165. Yamashita H, Goto C, Tajima R, Koparal AT, Kobori M, Ohki Y, Shitara K, Narita R, Toriyama K, Torii S, Niimi T, Kitagawa Y. Cryptic fragment alpha4 LG4-5 derived from laminin alpha4 chain inhibits de novo adipogenesis by modulating the effect of fibroblast growth factor-2. Dev Growth Differ 2008;50(2):97-107.

166. Klotzsch E, Smith ML, Kubow KE, Muntwyler S, Little WC, Beyeler F, Gourdon D, Nelson BJ, Vogel V. Fibronectin forms the most extensible biological fibers displaying switchable force-exposed cryptic binding sites. Proc Natl Acad Sci U S A 2009;106(43):18267-72.

167. Ruoslahti E. RGD and other recognition sequences for integrins. Annu Rev Cell Dev Biol 1996;12:697-715.

168. Shin H, Jo S, Mikos AG. Biomimetic materials for tissue engineering. Biomaterials 2003;24(24):4353-64.

169. RGD modified polymers: biomaterials for stimulated cell adhesion and beyond Ulrich Hersel Biomaterials 24 (2003) 4385–4415.

170. Gomes S, Leonor IB, Mano JF, Reis RL, Kaplan DL. Natural and Genetically Engineered Proteins for Tissue Engineering. Prog Polym Sci 2012;37(1):1-17.

171. Kyle S, Aggeli A, Ingham E, McPherson MJ. Production of self-assembling biomaterials for tissue engineering. Trends Biotechnol 2009;27(7):423-33.

172. Almine JF, Bax DV, Mithieux SM, Nivison-Smith L, Rnjak J, Waterhouse A, Wise SG, Weiss AS. Elastin-based materials. Chem Soc Rev 2010;39(9):3371-9.

173. Rodríguez-Cabello JC, Martín L, Alonso M, Arias FJ, Testera AM. "Recombinamers" as advanced materials for the post-oil age. Polymer 2009;50:5159-69.

174. Girotti A, Reguera J, Rodríguez-Cabello JC, Arias FJ, Alonso M, Matestera A. Design and bioproduction of a recombinant multi(bio)functional elastin-like protein polymer containing cell adhesion sequences for tissue engineering purposes. J Mater Sci Mater Med 2004;15(4):479-84.

175. Prieto S, Shkilnyy A, Rumplasch C, Ribeiro A, Arias FJ, Rodríguez-Cabello JC, Taubert A. Biomimetic calcium phosphate mineralization with multifunctional elastin-like recombinamers. Biomacromolecules 2011;12(5):1480-6.

176. Lee K, Silva EA, Mooney DJ. Growth factor delivery-based tissue engineering: general approaches and a review of recent developments. J R Soc Interface 2011;8(55):153-70.

177. King WJ, Krebsbach PH. Growth factor delivery: how surface interactions modulate release in vitro and in vivo. Adv Drug Deliv Rev 2012;64(12):1239-56.

178. Cross M, Dexter TM. Growth factors in development, transformation, and tumorigenesis. Cell 1991;64(2):271-80.

179. Russo L, Russo T, Battocchio C, Taraballi F, Gloria A, D'Amora U, De Santis R, Polzonetti G, Nicotra F, Ambrosio L, Cipolla L. Galactose grafting on poly(ε -caprolactone) substrates for tissue engineering: a preliminary study. Carbohydr Res 2015;405:39-46.

180. Hoffmann J, Paul A, Harwardt M, Groll J, Reeswinkel T, Klee D, Moeller M, Fischer H, Walker T, Greiner T, Ziemer G, Wendel HP. Immobilized DNA aptamers used as potent attractors for porcine endothelial precursor cells. J Biomed Mater Res A 2008;84(3):614-21.

181. Goddard JM, Hotchkiss JH. Polymer surface modification for the attachment of bioactive compounds. Prog Polym Sci 2007;32:698-725.

182. Hermanson GT. Bioconjugate Techniques 2nd ed. Academic Press, 2008.

183. Maheshwari G, Brown G, Lauffenburger DA, Wells A, Griffith LG. Cell adhesion and motility depend on nanoscale RGD clustering. J Cell Sci 2000;113(Pt 10):1677-86.

184. Hudalla GA, Murphy WL. Using "click" chemistry to prepare SAM substrates to study stem cell adhesion. Langmuir 2009;25:5737-5746.

185. Beer JH, Springer KT, Coller BS. Immobilized Arg–Gly Asp (RGD) peptides of varying lengths as structural probes of the platelet glycoprotein IIb/IIIa receptor. Blood 1992;79:117–2.

186. Hong Y, Guan J, Fujimoto KL, Hashizume R, Pelinescu AL, Wagner WR. Tailoring the degradation kinetics of poly(ester carbonate urethane)urea thermoplastic elastomers for tissue engineering scaffolds. Biomaterials 2010;31(15):4249-58.

187. Chen QZ, Efthymiou A, Salih V, Boccaccini AR. Bioglass-derived glass-ceramic scaffolds: study of cell proliferation and scaffold degradation in vitro. J Biomed Mater Res A 2008;84(4):1049-60.

188. Lee SH, Shin H. Matrices and scaffolds for delivery of bioactive molecules in bone and cartilage tissue engineering. Adv Drug Deliv Rev 2007;59(4-5):339-59.

189. Biondi M, Ungaro F, Quaglia F, Netti PA. Controlled drug delivery in tissue engineering. Adv Drug Deliv Rev 2008;60(2):229-42.

190. Simmons CA, Alsberg E, Hsiong S, Kim WJ, Mooney DJ. Dual growth factor delivery and controlled scaffold degradation enhance in vivo bone formation by transplanted bone marrow stromal cells. Bone 2004;35(2):562-9.

191. West JL, Hubbell JA. Polymeric biomaterials with degradation sites for proteases involved in cell migration. Macromolecules 1999;32:241-4.

192. Wang M. Developing bioactive composite materials for tissue replacement. Biomaterials 2003;24(13):2133-51.

193. Bonfield W. Composites for bone replacement. J Biomed Eng 1988;10(6):522-6.

194. Pêgo AP, Poot AA, Grijpma DW, Feijen J. Biodegradable elastomeric scaffolds for soft tissue engineering. J Control Release 2003;87(1-3):69-79.

195. Li Y, Thouas GA, Chen QZ. Biodegradable soft elastomers: synthesis/properties of materials and fabrication of scaffolds. RSC Adv 2012;2:8229-42.

196. Drury JL, Mooney DJ. Hydrogels for tissue engineering: scaffold design variables and applications. Biomaterials 2003;24(24):4337-51.

197. Discher DE, Janmey P, Wang YL. Tissue cells feel and respond to the stiffness of their substrate. Science 2005;310(5751):1139-43.

198. Cameron AR, Frith JE, Cooper-White JJ. The influence of substrate creep on mesenchymal stem cell behaviour and phenotype. Biomaterials 2011;32(26):5979-93.

199. Cox TR, Erler JT. Remodeling and homeostasis of the extracellular matrix: implications for fibrotic diseases and cancer. Dis Model Mech 2011;4(2):165-78.

200. Marx KA. 2010. Smart Biomaterials and Biosensors: Intelligent Properties of Biomolecules and Cells in Hybrid Devices. Encyclopedia of Industrial Biotechnology. 1–21.

201. Holzapfel BM, Reichert JC, Schantz JT, Gbureck U, Rackwitz L, Nöth U, Jakob F, Rudert M, Groll J, Hutmacher DW. How smart do biomaterials need to be? A translational science and clinical point of view. Adv Drug Deliv Rev 2013;65(4):581-603.

202. Rosso F, Marino G, Giordano A, Barbarisi M, Parmeggiani D, Barbarisi A. Smart materials as scaffolds for tissue engineering. J Cell Physiol 2005;203(3):465-70.

203. Place ES, Evans ND, Stevens MM. Complexity in biomaterials for tissue engineering. Nat Mater 2009;8(6):457-70.

204. Schenk S, Quaranta V. Tales from the crypt[ic] sites of the extracellular matrix. Trends Cell Biol 2003;13(7):366-75.

205. Hocking DC, Sottile J, McKeown-Longo PJ. Fibronectin's III-1 module contains a conformation-dependent binding site for the amino-terminal region of fibronectin. J Biol Chem 1994;269(29):19183-7.

206. Shaub A. Unravelling the extracellular matrix. Nat Cell Biol 1999;1(7):E173-5.

207. Rosso F, Marino G, Giordano A, Barbarisi M, Parmeggiani D, Barbarisi A. Smart materials as scaffolds for tissue engineering. J Cell Physiol 2005;203(3):465-70.

208. Backer MV, Patel V, Jehning BT, Claffey KP, Backer JM. Surface immobilization of active vascular endothelial growth factor via a cysteine containing tag. Biomaterials 2006;27:5452−8.

209. Zisch AH, Schenk U, Schense JC, Sakiyama-Elbert SE, Hubbell JA. Covalently conjugated VEGF--fibrin matrices for endothelialization. J Control Release 2001;72(1-3):101-13.

210. von Degenfeld G, Banfi A, Springer ML, Wagner RA, Jacobi J, Ozawa CR, Merchant MJ, Cooke JP, Blau HM. Microenvironmental VEGF distribution is critical for stable and functional vessel growth in ischemia. FASEB J 2006;20(14):2657-9. Epub 2006 Nov 9.

211. Hao X, Silva EA, Månsson-Broberg A, Grinnemo KH, Siddiqui AJ, Dellgren G, Wärdell E, Brodin LA, Mooney DJ, Sylvén C. Angiogenic effects of sequential release of VEGF-A165 and PDGF-BB with alginate hydrogels after myocardial infarction. Cardiovasc Res 2007;75(1):178-85.

212. Gama CI, Tully SE, Sotogaku N, Clark PM, Rawat M, Vaidehi N, Goddard WA 3rd, Nishi A, Hsieh-Wilson LC. Sulfation patterns of glycosaminoglycans encode molecular recognition and activity. Nat Chem Biol 2006;2(9):467-73.

213. Sakiyama-Elbert SE, Hubbell JA. Development of fibrin derivatives for controlled release of heparin-binding growth factors. J Control Release 2000;65(3):389-402.

214. Zhang L, Furst EM, Kiick KL. Manipulation of hydrogel assembly and growth factor delivery via the use of peptide-polysaccharide interactions. J Control Release 2006;114(2):130-42.

215. Ripamonti U, Roden LC, Ferretti C, Klar RM. Biomimetic Matrices Self-Initiating the Induction of Bone Formation. J Craniofac Surg 2011;22(5):1859-70.

216. Castaño O, Sachot N, Xuriguera E, Engel E, Planell JA, Park JH, Jin GZ, Kim TH, Kim JH, Kim HW. Angiogenesis in Bone Regeneration: Tailored Calcium Release in Hybrid Fibrous Scaffolds. ACS Appl Mater Interfaces 2014;6(10):7512-22.

217. Lendlein A, Langer R. Biodegradable, elastic shape-memory polymers for potential biomedical applications. Science 2002;296(5573):1673-6.

218. Lee J, Bae YH, Sohn YS, Jeong B. Thermogelling aqueous solutions of alternating multiblock copolymers of poly(L-lactic acid) and poly(ethylene glycol). Biomacromolecules 2006;7(6):1729-34.

219. Baroli B. Hydrogels for tissue engineering and delivery of tissue-inducing substances. J Pharm Sci 2007;96:2197−223.

220. Markland P, Zhang YH, Amidon GL, Yang VC. A pH- and ionic strength-responsive polypeptide hydrogel: synthesis, characterization, and preliminary protein release studies. J Biomed Mater Res 1999;47:595-602.

221. Matsusaki M, Akashi M. Novel functional biodegradable polymer IV: pH-Sensitive controlled release of fibroblast growth factor-2 from a poly(gamma-glutamic acid)-sulfonate matrix for tissue engineering. Biomacromolecules 2005;6:3351-6.

222. Ju XJ, Xie R, Yang L, Chu LY. Biodegradable 'intelligent' materials in response to chemical stimuli for biomedical applications. Expert Opin Ther Pat 2009;19(5):683-96.

CHAPTER 3

3. BIOFUNCTIONALIZATION OF POLY(METHYL METHACRYLATE) SURFACES

The integration of implants or medical devices into the body tissues requires of good cell-material interactions. However, most polymeric materials used for these applications lacks on biological cues, which enhanced mid- and long- term implant failure due to weak integration with the surrounding tissue. Commonly used strategies for tissue-material integration focus on functionalization of surface by means of natural proteins or short peptides. However, the use of these biomolecules involves major drawbacks like immunogenic problems and oversimplification of the constructs. Here, designed elastin-like recombinamers (ELRs) are used to enhance poly(methyl methacrylate) (PMMA) surface properties and compared against the use of short peptides. In this study, cell response has been analysed for different functionalization conditions in the presence and absence of the BSA protein, which interfere on surface-cell interaction by unspecific adsorption on the interface. ELRs can induce higher rates of cell attachment and stronger cell anchorages than short peptides, being a better choice for surface functionalization.

3.1. Introduction

Poly(methyl methacrylate) PMMA was firstly used into clinics, as dental device, for the fabrication of complete denture bases [1]. Due to its biocompatible characteristics, its reliability, ease manipulation and low toxicity, the use of PMMA was extended into other different medical applications like bone cements [2], contact and intraocular lens [3], screw fixation in bone [4], skull defects reparation [5], stabilization of vertebrae in osteoporotic patients [6], intradermal fillers [7] and mandibular reconstruction [8]. Despite numerous new biomaterials have appeared on the market, the versatility and reliability of PMMA cause it to remain a popular and frequently used material [9].

For many of these applications, such as screws, mandibular reconstruction or intraocular lenses, a good cell-biomaterial interaction is paramount for the integration of the implant, the stability of the fixation on the interface or the prevention of cataracts. However, PMMA shows weak or null interactivity against tissue cells, which promotes the formation of fibrotic tissue [10,11]. The formation of fibrotic tissue around the implant is known to be one of the most common causes of implant integration failure, which compromises long term viability of the implant [11].

In order to enhance tissue-biomaterial interaction, and therefore implant integration, many strategies are used, such as modification of surface properties. A common way to improve surface properties is done through chemical surface modification, which can be obtained through the addition of functional chemical groups or bioactive molecules [12,13]. The latter option, the addition of bioactive molecules, has proved to present stronger and more specific interaction towards cells, and have been widely exploited for cell-biomaterial interaction [13]. Especially noteworthy is the use of RGD (Arginine-Glycine-Aspartic acid) amino acidic sequence, which is a peptidic sequence that has been deeply studied because of its cell adhesion properties [14].

The use of amino acidic sequences that interact with integrins (adhesive cell membrane proteins) has clearly been proved to be useful on bioengineering [14]. However, there is great discussion about which is the best way to add these biological cues onto material surfaces, through the grafting of natural proteins or short peptides [15]. Traditionally there were two main strategies for the addition of biological cues on surfaces. The first one was based on the use of natural proteins, and the second one was based on the use of simplified artificial versions, this is, short peptides. Both strategies present advantages and disadvantages and there is no consensus of which is the best solution. For instance, the use of natural proteins is useful because allows the

incorporation of the full potential of the protein. Normally, natural proteins on its native form present synergistic sequences that trigger stronger cell response in a more specific and complex manner. However, natural proteins may present immunogenic problems, purification limitations, batch to batch variations and low functionalization control. Instead, short peptides are non-immunogenic, easier to purify, synthetized in a reproducible manner, and can be grafted in a controlled manner. Short peptides, however, are normally oversimplified constructs, with lower cell specificity, less effectiveness, weaker stability and cannot encode complex functionalities [16].

As an alternative, a third strategy appeared which is based on the use of recombinant proteins that were synthetized in order to gather the advantages of both previous systems, and avoid the major drawbacks [17]. Thus, recombinant proteins, obtained through biotechnological tools, started to gain interest. The study of these novel molecules raised high expectations because not only can be design to be non-immunogenic, and include tailored bioactive motifs, but they also can be design to perform complex activities [18,19]. In such a way, more stable, complex and easy-to-purify constructs can be obtained through smart designs.

A strategy to design these engineered proteins is based on the mimicry of natural proteins. Elastin-like recombinamers (ELRs) are a kind of synthetic biopolymers built from the combination of different modules derived from the natural protein elastin, which confer to the final construct the desired structural and functional properties [20]. ELRs are normally built using the VPGIG amino acidic building block, which mimics the natural non-immunogenic pentapeptide VPGVG from the natural elastin protein [21]. This pentapeptide confers to the synthetic construct the elastic properties of elastin, and can be modified to include other capabilities like cross-linking sites. Moreover, other modular sequences, like the integrin-recognized RGD sequence, can be introduced inside the construct to confer to this protein biological functionality [22]. ELRs are also interesting because they can be codified into synthetic genes in order to be expressed in Escherichia coli in large quantities, with great control on the amino acid sequence and the molecular weight, and can be easily purified through their inverse temperature transition properties as well.

On this chapter, the functionalization of model PMMA surfaces with ELRs is studied and compared with the use of short peptides and natural protein (fibronectin). The objective of the chapter is to explore the functionalization procedure of PMMA and analyse and detect the best functionalization strategy in terms of cell-biomaterial interaction, so it can be translated to the final device in order to improve the interface integration. Surface characterization results and in

vitro studies show that the highest cellular attachment efficiency is found on ELR functionalized PMMA surfaces.

3.2. Materials and Methods

3.2.1. Materials

Poly(methyl methacrylate) (PMMA, Acryl) was purchased from GoodFellow (Spain). Short peptides were purchased from Genscript (USA). Peptides were designed with an integrin ligand (RGDS) and a six-glycine tail in the amino end, to allow accessibility. A control peptide was designed with a scrambled sequence (RGE). Peptides were labelled G_6RGDS and G_6RGE respectively. They were received desalted and lyophilized.

Elastin-like recombinants (ELRs) were synthesized following already optimized protocols [23]. In short, ELRs were obtained from the expression of the ELRs recombinant gene inserted in an Escherichia coli strain BLR (DE3). Gene expression was induced in a 12L Applikon fermenter, in Terrific Broth (TB) medium with 0.1% of carbenicilin and 0.1% of glucose, under controlled conditions of temperature (37ºC) and pH (7.00). After fermentation, the culture was harvested by centrifugation, resuspended and lysed by ultrasonic disruption. Solid debris was separated by centrifugation. The lysate was subjected to several cycles of cold and warm centrifugations of 4 and 40ºC, respectively. All purifications steps were carried out in a 0.5M sodium chloride solution. The polymer solution was frozen at -24ºC and lyophilized.

An ELR with an RGD sequence ($HRGD_6$) and a control ELR without a RGD sequence (IK_{24}) were designed with the following sequences:

$HRGD_6$: MGSSHHHHHSSGLVPRGSHMESLLP[[(VPGIG)$_2$(VPGKG)(VPGIG)$_2$]$_2$AVTGRGD SPASS[(VPGIG)$_2$(VPGKG)(VPGIG)$_2$]$_2$]$_6$.

IK_{24}: MESLLP (VPGIG VPGIG VPGKG VPGIG VPGIG)$_{24}$.

VPGIG modules were substituted by VPGKG modules in order to introduce lysine residues (K) in the biomolecule sequence, to further be used to covalently attach the polypeptide to the surface.

All other chemicals were purchased from Sigma-Aldrich and used without further purification.

3.2.2. Poly(methyl methacrylate) Films Preparation

PMMA films were obtained by solvent casting. Briefly, PMMA was dissolved in $CHCl_3$ (2.5% w/v) and was poured into propylene well plates. The solvent was allowed to evaporate for 3 days in a solvent-saturated atmosphere. After this time, the obtained films were stored in vacuum and dry atmosphere until their use.

3.2.3. Surface Functionalization

Chemical surface composition was changed by means of covalent functionalization with different molecules. The functionalization protocol is composed of three steps. During the first step (surface pre-activation), the films were treated with sodium hydroxide (NaOH) 0.5M for 16h and carboxyl groups were obtained on the surface due to the hydrolytic cleavage of the ester bonds of the PMMA substrate. Before moving to the second step, films were gently washed with water. Then, films were activated with 1-Ethyl-3-(3-dimethylaminopropyl)carbodiimide and N-hydroxysuccinimide (EDC and NHS) 0.1/0.2M in phosphate-buffered saline (PBS) (pH 7.4). The time for the activation step was set to 1 hour, since the average time-life of the activated NHS molecule was found to be 1 hour in neutral aqueous solution [24]. When the surface activation was finished, films were washed twice with PBS. Finally, the biomolecules were functionalized using their amino-groups to create the covalent bond. This step was carried out overnight in PBS solution at 100 μg/ml. Finally, functionalized films were washed again with water and vacuum sealed until their use.

Parallel to this, model PMMA surfaces were functionalized with ELRs by physisorption. For that purpose, surfaces were simply soaked overnight with a solution of the desired biomolecule in PBS at 100 μg/ml. These surfaces were used in the comparative studies in order to analyse the role of the covalent bonding for the molecule stability as well as for the cellular response.

3.2.4. Contact Angle

Chemical surface composition affects the physical surface properties. For that reason, the hydrophobicity of PMMA surface was expected to change with each treatment step. Contact angle is a technique sensitive to substrate hydrophobicity that allows a fast qualitative analysis. In order to see the changes induced by reactions, PMMA thin films were analysed by the sessile drop method using a goniometer (OCA 15+, Dataphysics, Germany).

3.2.5. Time of Flight-Secondary Ion Mass Spectroscopy

Time of Flight-Secondary Ion Mass Spectroscopy (TOF-SIMS) was used as a complementary technique to analyse the chemical surface changes. TOF-SIMS (TOF-SIMS IV, Ion Tof) is a very sensitive technique used to detect components on the surface. In this study, nitrogenated components coming from the addition of biological molecules were analysed.

3.2.6. Surface Activation Test

The presence of activated sites was analysed using an ELISA assay following the manufacturer protocol. In short, surfaces were covalently functionalized with different ratios of Glycine (Sigma) and Amine-PEG biotinylated molecules (Pierce Protein Biology Products) using the previously described protocol. Then, functionalized surfaces were treated with blocking buffer [PBS + Tween20 0.05% (v/v) + BSA 2% (w/v)] during 1 hour at room temperature in order to block non-functionalized areas. Afterwards, the surfaces were washed three times with washing buffer [PBS + Tween20 0.05% (v/v)]. Next, a Streptavidin-HRP (Pierce Protein Biology Products) solution in blocking buffer was added and allowed to interact with the PEG-biotinylated molecules for 1 hour. Finally, the surfaces were washed six times with washing buffer, and ABTS (2,2'-Azinobis [3-ethylbenzothiazoline-6-sulfonic acid]-diammonium salt) (Pierce Protein Biology Products) substrate was incubated for 5-30 minutes. Obtained green product was measured by spectroscopy at 410 nm or 650 nm.

3.2.7. Mesenchymal Stromal Cells Culture

Rat mesenchymal stromal cells (rMSC) were extracted from bone marrow [25] and used at passages 4-6. Cells were expanded in Advanced DMEM medium supplemented with 15% fetal bovine serum (FBS), 1% Penicillin/Streptomycin and 1% L-Glutamine (A-DMEM). Cells were allowed to grow until ~80% confluence before passaging.

3.2.8. In Vitro Cell Adhesion Studies

For the cell attachment study, solvent casted films on 24-well plates were functionalized as previously described. Well plates were sterilized with ethanol 70% (v/v) and UV light. Then, plates were left in a sterile hood until they were dry. Afterwards, the wells were washed with PBS (pH 7.4) three times and, for some conditions, samples were blocked with a PBS (pH 7.4) + BSA 6% solution for 1 hour and washed again with PBS (pH 7.4). rMSC were expanded and collected. 10,000 cells were seeded per well (~5300 cells/cm^2) in serum free Advanced DMEM medium and cultured during 4 hours. Then, non-attached cells were removed with two PBS

washings steps. To evaluate the number of attached cells, a set of cultured well plates were treated with lysis buffer (PBS pH 7.4 + Triton X-100 0.01% (v/v). The cell lysate was analysed with Cytotoxicity Detection KitPLUS (LDH) (Roche) and cell number was obtained following the commercial protocol. To observe the cell morphology, a set of cultured well plates was treated with paraformaldehyde 6% to fix cells after 4 hours of incubation. Then, the cytoskeleton was stained with Rhodamine-Phalloidin (red), the nuclei with DAPI (blue) and the focal points with monoclonal anti-Vinculin antibody/Alexa Fluor® 488 goat anti-mouse IgG system (green). Fluorescence was observed with an Eclipse600 upright microscope (Nikon).

The aspect ratio (AR) and cell area were calculated from the fluorescence images. AR was defined as the relation between the major axis and the minor axis of the smallest ellipse that can fit the cell area and was obtained, like cell area values, through the processing of the images with the ImageJ software [22,26].

3.2.9. Statistics

Experiments were subjected to t-Student testing ($P < 0.05$). Results were presented as mean ± standard deviation. For population distributions, values were presented in box-plot format. In these cases, central boxes represented the 2nd and 3rd population quartiles (50 % of the population distribution) and bars represented the 1st and 4th population quartiles (50 % of the population distribution), indicating the minimum and maximum values of the distribution. In all distributions, the plotted population represented the 95% of the real measured events in order to not include extremely deviated results.

3.3. Results

3.3.1. Contac Angle

PMMA Wettability was evaluated at the different procedure steps in order to evaluate the effect of surface chemical changes (Table 7).

Results showed a first wettability increment with the incorporation of NHS molecule, and a second increment with the covalently functionalization of ELRs. Instead, the functionalization of bioactive molecules by physisorption left to same hydrophobic surface than non-treated surfaces.

Table 7. Contact angle of different treated PMMA surfaces

Treatment	Contact angle ± SD
PMMA non-treated	85.8º ±1.7
PMMA hydrolysed	82.5º ±1.3
PMMA activated (NHS)	77.4º ±0.9
PMMA $HRGD_6$ covalent	73.9º ±1.3
PMMA IK_{24} covalent	72.9º ±2.7
PMMA $HRGD_6$ physisorbed	88.3º ±2.5

3.3.2. Time of Flight-Secondary Ion Mass Spectroscopy

In order to validate the covalent functionalization of grafted molecules, the incorporation of nitrogen component into the surfaces was studied by means of TOF-SIMS analysis. Thus, non-treated surfaces, activated surfaces (with grafted NHS molecule), and functionalized surfaces (with short-peptide molecules) were studied (Figure 11). Only short peptides were used on this study because of their weak physisorbed retention on surface, which ensured complete cleaning of non-cross-linked molecules. Thus, incorporation of nitrogen component could be correlated to covalent bonding with more feasibility.

TOF-SIMS negative spectra showed the apparition of nitrogenised components on activated and functionalized samples but not on non-treated PMMA. Spectra showed new peaks on values associated to CN mass component (26 u) and CNO mass component (42 u).

3.3.3. Surface Activation Test

In order to evaluate grafting in a semi-quantitative manner, an ELISA assay was performed. In this case three different samples were evaluated: a covalently functionalized surface, a physisorbed surface without the NaOH treatment step, and a physisorbed surface with the NaOH treatment (Figure 12). Detection of molecular surface grafting was done for a PEG-biotin molecule, which was used as an analogue of a short peptide. Moreover, all samples were functionalized with different ratios of PEG-biotin/Glycine mixtures. The use of different molecular ratios was used to observe different amounts of PEG-b molecule grafted on different treated surfaces and ensure in such a way that the analysis was done inside the technique-sensitive region. Thus, it was possible to ensure that measured values were not given by a saturation signal and they could be compared between them in a semi-quantitatively manner. The physisorbed sample with pre-activation treatment was included to ensure that PEG-b reporter did not adsorb due to ionic forces.

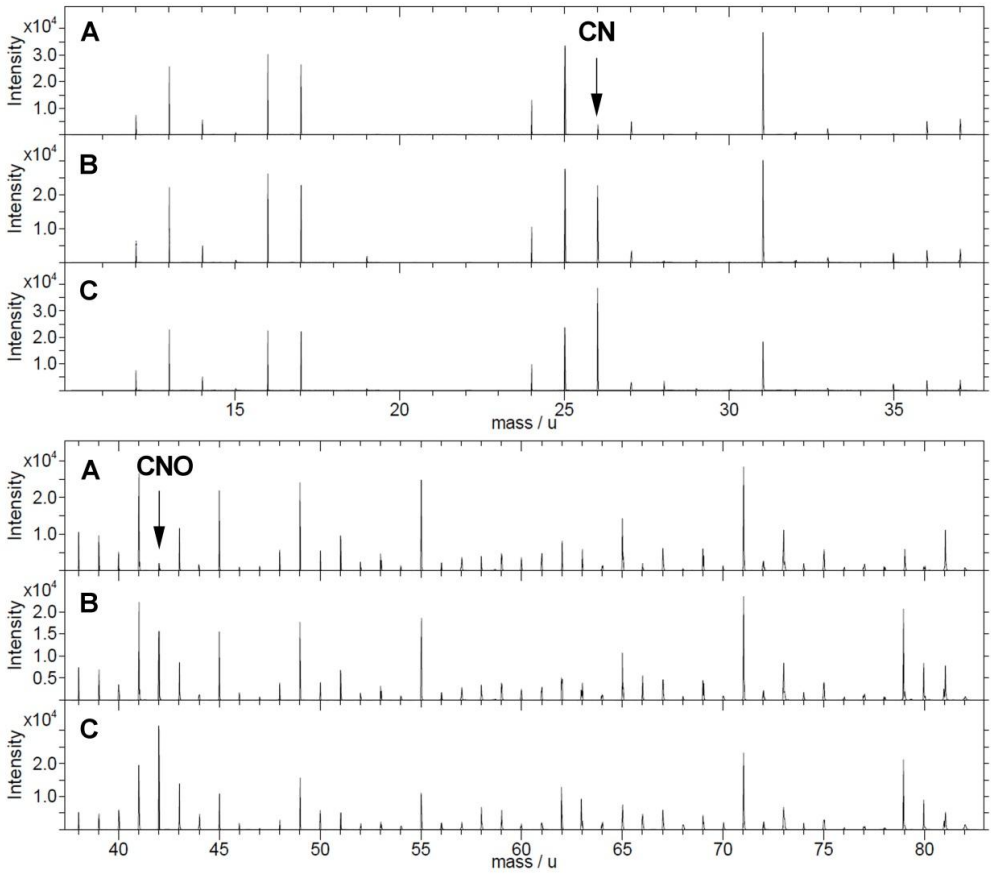

Figure 11. TOF-SIMS negative spectra of (A) non-treated PMMA surface, (B) NHS activated PMMA surface, (C) short peptide functionalized surface.

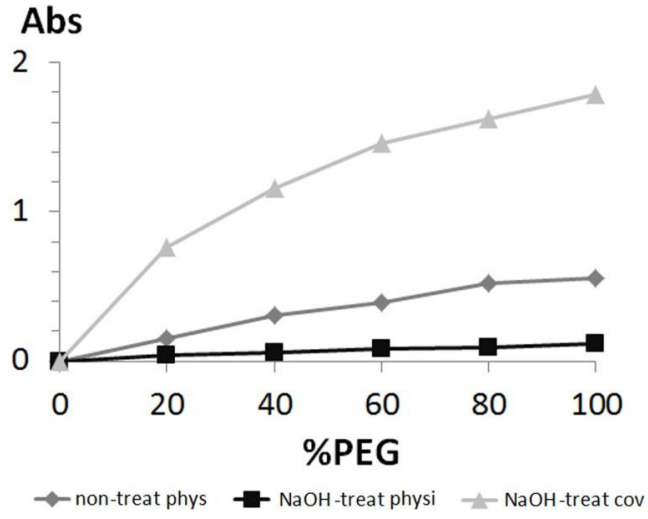

Figure 12. Absorbance levels for measured amounts of grafted PEG-b molecule under different conditions: non-treated PMMA surface by physisorption, 24h NaOH treated PMMA surface by physisorption and 24h NaOH treated PMMA surface by covalent ligation.

In Figure 12, it is shown that covalently functionalized samples presented higher levels of PEG-biotin reporter (3-fold times compared to physisorbed surfaces without pre-treatment step). Moreover, no signal was found on physisorbed samples with NaOH pre-treatment. Some unspecific adsorption of PEG-b reporter was found on physisorbed samples without NaOH pre-treatment, which revealed that week, but still existing, physisorbed functionalization occurred. Instead, PEG-b levels were almost zero for physisorption grafting on pre-treated samples.

3.3.4. In Vitro Cell Adhesion Studies

For the evaluation of cell attachment on PMMA surfaces, different conditions were tested. On one hand, non-treated PMMA (no treat) and BSA-blocked PMMA (BSA) were used as negative controls, while tissue culture polystyrene plate (TCP) and fibronectin-functionalized PMMA (Fn) were used as positive control. On the other hand, PMMA surfaces grafted with ELRs ($HRGD_6$) and short peptides (G_6RGDS), as well as PMMA surfaces grafted with their homologous without the RGD sequence (IK_{24} and G_6RGE), were used to analyse the role of the RGD and the role of the biomolecule nature in a comparative manner. Similarly, functionalized surfaces with same molecules but functionalized by physisorption were used to study the role of the grafting process. Moreover, covalent and physisorbed functionalized surfaces were studied as well under the effect of a BSA-blocking step before cell seeding, in order to evaluate the non-fouling properties of functionalized surfaces.

In order to evaluate short cell response, cell adhesion was quantified by measuring the number of attached cells after 4h of seeding. Comparison of different samples was done using TCP sample as reference, against which all other samples were normalized (Figure 13).

The adhesion study showed that functionalized PMMA samples enhanced cell adhesion far beyond positive controls. Indeed, $HRGD_6$ functionalized samples presented up to 100-150% more adhered cells than TCP control.

This adhesion study showed the effect of three different factors on cell attachment response. The first factor was the presence or absence of RGD sequence, which positively impacted on the number of adhered cells. Indeed, molecules with encoded RGD sequences ($HRGD_6$ and G_6RGDS) presented more cell adhesion levels than their homologues without the RGD motif (IK_{24} and G_6RGE). These differences between RGD-containing molecules and RGD-lacking molecules were increased on samples blocked with BSA.

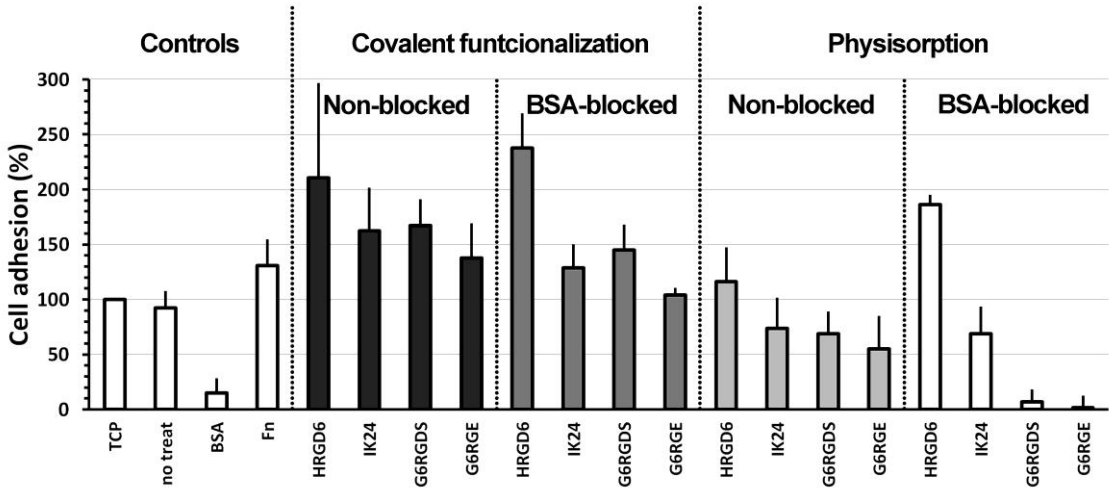

Figure 13. Adhesion assay performed on surfaces functionalized under different conditions. Cell number was calculated from LDH activity and normalized against positive control TCP. Error bars represented standard deviation.

The second factor was the nature of the functionalized molecule. Indeed, the use of ELRs presented larger adhered cell numbers compared to short peptides. More precisely, covalently functionalized $HRGD_6$ samples presented between 50 and 80% more adhered cells than covalently functionalized G_6RGDS samples, while physisorbed $HRGD_6$ samples presented between 50 and 180% more adhered cells than physisorbed G_6RGDS samples. Also, results showed that the presence of BSA on the medium affected in a stronger manner the short peptide functionalized surfaces, while had little or no effect on ELRs functionalized surfaces.

The third factor was the effect of the covalent grafting, this is, the grafting stability. In general, when comparing same functionalization conditions, moving from covalently functionalized to physisorption, decrease the amount of adhered cells on surface (between a 50% and a 100% difference). Indeed, most covalently functionalized surfaces presented amounts of adhered cells above TCP control, while only $HRGD_6$ physisorbed surfaces were above the TCP control levels. The other physisorbed surfaces (IK_{24} and short peptides) presented lower amounts of adhered cells than TCP. This effect was found to be stronger on peptidic functionalized surfaces.

The effect of covalent bond was also noticed with the introduction of BSA protein, which competed with adhered molecules for the unspecific adsorption on surface. In this case, the presence of covalent bond enhanced the amount of adhered cells between a 50% and a 100% more, depending on the functionalization conditions. Also it was observed that the presence of

covalent bonding was critical for the short peptide engraftment, since almost no cellular adhesion was found on physisorbed short peptides with blocking-BSA.

Cell adhesion strength was also evaluated by means of cell morphology. Thus, the cell shape was observed by fluorescence microscopy and classified using quantitative shape descriptors. During cell morphology studies, surfaces with physisorbed short peptides were not considered, since they presented not enough adhered cells for the statistic study. Then, AR was calculated from fluorescence images and median values represented on Table 8. Median values were represented instead of average values because population was distributed on a non-Gaussian shape.

Table 8. Aspect Ratio of cells seeded on different functionalized samples.

	Controls			Physisorbed		Covalent			
	No treat	Fn	TCP	$HRGD_6$	IK_{24}	$HRGD_6$	IK_{24}	G_6RGDS	G_6RGE
BSA-blocked PMMA	1.27	1.61	1.47	1.53	1.29	1.54	1.54	1.49	1.47
Non-blocked PMMA	1.35	1.49	1.47	1.69	1.41	1.56	1.51	1.45	1.36

Considering the results, values placed between 1.27 and 1.35 (negative controls) were used to define round and small shape (poor cell adhesion state). Instead, values placed between 1.47 and 1.61 (positive controls), were used to define elongated cell shape (advanced cell adhesion state). Other values found in between these two frames represented intermediate adhesion states. Using this scale, it was possible to see that in general, covalent functionalization presented the most advanced cell adhesion states after 4h of seeding, together with physisorbed $HRGD_6$ samples. Instead, surfaces with physisorbed IK_{24} and short peptides showed, in general, an intermediated cell adhesion state, or a poor adhesion state (star-like or round cell shapes, respectively).

To complement cell morphology study, spread cell area was analysed from different sets of fluorescence micrographies. Results were presented in a box-plot graph in order to clearly picture the distribution of cell population (Figure 14).

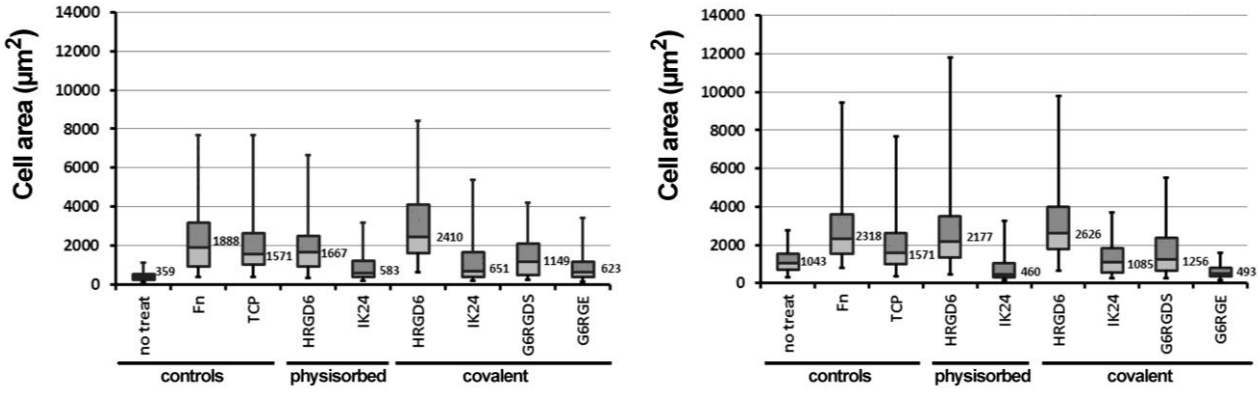

Figure 14. Box-plot graph of cell area distribution for different treated samples. The square boxes represented the second and third quartile of the distribution (50% of the population) and the bars represented the first and fourth quartile of the distribution (the remaining 50% of the population). Bars indicated the maximum and minimum values found on distribution. The 0.25% of the population found on both extremes of the distribution was excluded from the graph. The same TCP positive control (without blocking with BSA) was used on both graphs. Numerical values shown on each condition represented the median values of the distribution.

Cell spread area results showed that larger areas were found on RGD-containing ELRs ($HRGD_6$) functionalized surfaces, especially on covalently functionalized surfaces, which presented larger cell areas than positive controls. Instead, short peptides and IK_{24} functionalized surfaces presented smaller cell areas, which represented a weaker cell attachment. Interestingly, it was possible to observe that molecules presenting RGD sequence had larger cell areas on BSA blocked surfaces than non-blocked surfaces, while molecules without the RGD sequence, in general, presented an opposite behaviour (smaller cell areas with the presence of BSA protein). When crossing the cell area information with the adhered cell number results, it was interesting to observe that non-treated samples, despite adhering around ~80% of cells, they presented a completely round cell shape, which was a sign of a poor adhesion state. Similar behaviour was found on surfaces functionalized with IK_{24} and G_6RGE molecules.

The direct observation of cell morphology by fluorescence was in concordance with the numerical values calculated over cell populations (Figure 15). Thus, it was possible to observe round and small cell shapes on non-treated samples and IK_{24} physisorbed samples, while short peptides and IK_{24} covalent samples presented a star-like cell shape. Instead, positive controls and $HGRD_6$ functionalized samples (both covalent and physisorbed) were the only conditions presenting large cell areas with a clear cytoskeleton organization with well-formed actin stress fibres. Interestingly, when observing the formation of focal points, it was possible to observe that they were only present on samples functionalized with molecules containing RGD sequences. Moreover, it was possible to see that, generally, positive controls and covalently functionalized $HRGD_6$ surfaces presented cells with focal points along the entire cell body base, while

physisorbed $HRGD_6$ and G_6RGDS functionalized surfaces only presented focal points on the periphery of the cell body, this is the *lamellipodia*.

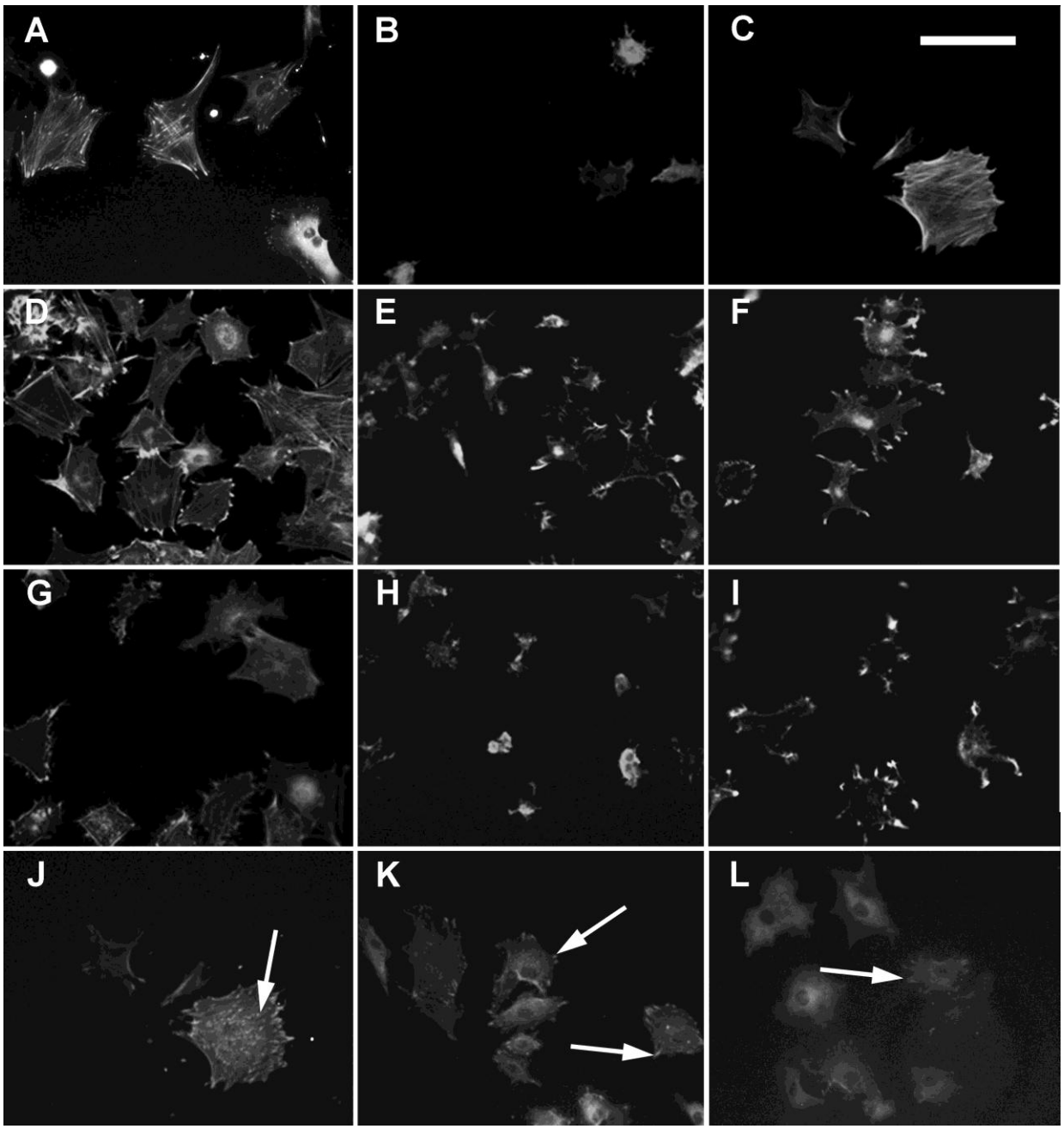

Figure 15. Immunofluorescence images of cells seeded on (A) TCP, (B) non-treated PMMA, (C) PMMA-Fn, (D), PMMA-$HRGD_6$ covalently functionalized, (E) PMMA-IK_{24} covalently functionalized, (F) PMMA-G_6RGD covalently functionalized, (G) PMMA-$HRGD_6$ physisorbed, (H) PMMA-IK_{24} physisorbed, (I) PMMA-G_6RGE covalently functionalized, (J) PMMA-$HRGD_6$ covalently functionalized, (K) PMMA-$HRGD_6$ physisorbed and (L) PMMA-G_6RGD covalently functionalized. A-I correspond to stained actin cytoskeleton of cells using rhodamin-phalloidin. Cytoskeleton organization is classified according the visualization of the stress fibres, a star cell shape or a round cell shape. Images J-L corresponds to stained vinculin using antivinculin antibody. White arrows indicate the presence of focal points. Cell cytoskeleton is stained with phalloidin-rhodamine. Scale bar = 100μm.

3.4. Discussion

A key aspect on tissue engineering is the integration of implants on hosting tissue, which is tightly correlated with a proper cell-material interaction on the interface. In this study, the cell-materials interaction for biofunctionalized PMMA surface is studied. A comparative study has been carried out involving commonly used strategies, like short RGD peptides and fibronectin, faced to a novel strategy based on the use of genetically modified protein, this is ELRs.

In order to validate the grafting of functionalized molecules, three different techniques were used. The first one, contact angle, was used to detect the chemical changes on surface occurred due to treatment steps. Hydrolyzation, activation and functionalization changed the composition of the functional groups shown on surface, and consequently the surface wettability. Surface wettability is correlated with the hydrophobicity of surface, which is an important parameter due to its role on protein non-specific adhesion and cellular attachment. Normally, hydrophobic surface adsorb unfolded proteins in an unspecific manner, and present low levels of cellular attachment [14,27]. Indeed, adsorption of proteins on hydrophobic surfaces tends to denature their native conformation, and, because it is unspecific, tends to accumulate high levels of adsorbed proteins from serum like BSA protein, which prevents a correct cell-material interaction and induce the formation of a cystic layer [28]. Contact angle results showed that PMMA non-treated surfaces were hydrophobic (85.77º), while successive treatments lowered it until 73.87º. The decrease of the contact angle revealed in an easy manner the chemical changes occurring at the interface, and also warned about the interactions of proteins and cells against the surface. For instance, the high hydrophobicity observed on all treated and non-treated surfaces defined these surfaces as highly attractive for BSA unspecific adsorption, while lower contact angles found on functionalized surfaces defined them as more cell appealing compared to non-treated surfaces.

The second technique was used to clearly corroborate the activation of PMMA surfaces and the molecular engraftment by means of covalent ligation. TOF-SIMS was used to analyse non-treated surfaces, activated surfaces and functionalized surfaces with short peptides. Only short peptides were used because it was easier to remove non-covalently grafted molecules and correlate the apparition of nitrogenised components with cross-linked engraftment. Thus, it was possible to observe the apparition of new peaks on the negative spectra on activated and functionalized surfaces, which were correlated with the CN and CNO mass component. The apparition of nitrogenized components was caused by the incorporation of NHS molecules and short peptides, which proved their grafting onto surfaces. Moreover, it was possible to observe

that peak intensities were higher on surfaces functionalized with short peptides than on activated surfaces, which agrees with the fact that a single peptidic molecule contains more nitrogen atoms than a NHS molecule.

The third technique was based on an ELISA test that used a PEG-biotin probe grafted under different conditions. The PEG-b probe was used as a reporter detected by means of biotin-streptavidin affinity through the ELISA test. PEG-b probe is a small molecule used as an analogue of a short peptide that can be easily removed by washing steps, so only strong grafted molecules were measured. PEG-b was grafted by physisorption on a non-treated surface and a 24h NaOH treated surface, and through covalent bonding on a 24h NaOH treated surface. Samples with physisorbed molecules on 24h NaOH treated surfaces were used as a negative control to ensure that no molecules were adsorbed due to unspecific electrostatic interactions. In the assay, different ratios of PEG-b/Glycine mixtures were functionalized. These mixtures were used as a control, so that detection of different quantities of grafted PEG-b molecules were a guarantee of assay sensibility. Results showed that covalently functionalized sample signal was 3-fold times more than physisorbed ones, which were found in much less quantities. Thus, it was indirectly proved the occurrence of the covalent functionalization. Negative control ensured that the probe did not adsorbed on treated surfaces, so the entire measured signal from covalent sample belonged to cross-linked molecules. It was important to notice that a certain extent of unspecific adsorption occurred on non-treated samples, but not on NaOH treated surfaces. This is important since it showed the low efficiency of functionalization processes by means of adsorption of small molecules.

Finally, in order to correlate the effect of the functionalization procedure with the biological response, the cell attachment was studied. Cell attachment was studied by means of number of adhered cells, cell morphology (elongation and cell area), cytoskeleton organization and focal point formation. Moreover, the BSA protein was used as competing agent in order to see the stability of grafted molecules and analyse the unspecific adhesion of albumin. Normally, on a system with more than one protein, the different molecules compete to adsorb on surface. In this way, it was possible to analyse if albumin, a protein found in large quantities on serum, could displace grafted proteins, or adsorb over them, blocking their biological capacities.

Cellular results concluded that the studied molecules were affected by BSA adsorption when they were grafted by physisorption. Indeed, short peptides and IK_{24} functionalized samples had reduced amounts of adhered cells when BSA was added on the media, especially under physisorption conditions. This was explained because these molecules were partially removed or

blocked by the unspecific adsorption of BSA protein. However, $HRGD_6$ functionalized samples were not affected by this interference and they maintained high amounts of adhered cells. This stability of $HRGD_6$ functionalized molecule was correlated to the non-fouling capability of ELRs [26], which prevented the BSA unspecific adsorption, and therefore ELR displacement or masking. BSA adsorption prevention is known to be important in order to have good tissue-implant integration, since BSA adsorption tends to trigger cystic encapsulation.

ELR covalent ligation not only showed higher amounts of adhered cells, but they also showed a more developed adhesion state. This was observed on cell morphology analysis, where $HRGD_6$ samples showed higher AR (more elongated cells). Moreover, highest cell areas where observed on $HRGD_6$ covalently functionalized, which means that cells could spread more when they had adhesive sequences strongly anchored on surface. Instead, physisorbed $HRGD_6$ showed smaller cell areas than their covalent homologous, which could be caused by the absence of fixed anchorage points that difficult the self-pulling and stretching of adhered cells. On the other hand, short peptides showed much less spread cell areas. This could be explained because ELRs molecules have certain degree of malleability because of their larger size and cells can stretch them in order to create focal points, while short peptides, because of their shorter nature, present less degree of malleability and focal point formation is less flexible. Interestingly, results also showed that, for those samples functionalized with RGD-containing molecules, cell areas found on PMMA-blocked surfaces were higher than cell areas found on PMMA-non-blocked surfaces. Instead, samples functionalized with RGD-lacking molecules did the contrary. This effect could be explained because BSA protein blocked unspecific cell adhesion regions, which promoted RGD-integrin interaction and, therefore, formation of stronger anchorage and cell spreading on surfaces functionalized with RGD-containing sequences. Equally important was the direct observation of cell morphology and cytoskeleton organization by fluorescence imaging. There, it was possible to observe that, except $HRDG_6$ functionalized surfaces, all other samples presented low cell adherence (round shape), or intermediate cell adherence (star shape), and only functionalized surfaces presented focal points on all cell base, which resulted from a good cell anchorage. Focal points found on the vertex of *lamellipodia* of star-like cell shapes were a sign of the stretching of the on-going spreading of cells. Thus, G_6RGDS functionalized samples and $HRGD_6$ physisorbed samples were defined as intermediate adhesion state, while covalent $HRGD_6$ was defined as advanced cell adhesion state.

3.5. Conclusions

The functionalization of PMMA surfaces using engineered proteins has been analysed in this manuscript. ELR engineered proteins have shown to be a good alternative to short peptides and natural proteins, which can enhance surface properties while avoiding problems like immunogenicity, purification, over-simplification and so on. Moreover, ELRs have shown better performance compared to both other strategies. ELRs not only have shown more cell adhesion capacity, but, because of their non-fouling properties, their biological activity is not diminished when BSA is present on the media. This property permits to ELRs to improve tissue-biomaterial interface and promote a better implant integration. The study also showed that better results are found when molecules are covalently grafted to surface, since adhered cells can spread better and have stronger adhesion points.

Because of the successful performance of ELRs, these molecules can be used for the functionalization of PMMA surfaces in order to obtain stronger and faster cell responses on tissue-biomaterial interface, thus, promoting better implant integration than short peptides functionalization.

3.6. References

1. Frazer RQ, Byron RT, Osborne PB, West KP. PMMA: an essential material in medicine and dentistry. J Long Term Eff Med Implants 2005;15(6):629-39.
2. Breusch SJ, Kühn KD. Knochenzemente auf Basis von Polymethylmethacrylat. Orthopade 2003; 32:41-50.
3. Wang B, Lin Q, Shen C, Tang J, Han Y, Chen H. Hydrophobic modification of polymethyl methacrylate as intraocular lenses material to improve the cytocompatibility. J Colloid Interface Sci 2014; 431:1-7.
4. Yu BS, Yang ZK, Li ZM, Zeng LW, Wang LB, Lu WW. Which is the preferred revision technique for loosened iliac screw? A novel technique of boring cement injection from the outer cortical shell. J Spinal Disord Tech 2011;24(6):E49-56.
5. Jaberi J, Gambrell K, Tiwana P, Madden C, Finn R. Long-term clinical outcome analysis of poly-methyl-methacrylate cranioplasty for large skull defects. J Oral Maxillofac Surg 2013;71(2):E81-8.
6. Sawakami K, Yamazaki A, Ishikawa S, Ito T, Watanabe K, Endo N. Polymethylmethacrylate augmentation of pedicle screws increases the initial fixation in osteoporotic spine patients. J Spinal Disord Tech 2012;25(2):E28-35.
7. Lemperle G, Ott H, Charrier U, Hecker J, Lemperle M. PMMA microspheres for intradermal implantation: Part I. Animal research. Ann Plast Surg 1991;26(1):57-63.
8. Goodger NM, Wang J, Smagalski GW, Hepworth B. Methylmethacrylate as a space maintainer in mandibular reconstruction. J Oral Maxillofac Surg 2005;63(7):1048-51.
9. McCord JF. Contemporary techniques for denture fabrication. J Prosthodont 2009;18(2):106-11.
10. Schaffner P, Meyer J, Dard M, Wenz R, Nies B, Verrier S, Kessler H, Kantlehner M. Induced tissue integration of bone implants by coating with bone selective RGD-peptides in vitro and in vivo studies. J Mater Sci Mater Med 1999;10(12):837-9.

11. Lye KW, Tideman H, Wolke JC, Merkx MA, Chin FK, Jansen JA. Biocompatibility and bone formation with porous modified PMMA in normal and irradiated mandibular tissue. Clin Oral Implants Res 2013;24 Suppl A100:100-9.

12. Benoit DS, Schwartz MP, Durney AR, Anseth KS. Small functional groups for controlled differentiation of hydrogel-encapsulated human mesenchymal stem cells. Nat Mater 2008;7(10):816-23.

13. Rodda AE, Meagher L, Nisbet DR, Forsythe JS. Specific control of cell–material interactions: Targeting cell receptors using ligand-functionalized polymer substrates. Prog Polym Sci 2014;39(7):1312-47.

14. Hersel U, Dahmen C, Kessler H. RGD modified polymers: biomaterials for stimulated cell adhesion and beyond. Biomaterials 2003;24(24):4385-415.

15. Williams, DF. The role of short synthetic adhesion peptides in regenerative medicine; The debate. Biomaterials 2011;32:4195-7

16. Barker, TH. The role of ECM proteins and protein fragments in guiding cell behavior in regenerative medicine. Biomaterials 2011;32:4211−4.

17. Nettles DL, Chilkoti A, Setton LA. Applications of elastin-like polypeptides in tissue engineering. Adv Drug Deliv Rev 2010;62(15):1479-85.

18. Rodríguez-Cabello JC, Martín L, Alonso M, Arias FJ, Testera AM. "Recombinamers" as advanced materials for the post-oil age. Polymer 2009;50:5159-69.

19. Girotti A, Reguera J, Rodríguez-Cabello JC, Arias FJ, Alonso M, Matestera A. Design and bioproduction of a recombinant multi(bio)functional elastin-like protein polymer containing cell adhesion sequences for tissue engineering purposes. J Mater Sci Mater Med 2004;15(4):479-84.

20. Zio KD, Tirrel DA. Mechanical Properties of Artificial Protein Matrices Engineered for Control of Cell and Tissue Behavior. Macromolecules 2003;36(5):1553−58.

21. McMillan RA, Lee TAT, Conticello VP. Rapid Assembly of Synthetic Genes Encoding Protein Polymers. Macromolecules 1999;32(11):3643-8.

22. Punet X, Mauchauffé R, Giannotti MI, Rodríguez-Cabello JC, Sanz F, Engel E, Mateos-Timoneda MA, Planell JA. Enhanced cell-material interactions through the biofunctionalization of polymeric surfaces with engineered peptides. Biomacromolecules 2013;14(8):2690-702

23. Costa RR, Custódio CA, Testera AM, Arias FJ, Rodríguez-Cabello JC, Alves NM, Mano JF. Stimuli-Responsive Thin Coatings Using Elastin-Like Polymers for Biomedical Applications. Adv Funct Mater 2009;19:3210−18.

24. Hermanson GT. The Chemistry of Reactive Groups, In: Elsevier (ed.). Bioconjugate Techinques (2nd ed). London: Elsevier, 2008, 169-212.

25. González-Vázquez A, Planell JA, Engel E, Extracellular calcium and CaSR drive osteoinduction in mesenchymal stromal cells. Acta Biomater 2014;106:2824-33.

26. Salvagni E, Berguig G, Engel E, Rodriguez-Cabello JC, Coullerez G, Textor M, Planell JA, Gil FJ, Aparicio C. A bioactive elastin-like recombinamer reduces unspecific protein adsorption and enhances cell response on titanium surfaces. Colloids Surf B Biointerfaces 2014;114:225-33.

27. Nakanishi K, Sakiyama T, Imamura K. On the adsorption of proteins on solid surfaces, a common but very complicated phenomenon. J Biosci Bioeng 2001;91(3):233-44.

28. Arima Y, Iwata H. Effect of wettability and surface functional groups on protein adsorption and cell adhesion using well-defined mixed self-assembled monolayers. Biomaterials 2007;28(20):3074-82.

CHAPTER 4

4. BIOFUNCTIONALIZATION OF POLY(LACTIC ACID) SURFACES

Research on surface modification of polymeric materials to guide the cellular activity in biomaterials designed for tissue engineering applications has mostly focused on the use of natural ECM proteins and short peptides, such as RGD. However, the use of engineered proteins can gather the advantages of these strategies and avoid the main drawbacks. In this chapter, recombinant engineered proteins called elastin-like recombinamers (ELRs) have been used to functionalize poly(lactic acid) (PLA) model surfaces. The structure of the ELRs has been designed to include the integrin ligand RGDS and the cross-linking module VPGKG. Surface functionalization has been characterized and optimized by means of ELISA and AFM. The results suggest that ELR functionalization creates a non-fouling canvas able to restrict unspecific adsorption of proteins. Moreover, AFM analysis reveals the conformation and disposition of ELRs on the surface. Biological performance of PLA surfaces functionalized with ELRs has been studied and compared with the use of short peptides. Cell response has been assessed for different functionalization conditions in the presence and absence of the BSA protein, which could interfere on the surface-cell interaction by adsorbing on the interface. This chapter shows that ELRs are able to elicit higher rates of cell attachment, stronger cell anchorages and faster levels of proliferation than peptides. The use of engineered proteins is a more efficient strategy to guide the cellular activity than the use of short peptides, because they not only allow for better cell attachment and proliferation, but also can provide more complex properties such as the creation of non-fouling surfaces.

4.1. Introduction

The degradability and resorbability of the materials into the body after implantation simplifies many surgical interventions. Poly(lactic) acid (PLA) and its copolymers are a class of biodegradable, biocompatible, FDA approved for several applications, synthetic polymers whose mechanical, ease-of-fabrication and degradability properties make them among the most often used polymers for biomedical applications [1]. Most medical uses of this material are related to load-bearing tasks (suture, fixation, bonding), obstruction (wound protection, blood flow arrest), organ protection or special sustention (nerve conduits, mandibular reconstruction, stents) [2]. However, when PLA is used to induce the regeneration of a damaged tissue, its hydrophobicity and lack of bioactive properties appear to be drawbacks for rapid and effective integration and healing [3]. To overcome this handicap, many biomaterials (including PLA) have been modified using different approaches [4-6]. The most frequently used modification is based on the incorporation of appropriate signals on the surface of the material in order to direct cellular activities. Normally, both functional groups and biomolecules are introduced on the surface of materials. However, if cell adhesion is desired to enhance cell growth and spreading, integrin ligands, such as extracellular matrix (ECM) proteins or their most reduced and essential amino acid sequences, are normally used [7,8]. Still, their use has opened a new and intense debate around the use of complex proteins and their artificial simplifications, remaining a controversial issue [9]. In fact, it has been observed that the use of proteins purified from the ECM in their native form allows the implementation of the integrin ligands with their full potential. This strong efficiency is obtained because the natural protein structure is preserved and the presence of other synergistic sequences, which increase the effectiveness of the protein. This strategy, however, presents some immunogenic problems, purification and functionalization control. Therefore, a second approach, based on the use of short peptides, has become the most frequently used strategy [10]. Short peptides are not only non-immunogenic, easy to purify and able to be introduced in a controlled manner, but also their sequence design can be well controlled [11]. Nevertheless, the use of these oversimplified constructs are not able to carry out the multiple and dynamic tasks that larger and more complex natural proteins can. Instead, they lose effectiveness, affinity and stability due to the simplification [12].

Parallel to these two approaches, recombinant proteins combine all the previous advantages and avoid major drawbacks, hence start to present a growing interest [13]. Obtained through biotechnological tools, they can be designed from non-immunogenic protein modules, which can include bioactive amino acid motifs such as the RGD (Arginine-Glycine-Aspartic

acid) sequence for cell attachment. These modules can be added, removed and permuted to include different properties in the final engineered protein. Modules can be included to introduce adhesive promoters, structural functions and sequences that trigger dynamic effects in time (like protein self-renewal or mineralizing nucleation points) [14-16]. Therefore, more stable, complex and easy-to-purify constructs can be obtained through these smart designs.

A practical way to design these engineered proteins is based on the use of modular amino acidic sequences already present in nature. Inspired by Nature and trying to mimic functionality and stability of natural proteins, the modified amino acidic module VPGIG from the pentapeptide VPGVG of the natural elastin has been used to synthesize a structural skeleton with similar elastic properties [17,18]. Moreover, the pentapeptide module VPGVG is a repetitive sequence that is codified in the tropoelastin gene along many species [19], which converts the structure VPGVG into a non-immunogenic repetitive sequence. This repetitive sequence, as well as the module VPGIG (which has shown to be biocompatible) [20], can be used to construct larger polymers that include other amino acid sequences as well. The obtained engineered proteins are called elastin-like recombinamers (ELRs).

Furthermore, ELRs are attractive because they can be codified in synthetic genes and expressed in Escherichia coli in large quantities, with greater control on the amino acid sequence and the molecular weight as compared with the chemical synthesis of large polypeptides [13]. Also, due to its inverse temperature transition property, they can easily be separated from the raw protein mixture. This results in a purified, biocompatible, biodegradable, non-immunogenic engineered protein [21]. In such a way, elastin and its special mechanical properties can be obtained and used for the design and production of biomedical devices. This success has been an important milestone, since its implementation has been restricted for many years due to the laborious purification procedures required for elastin protein [22].

In this work, the functionalization of model PLA surfaces with ELRs is studied. Moreover, this biofunctionalization strategy is compared with the use of short peptides, the most frequently used approach found in current literature to introduce adhesive RGD sequences on surfaces. The objective of the study is to explore the functionalization procedure of PLA with ELRs as alternative to the use of ECM proteins and peptides derived from them, as well as to evaluate the cell response of these modified surfaces. Surface characterization results show, in addition, that ELRs are able to diminish the unspecific adsorption of competing proteins. Subsequent cellular study results show enhanced efficiency of cellular attachment for ELR functionalized PLA samples.

4.2. Materials and Methods

4.2.1. Materials

Poly–L/DL lactic acid 70/30 (Purasorb PLDL 70/38, inherent viscosity midpoint 3.8 dl/g, Mw≈ 850,000 Da) was purchased from Purac Biomaterials (the Netherlands).

Short peptides were purchased from Genscript (USA). Peptides were designed with an integrin ligand (RGDS) and a six-glycine tail in the amino end, to allow accessibility. A control peptide was designed with a scrambled sequence (RGE). Peptides were labelled G_6RGDS and G_6RGE respectively. They were received desalted and lyophilized.

ELRs were synthesized following already optimized protocols [23]. In short, ELRs were obtained from the expression of the ELRs recombinant gene inserted in an Escherichia coli strain BLR (DE3). Gene expression was induced in a 12L Applikon fermenter, in Terrific Broth (TB) medium with 0.1% of carbenicilin and 0.1% of glucose, under controlled conditions of temperature (37ºC) and pH (7.00). After fermentation, the culture was harvested by centrifugation, resuspended and lysed by ultrasonic disruption. Solid debris was separated by centrifugation. The lysate was subjected to several cycles of cold and warm centrifugations of 4 and 40ºC, respectively. All purifications steps were carried out in a 0.5M sodium chloride solution. The polymer solution was frozen at -24ºC and lyophilized.

An ELR with an RGD sequence ($HRGD_6$) and a control ELR without a RGD sequence (IK_{24}) were designed with the following sequences:

$HRGD_6$: MGSSHHHHHSSGLVPRGSHMESLLP[[$(VPGIG)_2$(VPGKG)$(VPGIG)_2]_2$AVTGRGD SPASS[$(VPGIG)_2$(VPGKG)$(VPGIG)_2]_2]_6$.

IK_{24}: MESLLP $(VPGIG\ VPGIG\ VPGKG\ VPGIG\ VPGIG)_{24}$.

VPGIG modules were substituted by VPGKG modules in order to introduce lysine residues (K) in the biomolecule sequence, to further be used to covalently attach the polypeptide to the surface.

All other chemicals were purchased from Sigma-Aldrich and used without further purification.

4.2.2. Poly(lactic) acid Films Preparation

PLA films were obtained by solvent casting. Briefly, PLA was dissolved in $CHCl_3$ (2.5% w/v) and was poured into propylene well plates. The solvent was allowed to evaporate for 3 days in a solvent-saturated atmosphere. After this time, the obtained films were stored in vacuum and dry atmosphere until their use. The thickness of the resulting films is 500 μm.

4.2.3. Surface Functionalization

Chemical surface composition was changed by means of covalent functionalization with different molecules. The functionalization protocol was composed of three steps. During the first step (surface pre-activation) the films were treated with sodium hydroxide (NaOH) 0.5M and carboxyl groups were obtained on the surface due to the hydrolytic cleavage of the ester bonds of the PLA substrate [24]. Before moving to the second step, films were gently washed with water. Then, films were activated with 1-Ethyl-3-(3-dimethylaminopropyl)carbodiimide and N-hydroxysuccinimide (EDC and NHS) 0.1/0.2M in phosphate-buffered saline (PBS) (pH 7.4). When surface activation was finished, films were washed twice with PBS. Finally, the biomolecules were functionalized using their amino-groups to create the covalent bond. This step was carried out overnight in PBS solution at 100 μg/ml. Finally, functionalized films were washed again with water and vacuum sealed until their use.

The time for the pre-activation step was optimized to 30' according to the obtained results. The time for the activation step was set to 1 hour, since the average time-life of the activated NHS molecule was found to be 1 hour in neutral aqueous solution [25]. The final functionalization step was set overnight, to ensure the maximal binding.

Parallel to this, model PLA surfaces were functionalized with ELR by physisorption. For that purpose, surfaces were simply soaked overnight with a solution of the desired biomolecule in PBS. These surfaces were used in the comparative studies in order to analyse the role of the covalent bonding for the molecule stability as well as for the cellular response.

4.2.4. Roughness Study

Topographical changes induced during the hydrolytic treatment were analysed using atomic force microscopy (AFM). Topographical images were obtained by AFM (Dimension 3100, Nanoscope IV controller, Veeco, Digital Instruments, Santa Barbara, CA) in intermittent-contact mode using single-beam silicon cantilevers under ambient conditions. The surface roughness was quantified from the topographical images using the average roughness (Ra)

parameter. Specific area increase was calculated through the difference between the 2D image surface and the 3D recreation surface. Surface peak profile was characterized using Kurtosis (peak sharpness) and Skewness (symmetry of mountain and valleys distribution) parameters.

4.2.5. Surface Activation Test

The presence of activated sites was analysed using an ELISA assay following the manufacturer protocol. In short, surfaces were functionalized with Amine-PEG biotinylated molecules (Pierce Protein Biology Products) at 100 μg/ml in PBS (pH 7.4). Then, functionalized surfaces were treated with blocking buffer [PBS + Tween20 0.05% (v/v) + BSA 2% (w/v)] during 1 hour at room temperature in order to block non-functionalized areas. Afterwards, the surfaces were washed three times with washing buffer [PBS + Tween20 0.05% (v/v)]. Next, a Streptavidin-HRP (Pierce Protein Biology Products) solution in blocking buffer was added and allowed to interact with the PEG-biotinylated molecules for 1 hour. Finally, the surfaces were washed six times with washing buffer, and ABTS (2,2'-Azinobis [3-ethylbenzothiazoline-6-sulfonic acid]-diammonium salt) (Pierce Protein Biology Products) substrate was added to develop the colorimetric assay.

4.2.6. Micropatterning

Polydimethylsiloxane (PDMS) stamps with square features of 5 μm were created following literature protocols [26]. Briefly, silanized SiO_2 masters were cleaned in a mixture of absolute ethanol:isopropanol (50:50) in a sonicator for 10 min and then dried with a N_2 stream. Then, the desired master was placed in a Petri dish and covered with a mixture of Base Silicon Elastomer and Curing Agent (10% w/w). Bubbles were removed under vacuum at room temperature. Finally, the mixture was baked at 90ºC for 1h. Solidified PDMS was removed from the master, cleaned with ethanol and stored until further use. Correct topography was verified by interferometry.

The micropatterning technique was used for two different studies. The first study aimed to validate the ability to graft molecules onto surfaces through the proposed chemistry. That is, a PDMS stamp was wetted with a water solution of a fluorescently labelled protein (BSA-FITC) at 100 μg/ml during 1h at room temperature. Then, the stamp was rinsed with PBS and dried under a N_2 stream. Finally the stamp was softly pressed onto a PLA activated surface during 10 seconds. The PLA surface was kept for 2 hours in the dark and then vigorously rinsed with milli-Q water with 0.1% Tween20. Fluorescence was observed with a Nikon E1000 upright fluorescence microscope. As a negative control, a non-treated PLA surface was used.

The second analysis aimed to prove the anti-fouling behaviour of ELR. For that purpose PLA films were treated with NaOH and EDC/NHS as previously described. The functionalization step, however, was carried out by printing the biomolecule solution with the PDMS stamps, following the same protocol previously described. ELR, peptide and BSA solutions were microprinted in such a way, and ligation was carried out overnight in a water-saturated atmosphere, at 4ºC. Later, surfaces were gently washed with PBS. Finally, a BSA-FITC solution (20μg/ml) in PBS was used to cover the PLA films. Fluorescent protein was allowed to adsorb on the surface during 1h at room temperature. After, surfaces were gently rinsed with PBS and fluorescent patterns were checked with a Nikon E1000 upright microscope.

4.2.7. ELRs Surface Distribution and Conformation

ELR distribution and conformation was observed by AFM in intermittent-contact mode under liquid conditions. In addition, force spectroscopy was performed in order to evaluate the biomolecule attachment to the PLA surfaces. Force-distance curves were recorded and the maximum extension and adhesion force were evaluated. AFM imaging and force-spectroscopy were performed under liquid conditions using a 3D-MFP AFM set-up (Asylum Research, Santa Barbara, CA), and V-shaped Si_3N_4 cantilevers with nominal spring constant of 0.1 N/m. Individual spring constants were calibrated according to the thermal oscillation technique [27]. All the experiments were performed under Milli-Q water at ambient temperature. Force curves were acquired at piezoelectric actuator extension and retract constant velocity of 1μm/s, in the force-mapping mode over an area of 5 x 1.5 μm, i.e. the same exact spot was never probed twice.

4.2.8. Cell Culture

Rat mesenchymal stromal cells (rMSC) were extracted from bone marrow and used at passages 4-6 [28]. Cells were expanded in Advanced DMEM medium supplemented with 15% fetal bovine serum (FBS), 1% Penicillin/Streptomycin and 1% L-Glutamine (A-DMEM). Cells were allowed to grow until ~80% confluence before passaging them.

4.2.9. In Vitro Cell Adhesion Studies

For the cell attachment study, solvent casted films on 24-well plates were functionalized as previously described. Well plates were sterilized with ethanol 70% (v/v) and UV light. Then, plates were left in a sterile hood until they were dry. Afterwards, the wells were washed with PBS (pH 7.4) three times and, for some conditions, samples were blocked with a PBS (pH 7.4) + BSA 6% solution for 1 hour and washed again with PBS (pH 7.4). rMSC were expanded and

collected. 10,000 cells were seeded per well (~5300 cells/cm^2) in serum free Advanced DMEM medium and cultured during 4 hours. Then, non-attached cells were removed with two PBS wash steps. To evaluate the number of attached cells, a set of cultured well plates were treated with lysis buffer (PBS pH 7.4 + Triton X-100 0.01% (v/v). The cell lysate was analysed with Cytotoxicity Detection KitPLUS (LDH) (Roche) and cell number was obtained following the commercial protocol. To observe the cell morphology, a set of cultured well plates was treated with paraformaldehyde 6% to fix cells after 4 hours of incubation. Then, the cytoskeleton was stained with Rhodamine-Phalloidin (red), the nucleus with DAPI (blue) and the focal points with monoclonal anti-Vinculin antibody/Alexa Fluor® 488 goat anti-mouse IgG system (green). Fluorescence was observed with an Eclipse600 upright microscope.

4.2.10. In Vitro Cell Proliferation Studies

Cell growth was studied on functionalized PLA that had been poured on propylene 96-well plates beforehand. Cells were seeded at a ratio of 1000 rMSC per well (~3100 cells/cm^2). Cells were cultured within 8 days. Proliferation was assessed with Alamar Blue reactive and calculated in terms of cumulative population doubling levels (PDL) [29]. Maximum cumulative PDL is a value that indicates the proliferation capacity of a cell population. This value measures the times that a cell population duplicates itself after a chosen period. In this work eight days was chosen since it was the time needed to achieve the confluence, a state in which proliferation rate changes due to cell density.

4.2.11. Statistics

Experiments were subjected to t-Student testing ($P < 0.05$). Results were presented as mean ± standard deviation. For population distributions, values were presented in box-plot format. In these cases, central boxes represented the 2nd and 3rd population quartiles (50 % of the population distribution) and bars represented the 1st and 4th population quartiles (50 % of the population distribution), indicating the minimum and maximum values of the distribution. In all distributions, the plotted population represented the 95% of the real measured events in order to not include extremely deviated results.

4.3. Results

4.3.1. Roughness Study

For the pre-activation of the PLA surface it was necessary to generate and expose carboxyl groups at the interface. For this purpose, NaOH was used to hydrolyse the PLA chains on the surface and obtain functional groups such as carboxyl and hydroxyl groups, but this treatment entailed topography changes [30]. Therefore, the surfaces were characterized at the nanometre scale by means of AFM (Figure 16). Topographical images of the treated surfaces at different times are displayed in Figure 16A. Different surface parametric descriptors were evaluated: surfaces roughness (Ra) (Figure 16B), 2D/3D surface difference (Figure 16C), Kurtosis (Figure 16D) and Skewness (Figure 16E).

Topographical analysis revealed that the Ra values increase with hydrolysis time. However, a two-region behaviour was observed. During the first 10 minutes of treatment, an abrupt increase in roughness occurred, while after that time, roughness increased at much lower rate. These surface modifications, nevertheless, are framed in the nanometre scale and raised from a near-zero Ra value (for the non-treated PLA surface) to a 6 nm Ra value (for the 1h treated PLA surface).

The second region of the roughness evolution graph (with a lower-rate roughness increase) ensures a more reproducible performance of the experiments as small shifts from the selected time correlates to smaller changes in roughness. Therefore, a hydrolysis time above 10 minutes was selected for the functionalization protocol.

On the other hand, the 2D/3D surface difference showed no increase after 45 minutes of treatment. The values of Kurtosis (surface peakness) and Skewness (predominance of valleys or mountains) do not show a significant change or tendency along the treatment time as well. These three factors lead to the interpretation that after 10 minutes of hydrolysis, different treatment times induce similar random peaked and sharp topography, as observed in the topographic images.

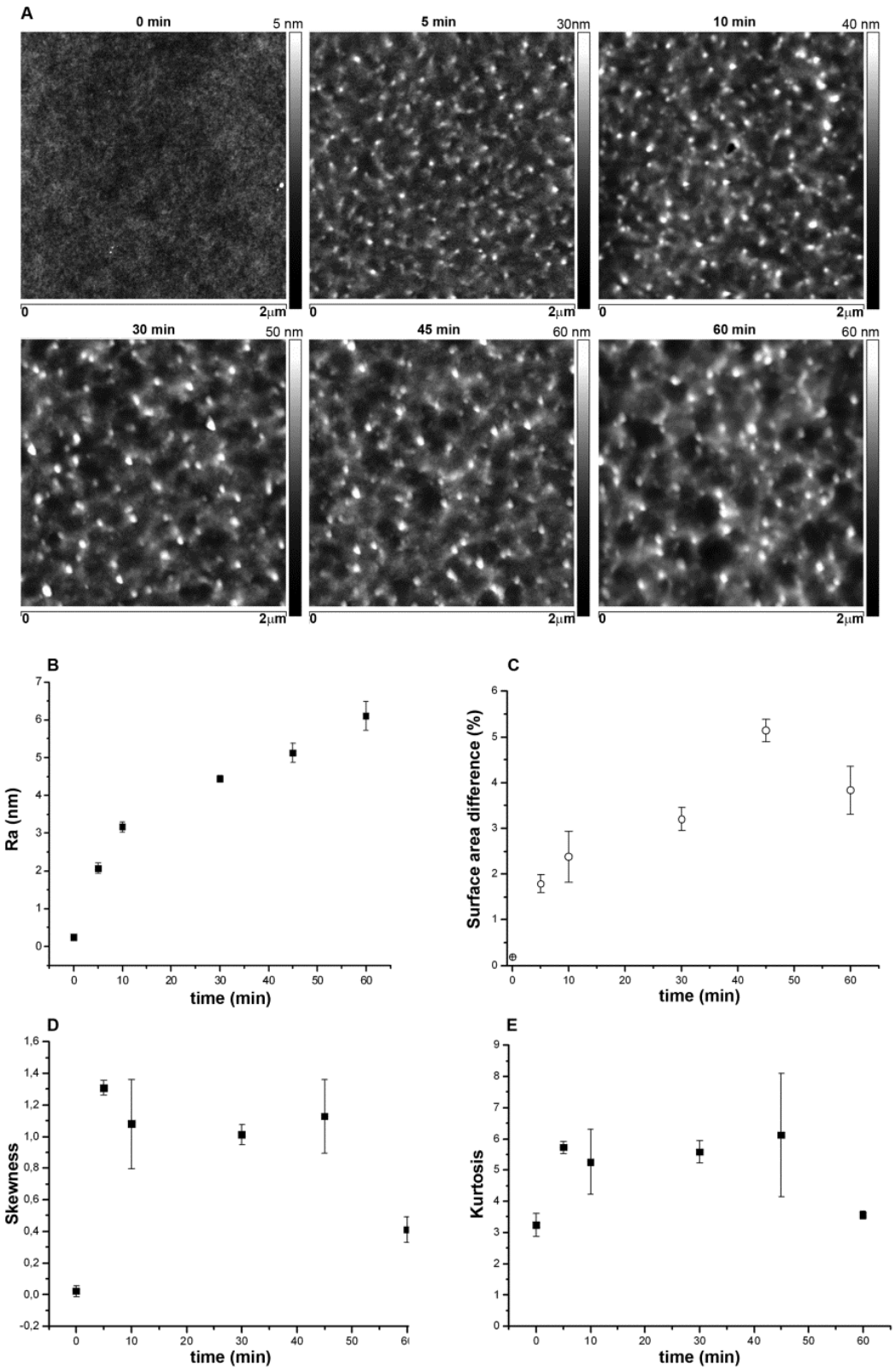

Figure 16. (A) AFM topographic images of PLA surfaces treated with NaOH 0.5 M at 0, 5, 10, 30, 45 and 60 min. 2μm x 2μm images were acquired using intermittent-contact mode in ambient conditions. For each condition, the following parameters were calculated: (B) the average roughness (Ra), (C) the surface area differences between the 2D projection and the 3D computed surface, (D) the Kurtosis values and (E) the Skewness values. Error bars in B-E indicates SD.

4.3.2. Surface Activation Test

After pre-activation, the carboxyl groups generated on the PLA surface were treated with EDC/NHS, which lead to the formation of an NHS activated ester group. These groups were able to react with the ε-amino groups of the bioactive molecules. The presence of available carboxyl groups obtained during the NaOH treatment and covalent ligation were analysed by means of two indirect studies: ELISA assay and micropatterning functionalization.

The ELISA assay was based on the detection of a biotin-labelled PEG probe (PEG-b) through an ELISA-like assay. This approach was not only used to show the covalent functionalization but it also provided semi-quantitative information about the amount of grafted PEG-labelled probe, an indirect measurement of the amount of available carboxyl groups. This procedure was then used to optimize the first step of the functionalization process.

In order to find the optimal hydrolysis time, several PLA surfaces were treated with NaOH 0.5 M for 0, 5, 30, 60, 120 minutes and overnight (O.N.). Then, the surfaces were functionalized with the PEG-b molecule using the proposed EDC/NHS protocol. PEG-b levels were measured following a standardized protocol of an ELISA assay and results were normalized against the sample treated for 120 minutes (Figure 17). It is clear that the absence of NaOH treatment lead to almost no-grafting of PEG-b. On the other hand, when NaOH treatment is used, the PEG-b levels decrease inversely proportional to the NaOH treating time. Since the ELISA assay included several washing steps with Tween20 0.1% (v/v) in PBS, it can be assumed that physisorbed molecules were completely removed from the surface, as proved with the sample without NaOH treatment (and therefore without available carboxyl groups).

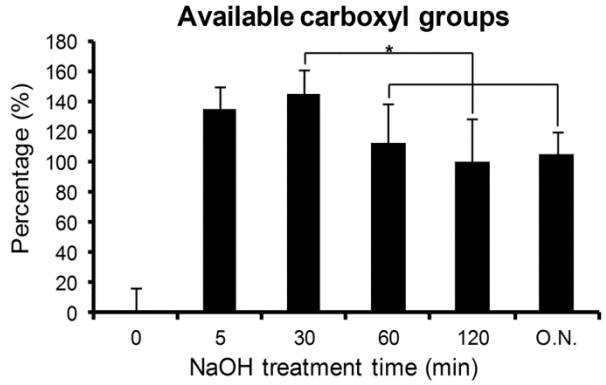

Figure 17. ELISA assay performed on samples functionalized with PEG-biotin probe using different hydrolysis times (0, 5, 30, 60, 120 minutes and over-night). The amount of PEG-b probe found on different samples was normalized against the sample treated for 120 minutes. Error bars indicates SD. Asterisk indicates statistical significance.

Samples with 5 and 30 minutes of hydrolysis treatment present the highest signal without significant differences between them. In view of this and previous results (see Figure 16B), 30 minutes hydrolysis time was selected for the pre-activation protocol step. In such a way, the amount of available carboxyl groups was maximized whereas the variability on the conditions of the experiments was minimized.

4.3.3. Micropatterning

Micropatterning was used to qualitatively corroborate surface functionalization and observe de non-fouling properties of the ELRs functionalized surfaces. The first study involved the use of a micropatterned PDMS stamp to functionalize surfaces with a fluorescent probe. The micropatterned stamp was wetted with the fluorescent reporter BSA-FITC, whose amino groups reacted with the activated NHS moieties. After vigorously washing with milli-Q water with 0.1% Tween20, a fluorescent pattern could be observed on the functionalized surface, and the contrast between the non-functionalized and functionalized regions indicates the presence of the fluorescence biomolecules (Figure 18). To further prove the presence of covalent ligation to the surface, a non-treated PLA surface was printed following the same protocol. After the washing steps, it was not possible to observe any fluorescence (Figure not shown).

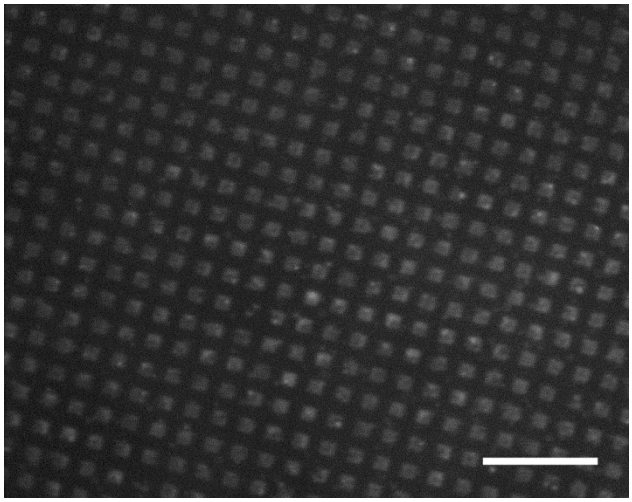

Figure 18. Fluorescence micrograph of a PLA surface functionalized with BSA-FITC. Functionalization was done using a micropatterned stamp. Bright squares correspond to BSA-FITC covalently functionalized regions. Scale bar = 40 μm.

For the detection of non-fouling properties, different PLA surfaces were functionalized with short peptides, ELRs and BSA biomolecules using the micropatterning technique. Later, functionalized surfaces were immersed in a solution of fluorescently labelled BSA-FITC and cleaned gently. Fluorescent microscopy reveals a negative pattern on surfaces functionalized

with BSA and ELRs, but not with peptide (Figure 19). Images show that BSA-FITC adsorb on biomolecule-free regions, but do not adsorb on regions functionalized with BSA (the positive control) or ELRs.

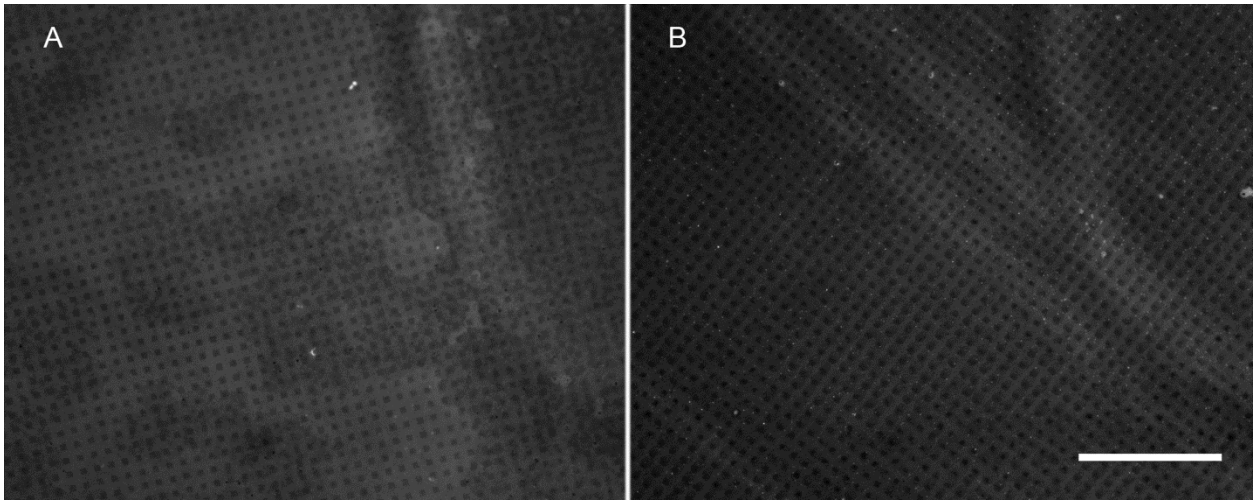

Figure 19. Fluorescence micrographs of PLA surfaces functionalized with (A) BSA and (B) ELR. Functionalization was done using micropatterned stamps. Functionalized surfaces were immersed in a BSA-FITC solution to obtain negative fluorescent patterns. Scale bar = 100 μm.

4.3.4. ELRs Surface Distribution and Conformation

The non-treated PLA and the ELR functionalized PLA surfaces were characterized by AFM. As shown in Figure 20, a flat PLA surface can be observed for non-treated samples visualized under ambient conditions. On the other hand, for functionalized surfaces, both physisorbed and covalently, the presence of ELRs is revealed. In the case of physisorbed ELRs, a distribution of agglomerates on a flat surface can be observed. This is more visible in the phase image, which shows different phase shifts between the agglomerates and the background. These differences in phase shifts are ruled by the nature of the material, which allow for the distinction between the globular aggregates of ELRs and the PLA background. For PLA covalently functionalized with the ELRs, the topography is determined by both the contribution of the PLA topography (due to the hydrolysis treatment) and the presence of ELRs.

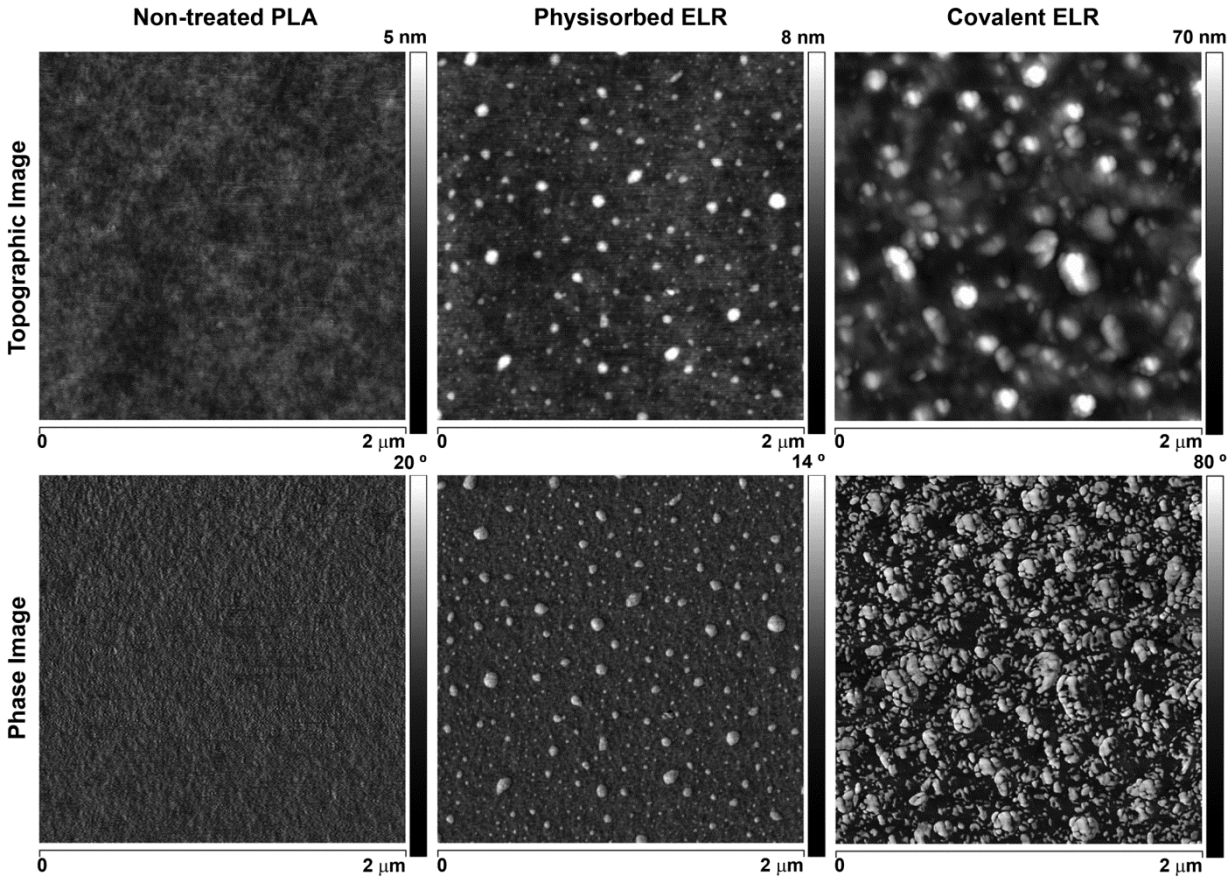

Figure 20. AFM topographic and phase images (2μm x 2μm) of non-treated PLA surfaces, PLA surfaces with physisorbed ELRs and PLA surfaces with ELR covalently functionalized. Images were acquired using the intermittent-contact mode under ambient conditions.

The analysis of the same surfaces under Milli-Q water at room temperature, allows the observation of the swelling of the aggregates of ELRs on phase images (Figure 21). Still it is not possible to determine from the images whether the ELR coverage of the PLA surface was homogeneous or not. In order to gain more insight into the distribution of ELRs on the surface, force spectroscopy was performed at different points of the surfaces and a force-map distribution was calculated.

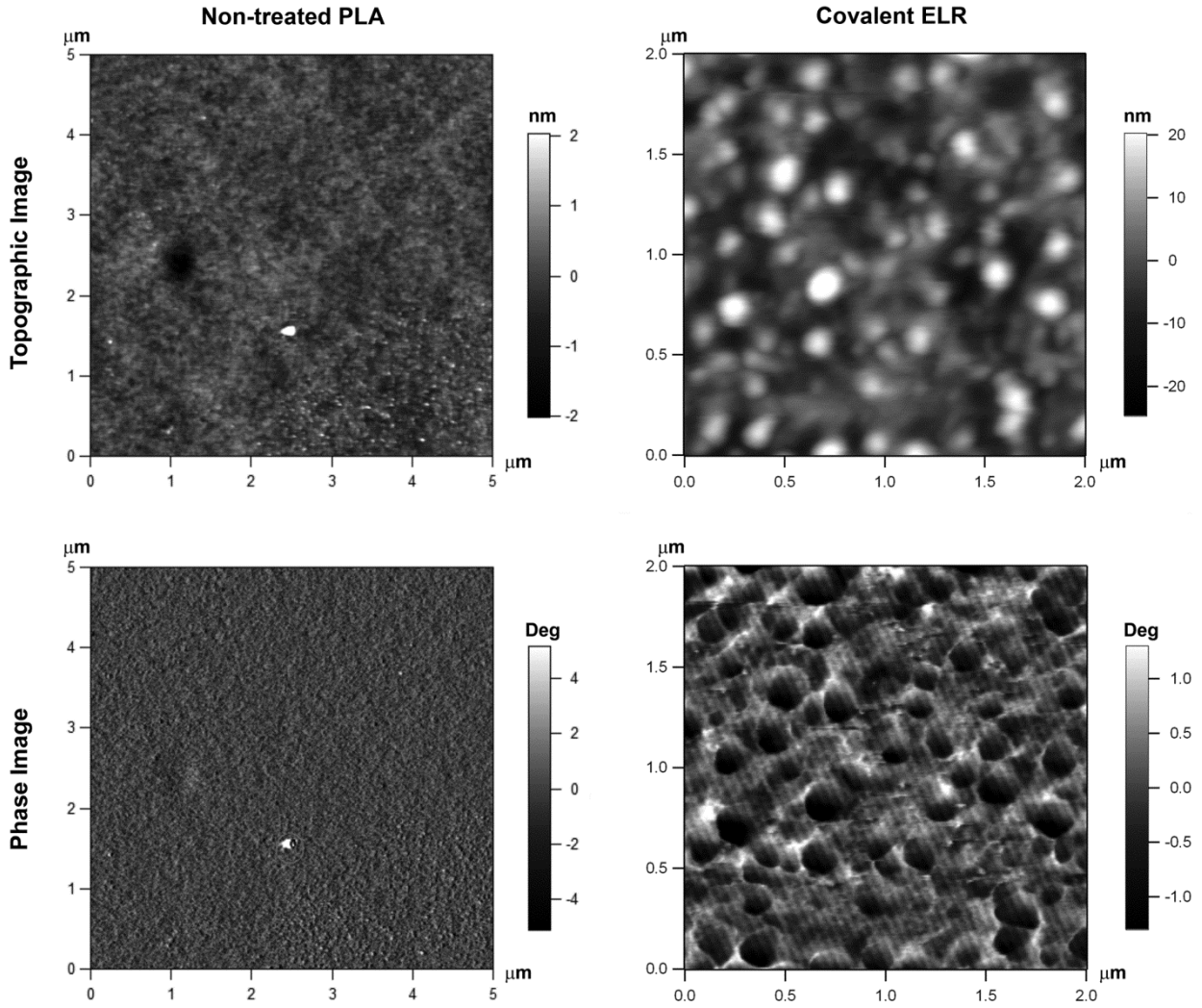

Figure 21. AFM topographic and phase images (2µm x 2µm) of non-treated PLA surfaces and PLA surfaces with ELR covalently functionalized. Images were acquired using the intermittent-contact mode under liquid conditions.

AFM-based force spectroscopy under liquid conditions was performed to observe the distribution of the ELR biomolecules on the surface as well as to observe the ELR degree of freedom depending on the functionalization procedures (physisorption or covalent grafting). In a typical AFM force spectroscopy experiment, the AFM tip approaches the surface at constant velocity. Once the tip is in contact with the surface and the cantilever is deflected upwards at a certain force, retraction takes place at the same constant velocity. The cantilever deflection is recorded against the Z-piezo movement and, when the spring constant of the cantilever is known, these data can be transformed into force vs. tip-surface separation. When a macromolecule, or a mesh of macromolecules, is anchored between the tip and the surface, it is uncoiled, or untangled if a mesh, and stretched during retraction. The untangling can be registered as a deflection of the cantilever towards the surface. Figure 22 presents typical force-distance curves obtained for (A) non-treated PLA, (B) ELR covalently functionalized PLA and (C) ELRs physisorbed on PLA.

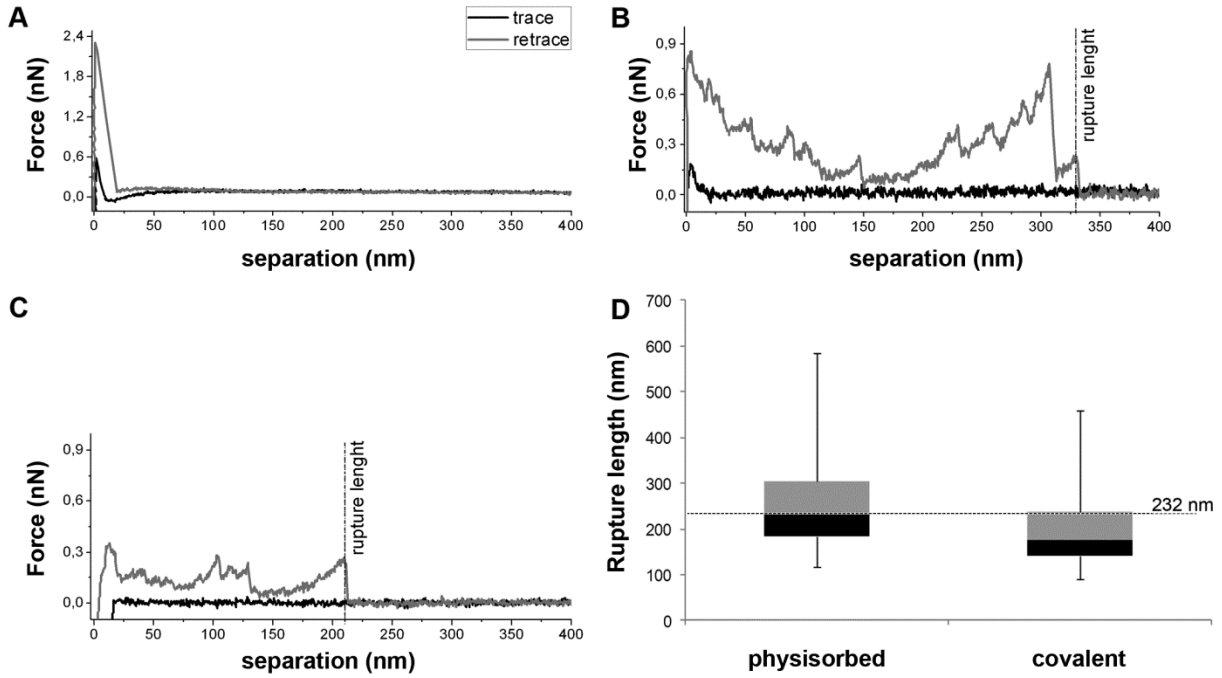

Figure 22. Typical force-distance curve for (A) a non-treated PLA surface, (B) a PLA surface with physisorbed ELR and (C) a PLA surface with ELR covalently functionalized. Maximum rupture lengths were measured from force-distance curves for covalent and physisorbed surfaces (352 curves per condition). (D) box-plot diagram for the rupture lengths distribution of the physisorbed and covalently attached ELRs.

For naked PLA samples, only a single non-specific adhesion pull-off peak can be observed, while for the ELR functionalized PLA a typical pattern for a polymeric mesh pulling is registered. These patterns are found through all the analysed area, which corroborates that the ELRs were covering the entire surface. Similar force profiles were obtained for both ELR modified samples. In order to evaluate possible differences between covalent and physisorbed ELR-PLA samples, a statistical analysis of the maximum extension of the ELR mesh was performed. This extension corresponds to the maximum length that the ELR meshes could be stretched before the contact with the tip was lost, called rupture length. The rupture length depends on the interactions between molecules themselves and between the molecules and the substrate or the tip. For instance, a single molecule attached to the substrate through many different covalent anchorages would be expected to be pulled a shorter distance than a molecule that is just physisorbed. A similar behaviour can be expected from an ELR mesh covalently grafted to the surface.

The rupture lengths of the different samples are plotted in a box plot graph in order to check the distribution of the events (Figure 22D). The results reveal a shift of the covalent

population to lower values of rupture length. In percentages, 75% of the covalently functionalized samples analysed had rupture length values less than 236 nm, while only 50% of the samples functionalized by physisorption cases showed a rupture length. ELR detached either from the tip or form the PLA surface- at less than 232 nm.

4.3.5. In Vitro Cell Adhesion Studies

For the early response, the number of attached cells and cell spread areas were quantified after 4 hours of culture. In order to observe the effect of different parameters on cell short response, various conditions were tested, including non-treated PLA (no treat) and BSA-blocked PLA (BSA) as negative controls; and tissue culture polystyrene plate (TCP) and fibronectin-functionalized PLA (Fn) as positive controls.

On the other hand, PLA surfaces grafted with ELRs ($HRGD_6$) and short peptides (G_6RGDS), as well as PLA surfaces grafted with their homologous without the RGD sequence (IK_{24} and G_6RGE) were used to analyse the role of the RGD and the role of the biomolecule nature in a comparative manner.

These functionalized surfaces also had a duplicate composed by the same kind of samples that, additionally, have been blocked with a BSA solution before cell seeding. This new condition was included in order to study the effect of a competing protein on surface adsorption. Finally, another duplicate of both blocked and non-blocked sets was added on the study. In this case, the covalent grafting of the biomolecules was changed by the functionalizing process based on the physisorption, in order to analyse the role of the grafting process.

For the early cell response, the cell adhesion was quantified by measuring the number of attached cells after 4 hours of seeding. In order to compare different samples between them, TCP was used as reference and all other samples were normalized against it (Figure 23).

In this adhesion study it is possible to see the effect of three different factors on the system. The first factor that plays an important role is the presence/absence of the RGD motif. When the surfaces functionalized with $HRGD_6$ or G_6RGDS are compared with the surfaces functionalized with IK_{24} or G_6RGE, the two former setups presented higher adhesive cell rates. This behaviour can be observed in all treatments (with significant differences in BSA-blocked set).

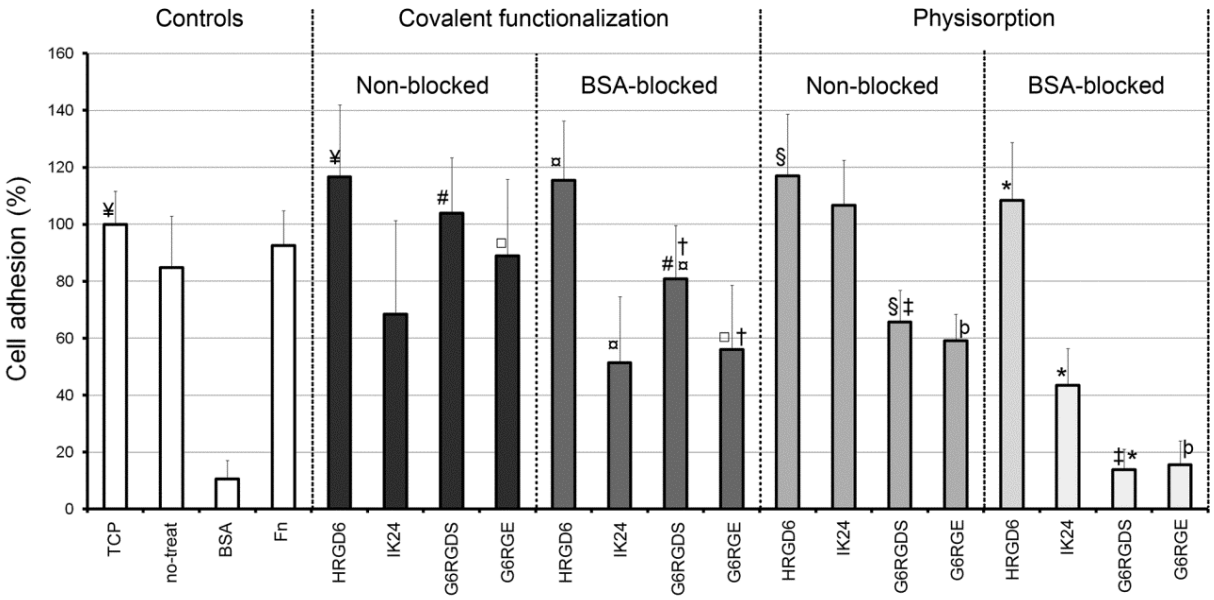

Figure 23. Adhesion assay performed on surfaces functionalized with different conditions. Cell number was calculated from LDH activity and normalized against positive control TCP. Error bars represented standard deviation. Statistical significance between paired data was represented with # (blocked and non-blocked G_6RGDS covalently functionalized), □ (blocked and non-blocked G_6RGE covalently functionalized), * (physisorbed $HRGD_6$, IK_{24} and G_6RGDS blocked with BSA), ¥ (non-blocked $HRDG_6$ covalently functionalized and TCP control), † (covalently functionalized G_6RGDS and G_6RGE peptides blocked with BSA), ‡ (blocked and non-blocked physisorbed G_6RGDS), § (non-blocked, physisorbed $HRDG_6$ and G_6RGDS), ¤ ($HRGD_6$, IK24 and G_6RGDS covalently functionalized molecules blocked with BSA), þ (blocked and non-blocked physisorbed G_6RGE) symbols.

The second factor relates to the nature of the construct used to present the RGD sequence (Mw, charge…). In this sense, the use of ELRs shows a stronger enhancement of cell adhesion compared to peptides. Quantitatively, on covalently functionalized samples the $HRGD_6$ surfaces shows ~13% more adhered cells than surfaces treated with peptides. On the other hand, on samples functionalized by physisorption, the $HRGD_6$ surfaces show a 51% more adhered cells.

The third factor that plays a role in the system is the presence/absence of the covalent bond (in terms of stability). The effect of the covalent attachment is strongly detected with the introduction of the BSA protein in the system, which competed with adhered molecules for the unspecific adsorption on surface.

For instance, $HRGD_6$ covalently functionalized samples shows 35% more adhered cells than peptides when BSA is added into the system (instead of the previous 13%). And in the case of physisorbed surfaces, the difference between ELRs and peptides raises to 95%. This means that when BSA is applied in the systems functionalized with peptides by physisorption, the cell attachment drops until almost null values. However, when the same situation is studied in a system with covalently functionalized peptides, the cell response drops significantly (23%

respect to the non-blocked sample), but there is still 81% of cells adhered. On the other hand, the functionalization procedure appears not to affect HRGD6 functionalized samples (in terms of adhered cell numbers) as the percentages for all treatments are similar: covalent/no-BSA: 117%, covalent/BSA: 115%, physisorbed/no-BSA:117%, physisorbed/BSA: 108%.

However the effect of the covalent ligation is observed on the spreading of cells along the surfaces. Quantitative measures of cell spreading reveal that the largest cell areas are found on PLA surfaces functionalized with $HRGD_6$ using the covalent ligation, with values higher than the TCP control and similar to the Fn control (Figure 24). On the other hand, physisorbed $HRGD_6$ shows cell areas similar than TCP control but lower than Fn and covalent $HRGD_6$ samples. Cell area measures also show that the lowest cell area values are found on non-treated PLA negative control (despite presenting 80% of adhered cells) as well as on PLA surfaces functionalized with IK_{24} and G_6RGE (the homologous synthetic biomolecules lacking the RGD sequence). Again, peptides are strongly affected by the presence of BSA, since cell areas are almost reduced by half when this protein is applied. Peptides functionalized by physisorption showed only 60% of cell adhesion (compared to control), thus they have not been included in the study.

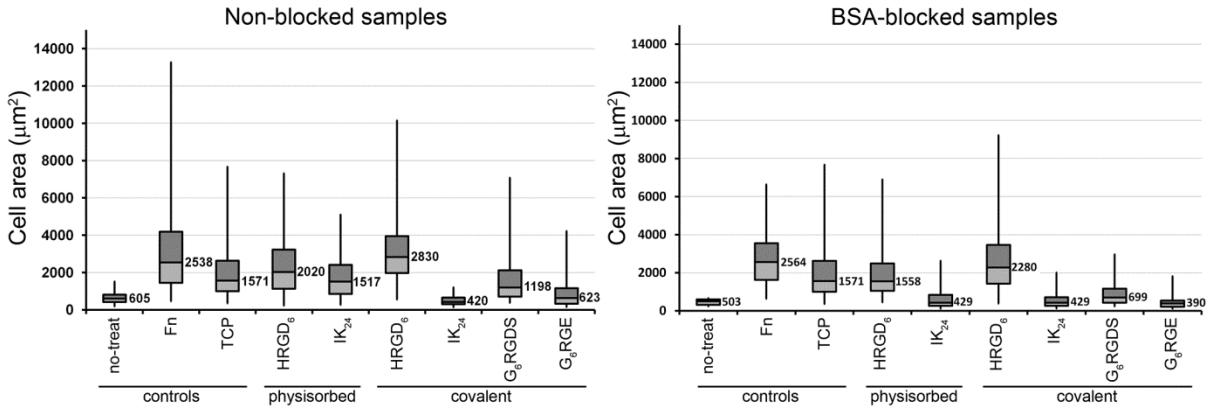

Figure 24. Box-plot graph of cell area distribution for different treated samples. The square boxes represented the 2nd and 3rd quartile of the distribution (50% of the population) and the bars represented the 1st and 4th quartile of the distribution (the remaining 50% of the population). Bars indicated the maximum and minimum values found on distribution. The 0.25% of population found on both extremes of the distribution was excluded from the graph. The same TCP positive control (without blocking with BSA) was used on both graphs. Numerical values shown on each condition represented the median values of the distribution.

To have the full view of the adhesion process, the morphology of cells has been studied as well and correlated with the adhesion and spreading results. The shape of the cells have been observed by fluorescence microscopy and classified following a quantitative shape descriptor.

For this purpose, the Aspect Ratio (AR) has been calculated from cell images. AR is defined as the relation between the major axis and the minor axis of the smallest ellipse that can fit the cell area and is obtained through the processing of the images with the ImageJ software (Table 9).

Table 9. AR median values of cell populations seeded on different treated samples.

	Controls			Physisorbed		Covalent			
	No treat	**Fn**	**TCP**	**$HRGD_6$**	**IK_{24}**	**$HRGD_6$**	**IK_{24}**	**G_6RGDS**	**G_6RGE**
BSA-blocked	1.08	1.69	-	1.53	1.28	1.55	1.36	1.62	1.32
Non-blocked	1.24	1.51	1.47	1.46	1.46	1.51	1.29	1.38	1.34

Median values are represented on the table, since population was distributed on a non-Gaussian shape (as observed in cell area studies). Considering the results, values placed between 1.08 and 1.24 (negative controls) are used to define round shape and, therefore, poor adhesion state. Instead, values placed between 1.47 and 1.69 (positive controls) are used to define elongated shape and, therefore, advanced adhesion state. Other values found in between these two frames represent an intermediate adhesion state. Using these quantitative data it is possible to see that only molecules with RGD sequence have values larger than 1.47, which include both $HRGD_6$ and G_6RGDS molecules. However, when these values are analysed in correlation with fluorescent images and spread area results, it is possible to observe that, while cells adhered on surfaces treated with G_6RGDS molecules present smaller cell areas and a star shape conformation with non-evident actin stress fibres formation, cells adhered on surfaces treated with $HRGD_6$ molecules present large cell areas as well as strong stress fibres formation. So, even if focal points are observed on all (and only) surfaces functionalized with molecules having RGD sequence, not all of them present the same advanced adhesion state. For that reason, when cytoskeleton organization is analysed by fluorescence microscopy, three cell shape states are used to define the degree of cell adhesion. Round shape is used to define the less advanced state of adhesion (non-anchored cells). The star shape represents an in-between stage in which cell has begun to spread its lamellipodia and to develop the first anchorages. And a full spread cell shape with clear stress fibres is defined as the stage in which cell is strongly attached. The qualitative results from cytoskeleton staining as well as focal points observation are shown on Figure 25.

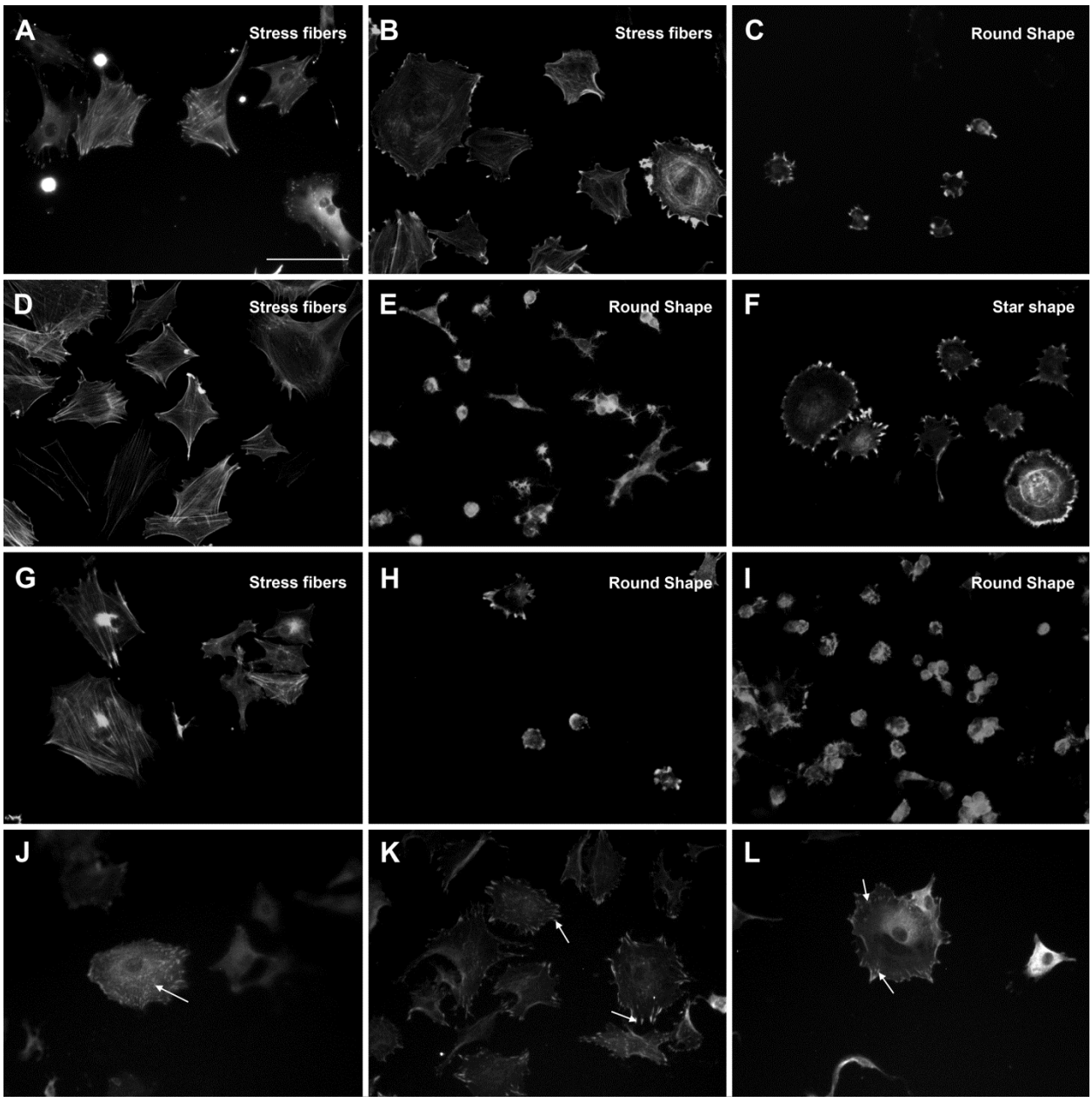

Figure 25. Immunofluorescence images of cells seeded on (A) TCP, (B) PLA-Fn, (C) non-treated PLA, (D) PLA-$HRGD_6$ covalently functionalized, (E) PLA-IK_{24} covalently functionalized, (F) PLA-G_6RGDS covalently functionalized, (G) PLA-$HRGD_6$ physisorbed, (H) PLA-IK_{24} physisorbed, (I) PLA-G_6RGDS, (J) PLA-$HRGD_6$ covalently functionalized, (K) PLA-$HRGD_6$ physisorbed and, (L) PLA-G_6RGDS covalently functionalized. Images A-I correspond to stained actin cytoskeleton of cells using rhodamin-phalloidin. Cytoskeleton organization is classified according the visualization of stress fibres, a star shape or a round shape (from more to less organized). Images J-L corresponds to stained vinculin using anti-vinculin antibody. White arrows indicate the presence of focal points. Cell cytoskeleton is stained with phalloidin-rhodamine. Scale bar = 100 μm.

Results show that the lack of the RGD sequence (non-treat, and IK_{24} control samples, see Figure 25C, E, F, H and I) led to an absence of focal points formation. Thus, the $HRGD_6$ treated surfaces (Figure 25D and G) are the only samples in which cells have an organized cytoskeleton with strong stress fibres (like in TCP and Fn positive control, see Figure 25A and B). On the

other hand, samples functionalized with G_6RGDS peptide present cells in a lower adhesion state. This means that, despite the presence of focal points, cells remain in star shape geometry, without defined stress fibres. Besides, cells seeded on IK_{24} and G_6RGE treated surfaces present the poorest cell interaction, having no focal points formation and even round shape geometry, both indicators of a weak cell attachment.

4.3.6. In Vitro Cell Proliferation Studies

For the long cell response study, cell proliferation was analysed (Figure 26). For that purpose cell growth was quantified with Alamar Blue and the cumulative population doubling level was calculated after 8 days of culture, which coincided with the beginning of cell confluence for Fn, TCP and $HRGD_6$ samples. Between functionalized PLA samples, the highest proliferation rate can be found on the covalently functionalized $HRGD_6$ surface, followed by the physisorbed functionalized $HRGD_6$ surface with no statistical differences. Other samples like non-treated surfaces or short peptide functionalized surfaces show significantly smaller differences compared to the first ones. These differences increase the evidence that the ELRs clearly improve cell response when compared with the use of short peptide.

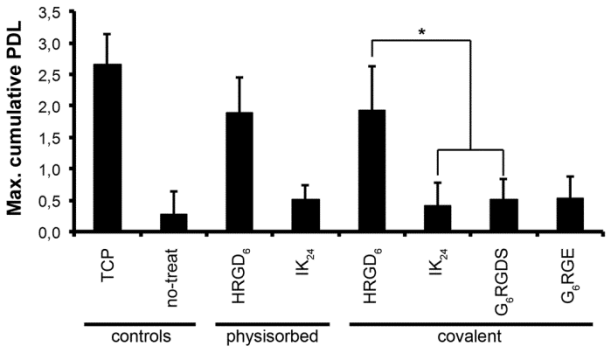

Figure 26. Proliferation assay of cells seeded on different treated samples. Growth ratio was represented by the maximum cumulative population doubling levels (PDL). Asterisk stands for statistical significance.

4.4. Discussion

One of the most difficult aspects on the study of biomaterials is to control and analyse the characteristics of the interface between the material and the surrounding cells and tissue. In this work the cell-materials interaction for biofunctionalized PLA surface is studied. A comparative study between the most used strategy to guide cell activity (introduction of the RGD peptide on the surface) and the use of a genetically modified protein derived from elastin (ELRs) has been carried out.

ELISA test was used to ensure the performance of the ligation step as well as optimize the functionalization procedure. Indirectly, the absence of PEG-b signal on the sample lacking NaOH treatment demonstrates the occurrence of the ligation step. Furthermore, the measured levels of the PEG-b probe frame the maximum yields of available carboxyl groups between 5 and 30 minutes of NaOH treatment. The decrease on the PEG-b signal along time observed during the ELISA assay may be correlated with the increasing surface roughness observed in the AFM assays and the subsequent steric hindrance. This might be the case, because the roughness dimensions are placed in the same range than the size of the PEG probe, which can affect its disposition and functionality [31]. Combining the observations from the ELISA tests and the roughness studies, a hydrolysis time of 30 minutes was selected as optimal for the functionalization, since it presented the maximum grafting capability and fell in the second region of the roughness evolution as function of time.

The analysis of the three-dimensional surface geometry revealed a constant and random surface, with a roughness range placed far below the cellular size. This roughness ensures that the topographic features do not play a role in the cellular response, as was observed in other previous studies. Indeed, it is known that roughness larger than 10 nm is needed for enhancing cell attachment or trigger an effective differentiation process [32,33].

The fluorescent micrographs of micropatterned functionalized PLA surfaces were used as a second and visual confirmation of the surface grafting. In such a way it was possible to corroborate that not only small molecules (like PEG-b or short peptides), but also larger molecules (like proteins), could successfully functionalize the model PLA surfaces.

Micropatterning was also used to analyse the expected non-fouling property of ELRs. Indeed, the reversed fluorescent pattern observed on samples functionalized with BSA and ELRs suggest that ELRs are able to cover the surface and protect it from non-specific protein adsorption. The inability of the BSA-FITC molecule to adsorb on functionalized regions with BSA or ELR may indicate the existence of a non-fouling surface. Meanwhile, the functionalization carried out by means of peptide does not show this capability. Probably, the small dimension of peptides does not allow a good coverage and protection of the surface.

Experiments based on AFM force-distance curve analysis were carried out to assess how covalent functionalization affected the ELR degree of mobility. The maximum rupture lengths for the functionalized ELR meshes (covalently and physisorption) were analysed. Distribution of the rupture lengths shows that, for the covalently functionalized samples, the mobility degree of

ELRs chains was restricted. Indeed, covalent samples present lower maximum rupture lengths. This corroborates the presence and the effect of the covalent attachment, which reduces the pulling distances, maintaining the ELR closely attached to the surface. However, ELRs covalently attached are still able to be stretched from ~90 nm to 458 nm, which confers a high degree of mobility to the ELRs mesh. This ELR mobility can be translated (in biological terms) as a capability to be rearranged by cells, which is a key factor for the development of the cell adhesion processes like the clustering of integrins during focal points formation [7].

Moreover, AFM studies showed that ELRs are distributed along the entire surface, since the polymer mesh pulling profile can be observed only for functionalized surfaces and all over the analysed area. Parallel to this, the ELRs swelling observed in the AFM images are able to explain the increased wettability of the surface noticed during the performance of the experiments (not shown). This increased wettability may contribute to the good performance of the ELRs, since they facilitate the interaction of cells and substrate [34].

Finally, to correlate the effect of the functionalization procedure with the biological response, the cell response was studied. For that reason, cell attachment was analysed by means of number of attached cells and spread cell area. Moreover, the BSA protein was used as a competing agent for the unspecific adhesion in order to see the effect of non-fouling ELR surfaces as well as the stability of biomolecules grafted on surface.

The biological results indicate that is possible to conclude that the studied molecules are affected by the adsorption of a competing protein when they are physisorbed. Especially, surfaces functionalized with short peptides have their biological response dramatically reduced to almost zero values. This effect can be explained by the displacement of functionalized molecules as a result of the BSA competing unspecific adsorption. On the other hand, surfaces with physisorbed $HRGD_6$ have shown to maintain similar cell attachment ratios without significant differences. This stability against BSA protein is supported by the non-fouling capability of ELRs. In such a way, BSA is not able to displace ELRs or to mask them to cells.

Despite the similar results found on ELRs functionalized samples in terms of amount of attached cells, cell areas values shows clear differences between the functionalization procedures. Actually, physisorbed ELRs samples blocked with BSA present only the 25% of the cell population over the 2500 μm^2 of spread area, while samples covalently functionalized with ELRs have more than the 50% of measured cell area values over the 2500 μm^2. This correlation between the covalent ligation and the cell area spreading may be related to the good transmission

of the mechanical properties that the covalent ligation causes between cell attachment points and the surface. In fact, the role of the covalent attachment of integrin ligands is known to be not only important for mechanical properties transmission, but also for the molecular stability in terms of prolonged efficacy and reproducibility [7]. IK_{24} modified surfaces shows small cell areas (similar to non-treated PLA samples), proving that no strong attachment occurred. When these results are compared with the larger cell areas found on $HRGD_6$, it is possible to conclude that ELRs can regulate the selective attachment of specific cell types through the incorporation or not of specific integrin ligands.

Also, when cell areas are compared between the ELRs and peptides sets, it is clear that peptides do not promote the same biological response. Despite the fact that peptides enhance cell attachment when compared to naked PLA, the measured cell areas are significantly smaller than the areas found on ELRs, TCP and Fn samples. Moreover, cell area differences between covalent $HRGD_6$ and physisorbed $HRGD_6$ are not related with a less developed cytoskeleton and focal points (in both cases actin fibres and focal points were found). However, the differences between peptides and ELR are correlated to the absence of stress fibres on the former. This lack of cytoskeleton organization after 4h of seeding confirms that peptides create a less suitable environment at the interface. These cell response differences between ELRs and peptides were emphasized with proliferation the studies, in which cells grew at smaller ratios over PLA samples functionalized with peptides than ELRs.

4.5. Conclusions

The functionalization of biomaterials surfaces using engineered proteins has been explored in this chapter. These molecules have shown to be a viable alternative to the use of natural proteins and short peptides, achieving similar or better performance than these two strategies. The functionalization of PLA model surfaces with ELRs has shown a strong potential to incorporate many tailored properties in one molecule. From the molecular point of view, ELRs have been demonstrated to provide more suitable conditions for cell attachment than short peptides. Their physico-chemical properties, closer to the natural protein than bioactive peptides, have been able to enhance the interaction of the cells and the material at the interface in a stronger manner than peptide (higher cell adhesion rates, better cell spreading, stronger attachment and faster proliferation). Moreover, ELRs seem to be non-fouling, which minimizes the unspecific adsorption of proteins. In a similar manner, the backbone of the ELR (represented with the IK_{24} molecule) has proved not to assess a good attachment of cells. However, when the RGD integrin ligand sequence was added to the backbone ($HRGD_6$), an enhancement of the cell

attachment was observed. This poor interaction of the module VPGIG ensured that cell attachment was driven by the integrin ligand sequences added in the molecule [35]. In such a way, specific cell interactions were obtained. Finally, the observations of the role of the covalent bond suggest that a tight attachment on the surface improves cell spreading, which is related with the transmission of the mechanical properties form surface to cell through the covalent grafting.

Given the successful performance of the ELRs, these molecules can be used to induce stronger and faster cell responses in biomaterials than peptides. Moreover, ELRs can be tailored to induce the attachment of specific cell types in a specific manner [36].

4.6. References

1. Suzuki S, Ikada Y. Medical Applications. In: Auras R, Lim LT, Selke SEM, Tsuji H. Poly(lactic acid): Synthesis, Structures, Properties, Processing, and Applications. John Wiley & Sons: New Jersey, 2010. p. 443-456.
2. Ueda H, Tabata Y. Polyhydroxyalkanonate derivatives in current clinical applications and trials. Adv Drug Deliv Rev 2003;55(4):501-18.
3. Puleo DA, Thomas MV. Implant surfaces. Dent Clin North Am 2006;50(3):323-38,v.
4. Rasal RM, Janorkar AV, Hirt DE. Poly(lactic acid) modifications. Prog Polym Sci 2010;35:338-56.
5. Wong LS, Khan F, Micklefield J. Selective covalent protein immobilization: strategies and applications. Chem Rev 2009;109(9):4025-53.
6. Desmet T, Morent R, De Geyter N, Leys C, Schacht E, Dubruel P. Nonthermal plasma technology as a versatile strategy for polymeric biomaterials surface modification: a review. Biomacromolecules 2009;10(9):2351-78.
7. Hersel U, Dahmen C, Kessler H. RGD modified polymers: biomaterials for stimulated cell adhesion and beyond. Biomaterials 2003;24(24):4385-415.
8. Delaittre G, Greiner AM, Pauloehrl T, Bastmeyer M, Barner-Kowollik C. Chemical approaches to synthetic polymer surface biofunctionalization for targeted cell adhesion using small binding motifs. Soft Matter 2012;8:7323-47.
9. Williams, DF. The role of short synthetic adhesion peptides in regenerative medicine; The debate. Biomaterials 2011;32:4195-7.
10. Collier JH, Segura T. Evolving the use of peptides as components of biomaterials. Biomaterials 2011;32(18):4205-10.
11. Bellis SL. Advantages of RGD peptides for directing cell association with biomaterials. Biomaterials 2011;32:4205-10.
12. Barker, TH. The role of ECM proteins and protein fragments in guiding cell behavior in regenerative medicine. Biomaterials 2011;32:4211−4.
13. Nettles DL, Chilkoti A, Setton LA. Applications of elastin-like polypeptides in tissue engineering. Adv Drug Deliv Rev 2010;62(15):1479-85.
14. Rodríguez-Cabello JC, Martín L, Alonso M, Arias FJ, Testera AM. "Recombinamers" as advanced materials for the post-oil age. Polymer 2009;50:5159-69.
15. Girotti A, Reguera J, Rodríguez-Cabello JC, Arias FJ, Alonso M, Matestera A. Design and bioproduction of a recombinant multi(bio)functional elastin-like protein polymer containing cell adhesion sequences for tissue engineering purposes. J Mater Sci Mater Med 2004;15(4):479-84.

16. Prieto S, Shkilnyy A, Rumplasch C, Ribeiro A, Arias FJ, Rodríguez-Cabello JC, Taubert A. Biomimetic calcium phosphate mineralization with multifunctional elastin-like recombinamers. Biomacromolecules 2011;12(5):1480-6.

17. Zio KD, Tirrel DA. Mechanical Properties of Artificial Protein Matrices Engineered for Control of Cell and Tissue Behavior. Macromolecules 2003;36(5):1553−58.

18. Lee J, Macosko CW, Urry DW. Phase transition and elasticity of protein-based hydrogels. J Biomater Sci Polym Ed 2001;12(2):229-42.

19. Sandberg LB, Soskel NT, Leslie JG. Elastin structure, biosynthesis, and relation to disease states. N Engl J Med. 1981 Mar 5;304(10):566-79.

20. Urry DW. Molecular Machines: How Motion and Other Functions of Living Organisms Can Result from Reversible Chemical Changes. Angew Chem Int Ed Engl 1993;32:819-41.

21. Meyer DE, Chilkoti A. Purification of recombinant proteins by fusion with thermally-responsive polypeptides. Nat Biotechnol 1999;17(11):1112-5.

22. Daamen WF, Hafmans T, Veerkamp JH, Van Kuppevelt TH. Comparison of five procedures for the purification of insoluble elastin. Biomaterials. 2001 Jul;22(14):1997-2005.

23. Costa RR, Custódio CA, Testera AM, Arias FJ, Rodríguez-Cabello JC, Alves NM, Mano JF. Stimuli-Responsive Thin Coatings Using Elastin-Like Polymers for Biomedical Applications. Adv Funct Mater 2009;19:3210−18.

24. Jiao YP, Cui FZ. Surface modification of polyester biomaterials for tissue engineering. Biomed Mater 2007;2(4):R24-37.

25. Hermanson GT. The Chemistry of Reactive Groups, In: Elsevier (ed.). Bioconjugate Techinques (2nd ed). London: Elsevier, 2008, 169-212.

26. Xia Y, Whitesides GM. Soft Lithography. Angew Chem Int Ed Engl 1998;37:550-75.

27. Hutter JL, Bechhoefer J. Calibration of Atomic-Force Microscope Tips. Rev Sci Instrum 1993;64:1868-73.

28. González-Vázquez A, Planell JA, Engel E, Extracellular calcium and CaSR drive osteoinduction in mesenchymal stromal cells. Acta Biomater 2014;106:2824-33.

29. Cristofalo VJ, Allen RG, Pignolo RJ, Martin BG, Beck JC. Relationship between donor age and the replicative lifespan of human cells in culture: a reevaluation. Proc Natl Acad Sci U S A 1998;95(18):10614-9.

30. Cao Y, Liu W, Zhou G, Cui L. Tissue engineering and tissue repair in immunocompetent animals: tissue construction and repair. Handchir Mikrochir Plast Chir 2007;39(3):156-60.

31. Kasemo B, Gold J. Implant surfaces and interface processes. Adv Dent Res 1999;13:8-20.

32. Chung TW, Liu DZ, Wang SY, Wang SS. Enhancement of the growth of human endothelial cells by surface roughness at nanometer scale. Biomaterials 2003;24(25):4655-61.

33. Khang D, Choi J, Im YM, Kim YJ, Jang JH, Kang SS, Nam TH, Song J, Park JW. Role of subnano-, nano- and submicron-surface features on osteoblast differentiation of bone marrow mesenchymal stem cells. Biomaterials 2012;33(26):5997-6007.

34. Wilson CJ, Clegg RE, Leavesley DI, Pearcy MJ. Mediation of Biomaterial–Cell Interactions by Adsorbed Proteins: A Review. Tissue Eng 2005;11(1-2):1-18.

35. Nicol A, Gowda DC, Urry DW. Cell adhesion and growth on synthetic elastomeric matrices containing Arg-Gly-Asp-Ser-3. J Biomed Mater Res 1992;26(3):393-413.

36. Garcia Y, Hemantkumar N, Collighan R, Griffin M, Rodriguez-Cabello JC, Pandit A. In vitro characterization of a collagen scaffold enzymatically cross-linked with a tailored elastin-like polymer. Tissue Eng Part A 2009;15(4):887-99.

CHAPTER 5

5. A NOVEL AND VERSATILE SCAFFOLDING TECHNIQUE

Scaffolds play an important role on regenerative medicine owing to their capacity to direct tissue reconstruction by means of physical and chemical cues. Indeed, scaffolds are necessary on the regeneration processes in which cells have to form and develop a new tissue in a three-dimensional space. However the presence of scaffolds into the clinics is reduced and most existing products stand for epithelium regeneration (like skin or internal ulcers). The current challenges for the translation into the clinics are centred on the development of processes that are able to create scaffolds in a reproducible, cheap and easy manner, while at the same time control the scaffold physical properties in a tailored way (i.e., architecture, mechanical behaviour, porosity and diffusivity). This chapter will present, describe and analyse a novel process able to obtain scaffolds with high control on their properties by means of a two-step methodology that uses, exclusively, biocompatible materials.

5.1. Introduction

There are many strategies for a technology to enter into the market minimizing risks and capturing value. For instance, an incremental approach based on already tested and approved technology reduces the risk and uncertainties and facilitates regulatory approval and clinical acceptance. On this chapter, a technique with a strong potential to be used on scaffold design and production is developed and characterized. This technique uses as raw material two different components that are already present in commercial devices, clinical products and food products, and therefore, their safety has been already accepted by regulatory organisms like the Food and Drug Administration (FDA).

The first component is the poly(lactic) acid (PLA) synthetic polymer and its co-polymers. PLA has been extensively used in surgery and medical device implantation [1], and therefore the regulatory constrains regarding him are very low. The most interesting properties of PLA are the degradability, biocompatibility and mechanical properties as well as its easy processing. Moreover, PLA is an accessible product, manufactured and commercialized by many companies. Furthermore, PLA degradation can be regulated through their crystallinity, molecular weight (Mw), glass transition temperature (Tg), hydrophobicity and surface area exposure [2-7]. PLA is biocompatible and is degraded by hydrolytic chain scission [5]. Their by-products are also non-toxic and can be resorbed by the body, which is ideal for regenerative purposes [8]. PLA is a chiral molecule, and can refer to the L- and D- isomer, or a combination of both. While the L-isomer is the biological metabolite, no adverse physiological effects are reported for the D-isomer [9]. All kind of PLA racemic combinations and copolymers can be found on the market, produced under GMP processes for reasonable good prices [10].

The second component is ethyl lactate (EtLac). EtLac is an FDA approved organic solvent with dipolar properties that confers to him the special capability to wet and dissolve PLA while being miscible with water [11,12]. Moreover, this solvent is non-toxic in low quantities [13], and can be metabolized into the body, being an interesting green product for the pharmaceutical industry [14].

The scaffolding technique that combines both components implies the inherent and special characteristic of EtLac to dissolve PLA at high temperatures, and produce an organogel when the solution is cooled down. Organogels are gels formed by an apolar phase (i.e. EtLac) that is immobilized within the spaces of a three-dimensional network formed due to the physical interactions amongst the self-assembled structures of compounds regarded as gelators (i.e. PLA

molecules). These gels are characterized for being thermodynamically stable and having a thermoreversible gelation behaviour which depends on temperature, gelator concentration and gelator molecular structure. Moreover, organogels can present a series of different interesting characteristics like optical and viscoelastic properties, biocompatibility and the capability of being used as drug delivery agents [15,16].

Organogels can be obtained from very different systems (small peptides, low molecular weight molecules, polymers and so on) [15,17]. Polymers, especially poly(α-hydroxy acids), have been used on the production of biomaterials scaffolds. More specifically, PLA-based polymers were used in combination with tetrahydrofuran (THF) solvent to obtain organogels which were later phase separated by water immersion or freeze drying, in order to obtain highly porous nanofibrous matrices [18,19]. This technique was very innovative and allowed the formation of nanostrured fibrous matrices using few and easy steps. However, it was based on the gelation of PLA in a very toxic component which is an important setback during safety regulation. Actually, the use of toxic solvents many times is not considered during research development, but it is an issue of great concern. For instance, when using chloroform for the obtaining of scaffolds, it has been studied that, even after one week of drying, the remaining amount of chloroform can be up to 0.5% wt., which is equivalent to 5000 ppm [20]. However, the amount of residual chloroform permitted in drugs, in the US, is 60 ppm [21].

Because the use of toxic organic solvent is of great concern not only on safety terms but also on operative terms (residual by-products management), this chapter will present a novel alternative based on the system composed by PLA and EtLac. The PLA/EtLac system can form an organogel by means of gelation, which can be phase-precipitated into water to obtain highly porous scaffolds with nanofibrous structure that resembles the extracellular matrix (ECM). Moreover this chapter will go deeply in the analysis of organogelation and the study of the properties of the resultant scaffolds, gathering in such a way a comprehensive study in which initial inputs (gelation time, gelator concentration, gelating temperature and warming conditions) are correlated with the resultant outputs (mechanical and viscoelastic properties, porosity, nanostructure, diffusion rate and shrinkage). Thus, with the present technique, highly porous scaffolds with tailored properties are obtained by means of a cheap, easy, clean, safe and reproducible two-step process.

5.2. Material and Methods

5.2.1. Materials

Poly–L/DL lactic acid 70/30 (Purasorb PLDL 70/38, inherent viscosity midpoint 3.8 dl/g, Mw≈ 850,000 Da) was purchased from Purac Biomaterials (The Netherlands).

Ethyl Lactate 99% photoresist grade was purchased from Sigma and used without further purification.

5.2.2. Poly(lactic) acid Scaffolds Preparation

PLA was dissolved in EtLac at 54ºC and stirring conditions until complete dissolution. Then, the PLA/EtLac solution was poured into the desired mould avoiding the formation of bubbles and placed at cold temperatures until complete gelation occurred. When the gel was completely formed, it was removed from the mould and immersed into Milli-Q water. Finally, due to the diffusion of EtLac into water, solvent was exchanged and PLA precipitated by phase separation. The scaffolds were washed several times with water.

For long storages or experimental needs, PLA scaffolds were lyophilized and kept in dry conditions. Reconstitution was carried out by immersing lyophilized scaffolds into ethanol and exchanging the ethanol phase by water with several washing steps.

5.2.3. Rheometry

Rheometric assays were performed in a DHR rheometer system (TA Instruments) with a Peltier Plate as temperature control system.

For the viscosity measurements, PLA/EtLac solutions of 4%, 7% and 10% concentrations were heated until 70 ºC and studied in flow mode. Viscosity was measured for a range of shear rates going from 10^{-5} till 10^{3} s^{-1}.

Gel Temperature (T_{GEL}) was found following a methodology based on the gelator concentration independency principle [22]. For this purpose, the gelation time as a function of temperature was studied for the different concentrations. Obtained gelation curves were plotted, and the convergence point was found by extrapolation. The gelation times (t_{gel}) needed for the creation of the gelation curves were found by analysing the crossing of the tanδ during the gelation process for each sample at each temperature in a tanδ versus time plot [23]. Studied concentrations ranged from 4% until 8% and studied temperatures ranged from 5ºC until 25ºC.

The study of the tanδ evolution was carried out in oscillatory mode conditions. Frequencies used for the assay were ranged between 0.5 and 2 Hz and the applied strain was 0.5%.

Gelation kinetics was studied in oscillatory conditions, using frequencies ranged between 0.5 and 2 Hz and a 0.5% strain. The evolution and completion of the gelation process was followed by recording the evolution of the storage modulus (G') in time, until a Plateau level was reached. PLA/EtLac concentrations of 4%, 7% and 10% pre-warmed at 50 ºC were used for the analysis, and two different temperatures were assayed: 5ºC and 10ºC. Additionally, 4% solution pre-warmed at 46ºC was analysed as well.

The shrinkage occurred during the gelation process was studied through the gap variance regulated by the axial force control of the rheometer. During the gelation process of the sample, the upper plate was set to maintain a constant normal force of zero value through the modification of the gap between plates. Therefore, when shrinkage occurred, the sensed force was modified and the gap distance was changed to restore the initial setting of zero value. Thus, the diminution of the gap was recorded in order to measure the volume reduction during the shrinkage. Same settings from kinetics studies were applied.

5.2.4. Structure Characterization

Material structure was observed by Scanning Electron Microscope (SEM). Images were obtained at intensities between 3-10 kV with a Nova NanoSEM 230 microscope. Samples were covered with 10 nm gold by sputtering.

Dry weight percentage was calculated from the ratio between the PLA and the water content. For these purpose, scaffolds were weighted after and before lyophilisation.

Diffusion was analysed by immersing cylindrical scaffolds in an aqueous dissolution of rhodamine at 0.05% (w/v) concentration. Then, scaffolds were cut transversally in order to observe rhodamine internalization. The penetrated distance to the centre was measured by image analysis with ImageJ software.

5.2.5. Mechanical Assays

Mechanical assays were carried out in a Zwick/Roell BT1-FR0.5TN.D14 testing machine. Samples were fixed using a 60N Grip system. Samples were shaped following the Standard Test Method for Tensile Properties of Plastics (ASTM D 638). The dumbbell-shaped

test specimens were fabricated by moulding process. Different PLA/EtLac concentration solutions, ranging between 4% and 10%, were used to produce test specimens.

Traction tests were carried out following the ASTM D 638 guidelines at room temperature. From the resulting stress-strain curves, several properties were calculated: Young Modulus (E modulus), tensile strength (σ_{max}), strain at tensile strength (dL_{max}), work at tensile strength (W_{max}), 0.2% offset yield strength (σ at 0.2%), 0.2% offset yield strain (dL at 0.2%) and 0.2% offset yield work (W at 0.2%).

Creep-Recovery tests were also carried out. Test specimens were fastened at 1% of strain at 1%/s speed. Then, applied stress was maintained constant for 300 seconds and elongation (dL) was recorded. Later, stress was released and maintained at zero constant value. Strain recovery was recorded for an extra 300 seconds. From Creep-Recovery test curves, the following properties were calculated: the Creep Rate (dL/dt) during the secondary creep stage (linear creep phase) and the Strain Recovery portion (dL_f/dL_{max}).

Relaxation test were carried out as follows. Test specimens were fastened at 1% of strain at 1%/s speed. Then, 1% of deformation was maintained constant for 600 seconds and stress (σ) was recorded. Relaxation ratio was calculated between initial and final stress (σ_0/σ_f).

5.2.6. Statistics

Experiments were subjected to t-Student testing ($P < 0.05$). Results were presented as mean ± standard deviation.

5.3. Results

5.3.1. Rheometry

Rheometric assays were performed to study and characterize the viscosity of PLA/EtLac solutions, the temperature at which gel starts to form (T_{GEL}), the kinetics behaviour of the gelation process and the shrinkage degree during the formation of the gel. These parameters were studied at different ratios of PLA/EtLac ranging from 4% to 10%. These parameters were selected for their relevance on the designing and setting of a production protocol.

Viscosity was studied for its importance and role on the pumping, moulding and injecting of viscous solutions during the processing. Viscosity also plays a role on the design of colloids

and suspensions, since they determine the sedimentation speed, which is important for the homogeneous application of porogen agents or other kind of particles. Therefore, among all variables affecting viscosity, temperature and shear rate were studied. For this reason, temperature was fixed at a working temperature of 70ºC, while shear rate was varied from 10^{-3} to 10^{3} s^{-1} values. This range of shear rates was selected because comprised the viscosity behaviour along different states of interest, like the steady state at low shear rates (used for the study of particle sedimentation) or the stressed state at high shear rates (used for the study of volume flow).

Figure 27 showed the viscosity of the different polymer concentrations as a function of shear rate. PLA/EtLac solutions had an inherent viscosity of about 30 to 2000 times the viscosity of water. It was also possible to observe the increasing viscosity levels when moving to shear rates below 1 – 10^{-2} s^{-1} (depending on the concentration studied), and the decreasing viscosity levels when moving to shear rates close to the 10^{3} s^{-1}. Also, after the first slope, all studied concentrations presented a plateau.

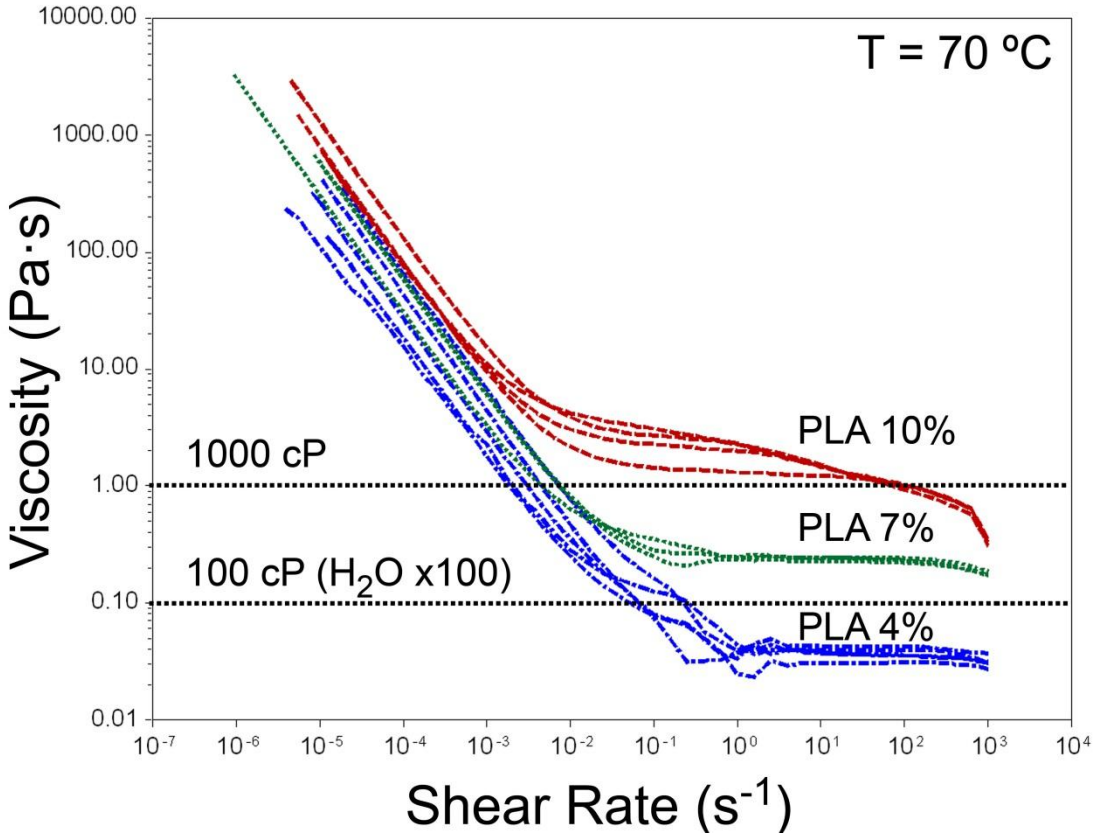

Figure 27. Viscosity behaviour as a function of shear rate for three different PLA/EtLac concentrations (4%, 7% and 10%) at 70 ºC.

Gelation curves studied by rheometry were plotted in Figure 28, and the concentration independency point was found by extrapolation. Used PLA/EtLac concentrations were 4%, 6%, 7% and 8%. The graph showed that the different curves converged into one point which determined the gel temperature point at 44.5 ºC.

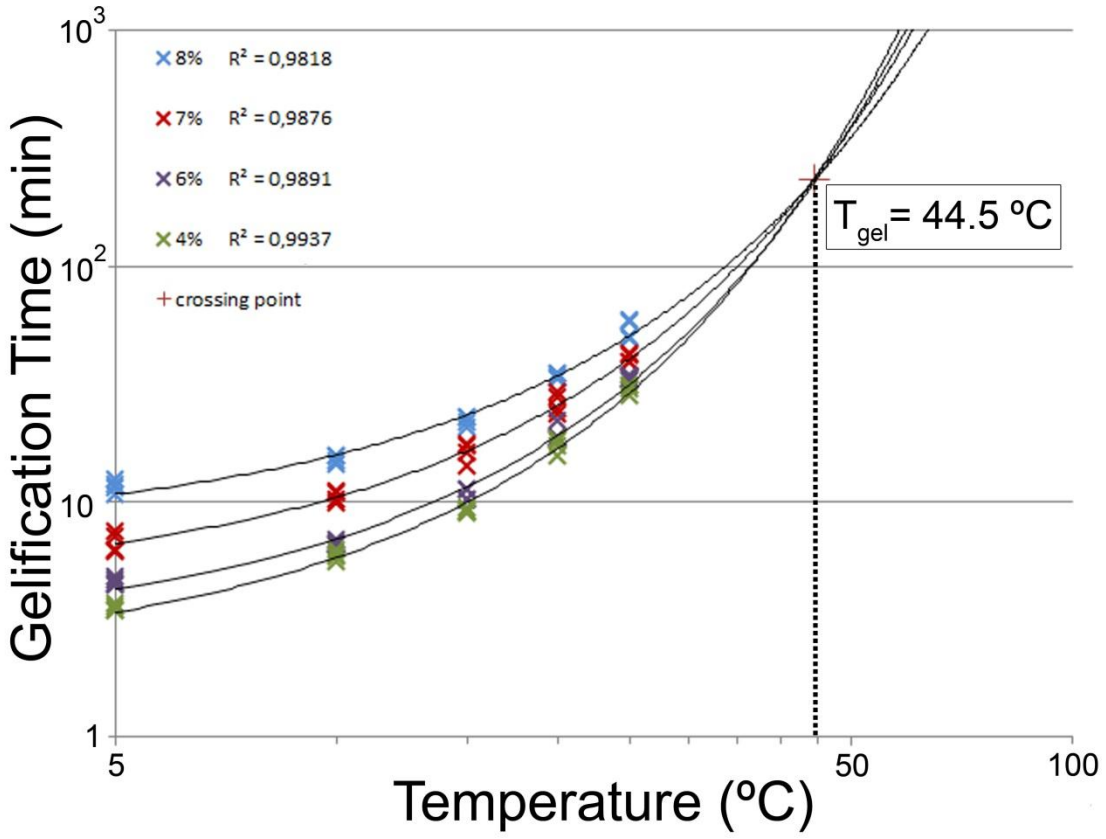

Figure 28. Gelation curves of the PLA/EtLac 4%, 6%, 7% and 8% solutions. The extrapolated crossing point defines the T_{GEL}.

Parallel to the T_{GEL} study, some of the specimens used for the analysis of the gelation time were studied for extended times (after the tanδ convergence) in order to evaluate the gelation kinetics. On this analysis, the evolution of the storage modulus (G') was recorded and plotted (Figure 29). As it is shown, the gelation kinetics was studied for sample concentrations of 4%, 7% and 10% at 5ºC and 10ºC experimental temperatures. All solutions were warmed at 50ºC prior to the study and then solutions were brought to the selected experimental temperatures (5ºC or 10ºC) to analyse the gelation kinetics and behaviour. In addition, for the 4% samples, two extra specimens were pre-warmed at 46ºC prior the gelation process. Results showed that all gelation curves achieved a plateau level after the completion of the gelation process. This final stable state was dependant on the initial gelator concentration, but independent on the experimental temperature used or the pre-warming applied. In that sense, it was possible to observe that higher concentrations were related to higher levels of storage modulus (higher levels

of stiffness). Another appreciation about the kinetics was that higher experimental temperatures (10ºC) correlated to slower speeds of gelation, this means, it was necessary more time to achieve the plateau equilibrium. Kinetics also showed, on all samples, a peak on the storage modulus achieved before the plateau level. On the first slopes before the peak, it was possible to observe higher slopes (higher speeds of gelation) for higher concentrations. Finally, when looking at 4% samples, it was possible to observe that, for same experimental temperatures, samples pre-warmed at higher temperatures (50ºC) needed more time to achieve the plateau level than samples pre-warmed at lower temperatures (46ºC).

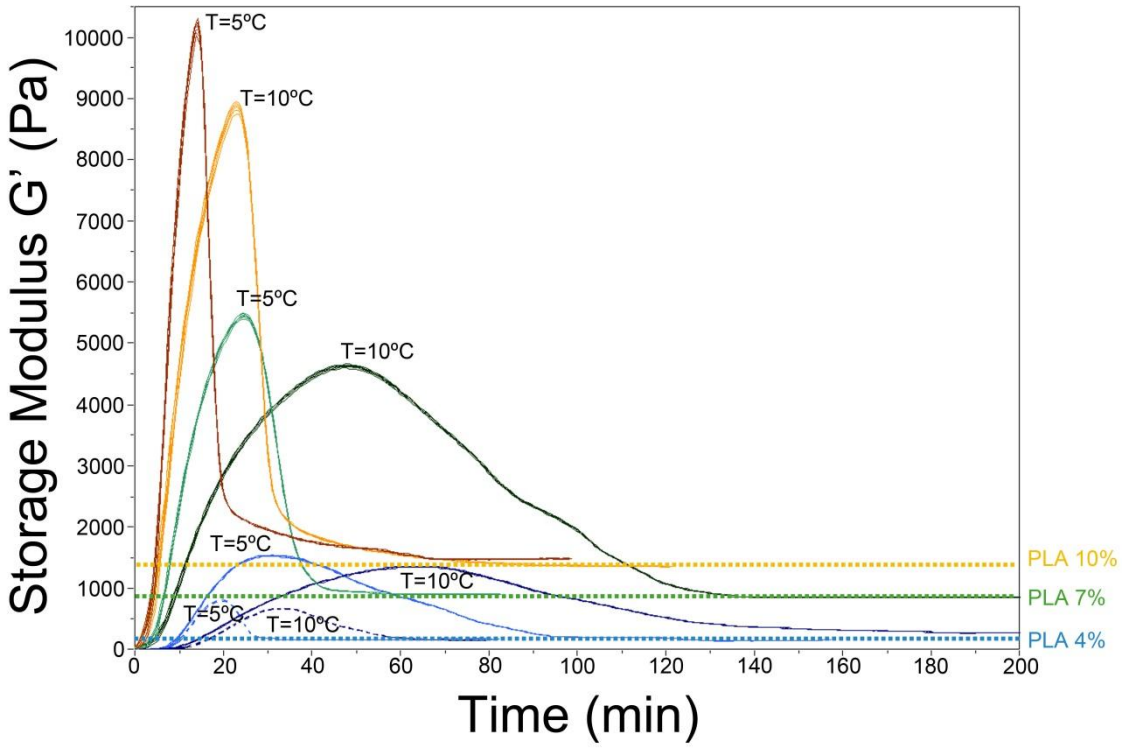

Figure 29. Gelation kinetics curves of the PLA/EtLac 4% (blue), 7% (green) and 10% (brown) solutions. Samples were studied at two different gelating temperatures (5 ºC and 10 ºC). Continuous curves stands for samples pre-warmed at 50 ºC and doted curves (only 4%, blue) stands for samples pre-warmed at 46ºC.

The last studied parameter by rheometry was the shrinkage ratio. This side effect, which was consequence of the packaging of the system during the gelation process, could be very relevant for the designing of moulds and scaffold formation. Therefore it was necessary to evaluate the magnitude of the shrinkage of the PLA/EtLac system. For this purpose, the evolution of the distance between the plates of the rheometer was analysed. During the gelation experiments, the plate to plate gap was controlled in order to maintain the normal force at a constant zero value. In such a way, when the material shrunk, the force diminution sensed by the upper plate was compensated with a reduction of the gap length. Therefore, it was possible to

know at the end of the experiment the change in volume during the gelation process. Figure 30 shows that lost volumes were ranged between 0.8% and 3.5%, with the larger shrinkage ratios found in the more concentrated samples.

Δ GAP (%)	4% PLA/EtLac	7% PLA/EtLac	10% PLA/EtLac
	0.88 ± 0.45	1.63 ± 0.41	3.51 ± 0.55

Figure 30. Measured shrinkages presented as gap reduction percentage ± standard deviation.

5.3.2. Structure Characterization

The study of gelation kinetics revealed that thermostable gels were obtained at 5ºC after 2h of gelation. Therefore, these settings were selected to obtain gels, which would be used for the formation of scaffolds. These gels, formed from different initial PLA/EtLac concentrations ranging from 4% to 10%, were used for the creation of solid scaffolds through a two-step protocol. First, solutions were gelated, and then, gels were immersed into water in order to exchange the EtLac solvent by water and induce the PLA precipitation through a phase separation process. In this way, scaffolds were obtained, whose mechanical, porous and diffusion properties depended on the initial PLA/EtLac concentration.

To observe the micro and nanostructure of the obtained scaffolds, SEM analyses were performed. SEM images from 4%, 7% and 10% concentrated samples are shown in Figure 31. From visual observation it was not possible to discern clear differences between concentrations. As it is possible to see, all images showed a random structured network conformed by nanofibers ranged below de 200 nm. Expected differences on network densities were difficult to observe by image analysis, because PLA quantities variations represented small percentages.

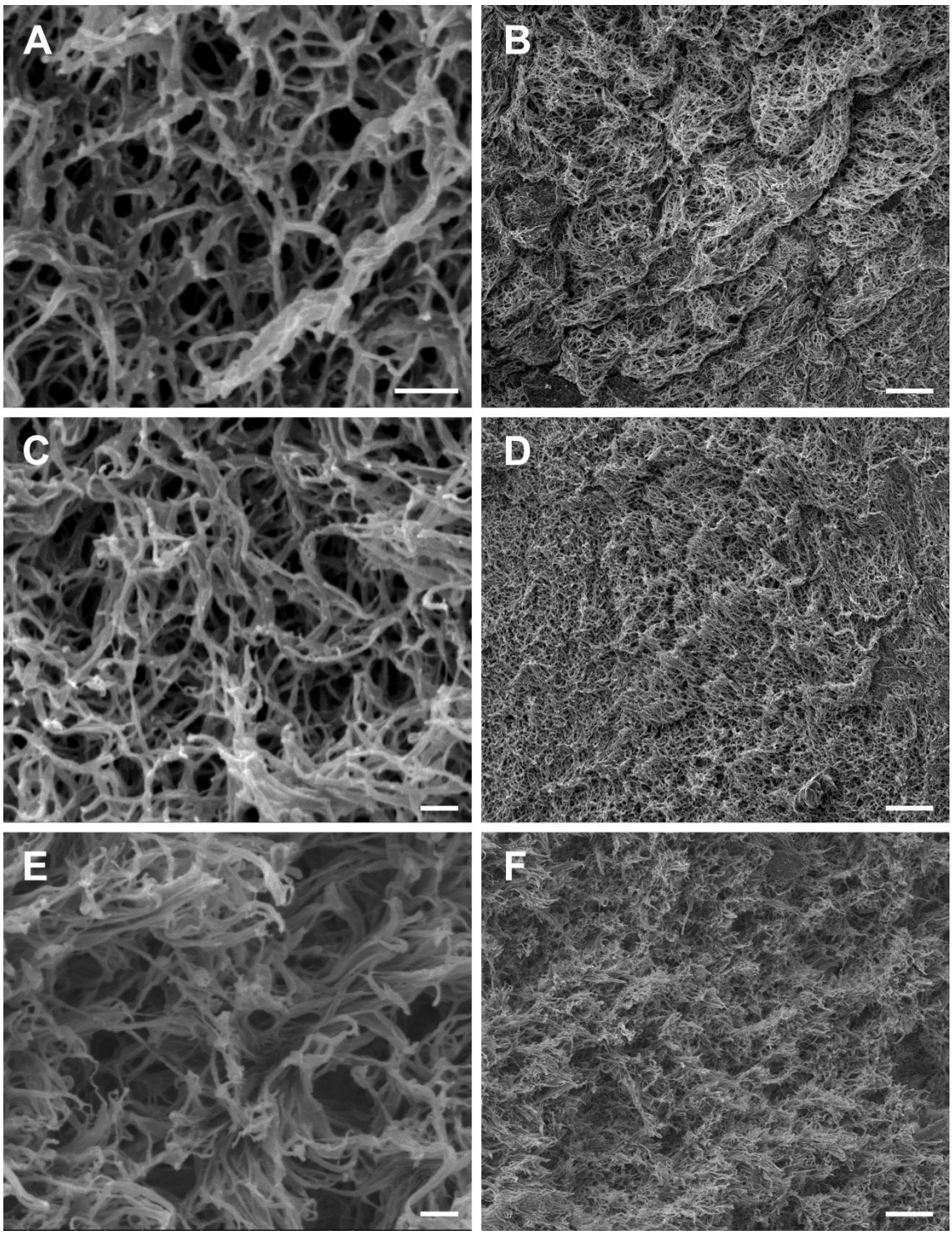

Figure 31. SEM Images of lyophilized scaffolds obtained from PLA/EtLaC concentrations of (A-B) 4%, (C-D) 7% and (E-F) 10%. Scales bars represent 1 μm on (A), (C) and (E) images; and 10 μm on (B), (D) and (F) images.

In order to verify the differences between material densities, the weight of wet scaffolds (with water entrapped inside) and the weight of lyophilized scaffolds were compared. Results showed in Table 10 revealed that the water entrapped inside represented between the 87.3% and

the 94.6% of the weight of the scaffold (10% and 4% samples respectively), which is a clear evidence of the high porosity of the scaffolds and the differences between them.

Table 10. Dry weight percentage of the scaffolds obtained from the different PLA/EtLac concentrations.

PLA/EtLac ratio	4% PLA/EtLac	7% PLA/EtLac	10% PLA/EtLac
Dry weight percentage (%)	5.39 ± 0.04	8.92 ± 0.03	12.76 ± 0.06

Since different ratios of PLA/water were observed for the different scaffolds, diffusion assays were performed (Figure 32). These assays were intended to evidence the diffusion effects due to the existing differences on the nanofibrous network density, as well as to analyse the potential capability of using such a scaffold as entrapping agents for controlled release. For the diffusion assays, cylindrical scaffolds formed from different concentrations (4%, 7% and 10%) were immersed into a rhodamine aqueous solution. Scaffolds were taken after 2h, 6h and 22h and cut transversally. The dye penetration was measured at each time point and the evolution in time was plotted (Table 11). From results, it was possible to notice a clear restriction on the dye diffusion correlated with an increase of the sample PLA concentration.

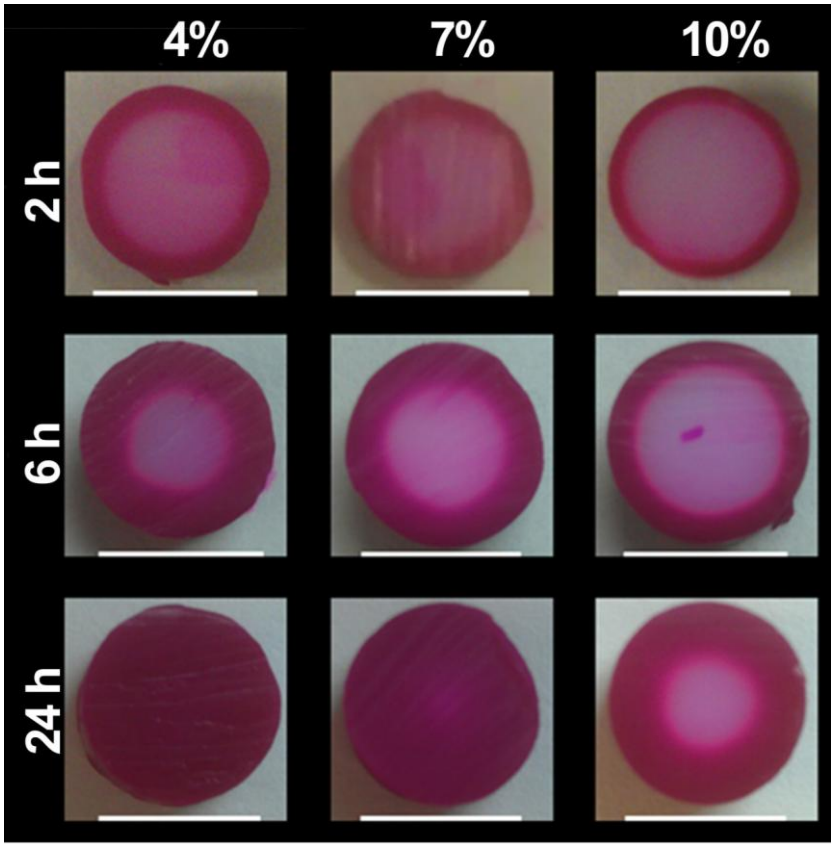

Figure 32. Images of rhodamine diffusion at different time points (2h, 6h and 22h) for different scaffold compositions (4%, 7% and 10%). Scale bars equal 1 cm.

Table 11. Measured diffusion distance as percentage of the total radius distance (± standard deviation).

	DIFFUSION DISTANCE (%)		
	4% PLA/EtLac	**7% PLA/EtLac**	**10% PLA/EtLac**
2h	22.77 ± 2.18	22.22 ± 2.48	14.39 ± 2.40
6h	46.42 ± 1.46	35.36 ± 1.92	24.09 ± 1.39
24h	97.64 ± 3.64	81.06 ± 3.66	55.41 ± 1.79

5.3.3. Mechanical Assays

Because the two-step methodology proved to form highly porous scaffolds with a nanofibers network entrapping water, the new poro-elastic properties conferred to the scaffold were studied. In order to study and characterize these properties, dumbbell test specimens with shapes and sizes according to the ASTM D638 norm were prepared by moulding. Because different initial concentration of PLA/EtLac could result in different mechanical and viscoelastic properties, scaffolds formed from concentrations framed between the 4% and the 10% ratios were used.

On first place, traction tests following the ASTM D638 protocol were carried out. This study was used to evaluate the elastic modulus of the material as a function of the initial PLA/EtLac concentration. The assay was also used to define the tensile properties before rupture, and at 0.2% yield offset, which is the standard offset that defines the end limit of the elastic region. Results on Figure 33A, showed that elastic modulus increased with the crescent PLA/EtLac percentage. The values of the elastic modulus ranged from 3.69 MPa, to 45.39 MPa.

For the tensile properties at the vicinity of the material rupture, it was possible to observe maximum elongations (dL_{max}) around the ~35% for all concentrations except the 10% concentration, which was correlated with a statistically significant reduction of the maximum elongation (25.33%) (Figure 33B). Instead, elongations measured at the 0.2% yield offset were smaller (2.9% to 1.35%) and presented a minimum level after the 7% concentration (Figure 33C). Results also showed that tensile strengths (σ_{max}) increased from 0.36 MPa to 1.66 MPa for the 4% and 10% concentrations respectively (Figure 33D). Instead, strengths found at 0.2% yield offset were four times smaller (0.11 to 0.55 MPa) (Figure 33E). Because stiffness was found to increase along the concentration range, but strain until rupture was not, the energy that the material was able to store until the tensile strength point showed a maximum at the 8% concentration (251.81 mJ) (Figure 33F). However, the energy stored on the elastic deformation range was found to be two order of magnitude smaller (1.34 to 3.23 mJ) (Figure 33G).

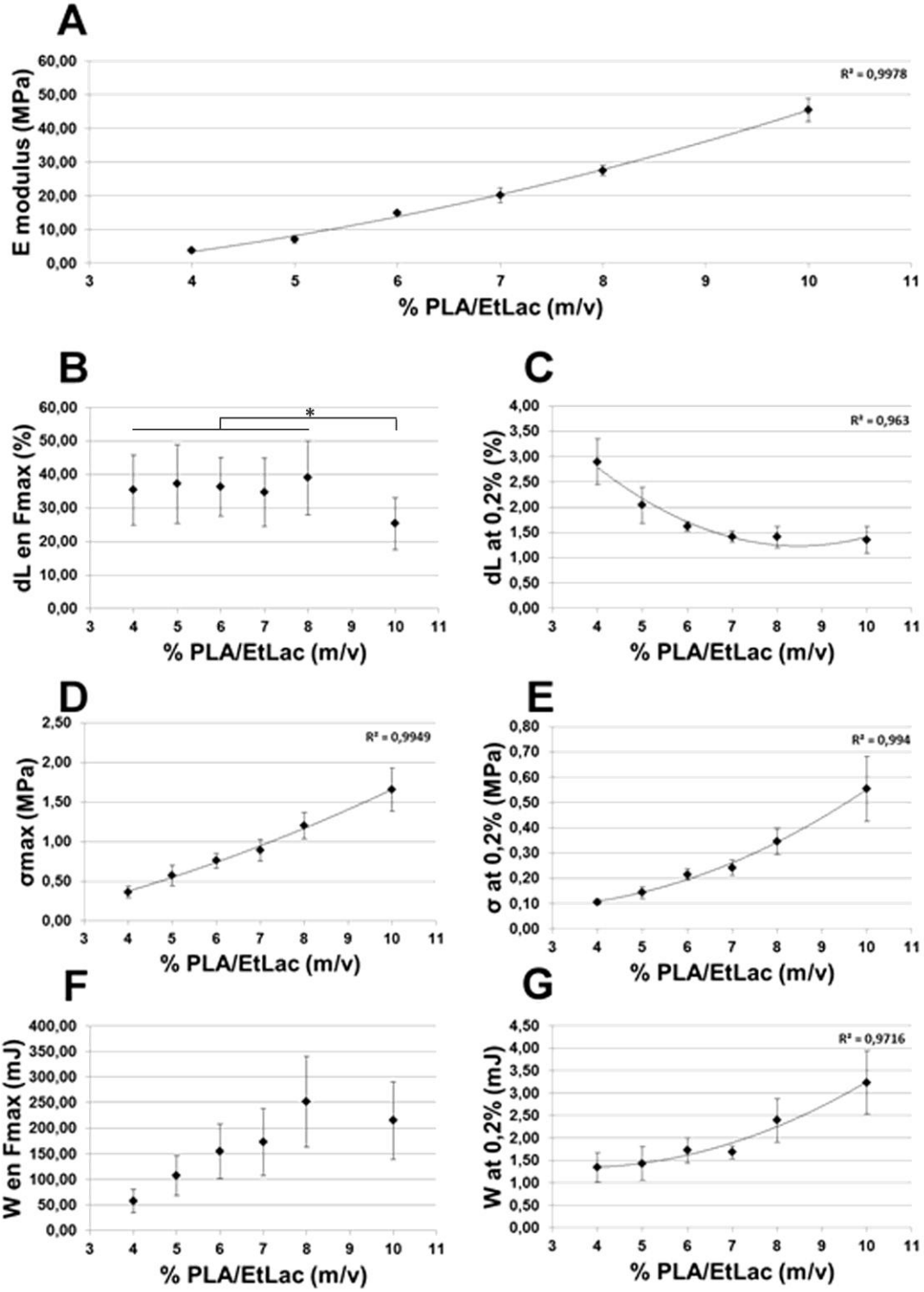

Figure 33. Tensile mechanical properties obtained from scaffolds formed with different PLA/EtLac concentrations. Analysed properties were (A) Young modulus, (B) strain at tensile strength (dL at Fmax), (C) strain at 0.2% offset (dL at 0.2%), (D) tensile strength (σmax), (E) stress at 0.2% offset (σ at 0.2%), (F) Work at tensile strength (W at Fmax) and (G) Work at 0.2% offset (W at 0.2%).

Given that the scaffold was composed by a polymer in a fibrous structure with a high level of porosity, it was also necessary to study the viscoelastic behaviour as function of PLA/EtLac ratio. For such a reason, creep and relaxation tests were performed on test specimens with the same dumbbell shape.

The creep test was used to study the speed of deformation that a constant load produced on test specimens. It is known that materials normally go through three different creep phases. A primary phase in which deformation decelerates. A secondary phase in which deformation stays constant. And a tertiary phase in which deformation accelerates and rupture occurs. For this comparison study, the creep rate was measured during the steady phase, this is the secondary phase. Results from Figure 34A showed that specimens obtained from lower concentrated solutions (4%) presented higher creep rates (0.2 strain %/h) when compared to specimens obtained from higher concentrated solutions (10%), which presented lower creep rates (0.03 strain%/h). The differences became more significant when it is considered that stresses used for the creep study, which were obtained by deforming all specimens at 1% of deformation and setting them constant at this point, resulted to be lower on those samples obtained from lower concentrated solutions (Figure 34B). This means that, even smaller stresses were applied on 4% samples, they presented higher creep rates compared to 10% samples.

On the other hand, the strain recovery measured at the end of the creep-recovery tests, showed that 10% samples allowed up to a ~95% of strain recovery, while lower concentrated samples like 4% and 7% only recovered the ~80% of the deformation (Figure 34C).

Finally, relaxation tests were carried out to observe the effect of a constant deformation in the rearrangement of the polymeric structure. Since different ratios of PLA/EtLac have proved to give place to different network structures (in terms of network density), it was expected that the forces applied in the specimens were distributed on a different way through the fibrous network and, therefore, the viscoelastic response of the whole specimen appear to be different as a function of PLA/EtLac ratio. For this study, samples from different PLA/EtLac ratios were fastened and maintained at 1%. And then, stress relaxation was recorded during 600 seconds and relaxation ratio was measured at the end of test. When results were observed, it was possible to observe that lower concentrations (4%) correlated with higher relaxation ratios (1.94), and higher concentrations (10%) correlated with lower relaxation ratios (1.75) (Figure 35A), which means that viscoelastic effects were more acute for the 4% samples. These differences became again more significant, when it is considered that for the same applied deformation, the 4% samples showed lower initial stresses than the 10% samples (Figure 35B).

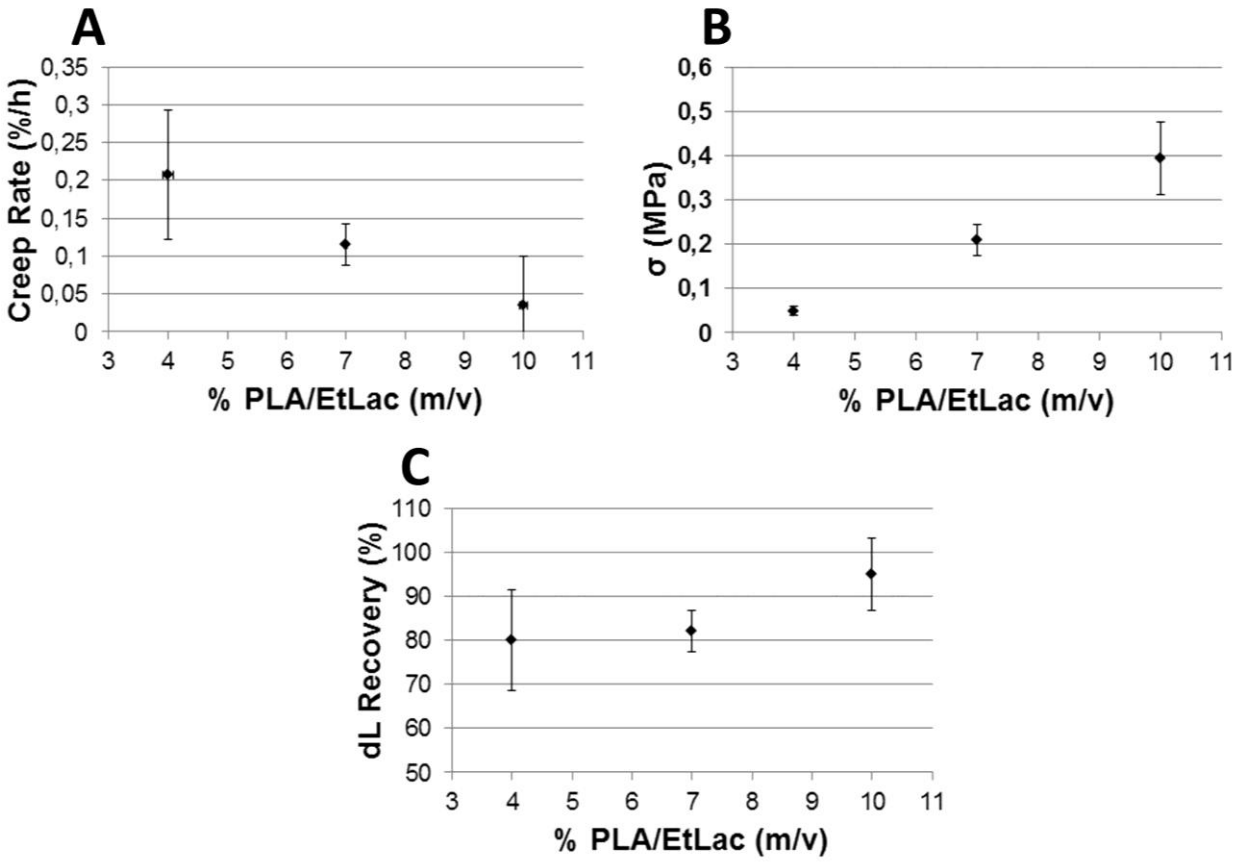

Figure 34. Creep/Recovery test results from different PLA/EtLac concentration. (A) Creep rate evaluated during the secondary creep phase (constant phase). (B) Stresses obtained after 1% deformation. (C) Recovered strain at the end of the test.

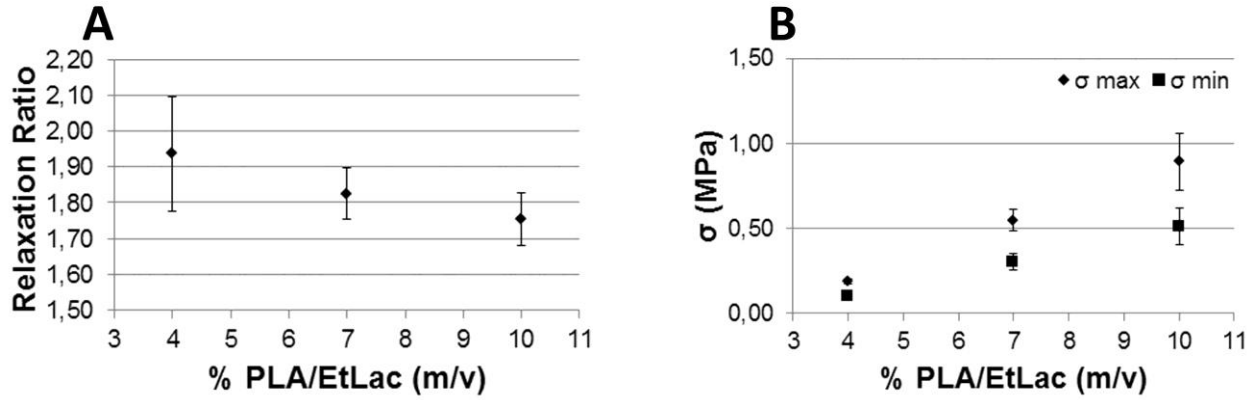

Figure 35. Test relaxation test results from different PLA/EtLac concentration. (A) Relaxation ratio measured from samples fastened at 1% and maintained for 600 seconds. (B) Stresses obtained at the initial point of the assay.

5.4. Discussion

It was important for the characterization of the methodology to study the different parameters that were relevant on the viability of the technique and that were as well key factors on the control of the obtained characteristics. Therefore, properties like viscosity, T_{GEL}, gelation kinetics and shrinkage, were analysed for the optimization and control of the processing, while properties like porosity, diffusion rates, mechanical properties and viscoelastic properties were analysed and correlated to the initial inputs in order to prove the control and plasticity of the final properties of the scaffolds.

Viscosity analysis revealed that liquid PLA/EtLac solutions presented high viscosity levels, from 10 to more than 1000 cP. The difference of viscosity between the lower concentration (4%) and the higher concentration (10%) were of about two orders of magnitude. It was observed that samples presented a Newtonian plateau, a region in which viscosity was independent of shear rate. The importance of detecting this Newtonian region lays on the need of confining a frame in which viscosity stays constant, and therefore can be used as a designing parameter. Also, it was possible to observe that viscosity increased up to 1000 Pa·s (10^6cP) with lower shear rates. This behaviour reflected the resistance against flow produced by the polymer-polymer interactions and the chain entanglements. At the other side of the scale, it was possible to observe the beginning of a non-Newtonian region close to the 10^3 s^{-1} shear rates. This change on behaviour could belong to the starting of a shear-thinning phase. However, for designing purposes the important range is framed between the 10^{-2} - 10 s^{-1} shear rates, which stand for the typical values used on compression and moulding processes. The analysis of the viscosity behaviour revealed that solutions presented a Newtonian region and, therefore, were suitable for the processing purposes. Finally, from the viscosity data, it could be calculated, as well, the characteristics needed for the formation of homogeneous suspensions or colloids. In this sense, knowing the properties (size and density) of the selected particles for the suspension (glass particles, salt particles…), it is possible to calculate the sedimentation speed with the Stokes law and adjust the system (through the gelator concentration), in order to obtain a viscosity able to maintain the homogeneity of the mixture until the gel is formed. In this way, the design of composites or the addition of porogen agents could be applied avoiding undesired precipitation. Thus, this gelation technique could be combined with a porogen leaching technique avoiding one of the main drawbacks of such a methodology, which is the incapacity to remove isolated deep porogen particles. The problem could be dodged because the high porosity of obtained scaffolds would allow the entrance of water through the entire scaffold.

T_{GEL}, which is an intrinsic value of the PLA/EtLac system, only depends on the molecular structure of the solvent and the gelator, and will be independent of gelator to solvent ratio [22]. Such a temperature will define below which level it is possible to obtain a thermostable gel. Thus, when solution is placed below T_{GEL}, the gelation process will start at a speed proportional to the difference between T_{GEL} and selected temperature. On the other hand, when solution is placed above the T_{GEL}, solution will stay liquid, defining in such a way the lower limit of the working temperature at which the material can be mixed, pumped and moulded.

The T_{GEL} was found at the convergence point of the concentration curves in a gelation time versus temperature graph. Since gelation is temperature dependent, it was very complex to find the T_{GEL} by direct observation. The reason is that gelation speeds near the vicinity of T_{GEL} occur at very low rates. Therefore, indirect methodologies had to be used. There are several techniques to analyse the $T_{GEL,}$ but most of them strongly underestimated it [22,24]. One proved strategy for the accurate determination of T_{GEL} is based on the extrapolation of gelation curves in a time-temperature graph, and the determination of the convergence point of different gelator concentration curves. This crossing point, which defines the gel temperature, is a temperature point in which polymer to polymer interactions are breaking and reforming at the same rate (gelation point), and therefore, the concentration of polymer is inconsequential [22]. Thus, the concentration independency of such a temperature point revealed the $T_{GEL.}$

However, in order to create the gelation time versus temperature graph as a function of concentration, there was a need to find a technique that determined with exactitude when the gelation of a specific solution for a specific temperature occurred. Normally, in literature it is used the study of the crossover between the loss modulus (the viscous component, G'') and the storage modulus (the elastic component, G') in order to determine the point in which a solution started to behave like a solid, this is, started to gelate. However, many studies have pointed out that the G'-G'' crossover point correlated with the precise gelation point only for a few number of cases, while normally, due to different mechanical and stoichiometric effects, it was common that gelation point occurred shifted in time respect to the G'-G'' crossover [25]. Therefore, in order to avoid these mismatches, an alternative strategy based on the study of the evolution of tanδ (G''/G') along time in a multifrequency rheology test was used. Such a strategy has proved in literature to be more accurate, since the frequency independency of tanδ was able to determine with exactitude when the infinite gel network (this is, a gel network that occupy all the available volume) started to form [23].

Using these strategies for the obtaining of the time-temperature graph, it was possible to corroborate the concentration independency of the T_{GEL} point and determine its value at 44.5 ºC. The accurate definition of the T_{GEL} value was relevant not only for the fixation of the minimum working temperature and maximum gelation temperature, but also for the optimization of the gelation process. This process is thermodynamically guided and molecules rearrange and pack to achieve a lower energetic state. Therefore the pre-warming of a PLA/EtLac solution can modify the initial energetic state of the system, and affect the consequent gelation step. This means that, for instance, a solution pre-warmed at 60 ºC will acquire a higher energetic state than a solution pre-warmed at 50ºC, which means that will need more time to dissipate the energy and achieve the thermostable gel state when this is cooled down. Therefore, the control of the T_{GEL} became important because allowed the characterization of the system and the optimization of the formation of gel structures by keeping warming temperatures close to the T_{GEL}.

Regarding the gelation kinetics it was interesting to notice that, while tanδ convergence occurred first on lower concentrations, complete gelation occurred first and faster on higher concentrations. This behaviour could be explained due to the dissipation of energy and the polymer interaction ratios. For instance, low concentrations, due to the reduced quantity of polymer, achieve lower states of energies compared to high concentrations when they are warmed at the same temperatures. Therefore it is easy and faster for them to dissipate the energy and achieve the point in which the gel starts to form, this is the tanδ convergence. However, due to the same reduced quantity of polymer, the chances of polymer to polymer interaction for the packaging process and gel formation are lower and, therefore, the process of gel formation is slower. Instead, high concentrations warmed at the same temperature have more energy in the system and require more time to dissipate it, but gel formation and hardening become faster due to the elevated presence of interacting polymer chains.

It was also possible to notice in the kinetics study, that the temperature used for the gelation process determines the time needed for the gelation to finish, but had no effect on the final equilibrium state. This information reveals that, for the formation of gels, any temperature below T_{GEL} (like room temperature) can be used without changing the final gel properties. This is an interesting issue, because, compared to the PLA/THF system [18], the PLA/EtLac system can perform at different temperatures above de 0ºC. Instead, PLA/THF system had to adjust gelating temperature around -18ºC in order to achieve nanofibrous structure, while gelating temperatures near room temperature gave place to platelet-like structures with notably worst mechanical properties. In this sense, the improvements are twofold. First, the formation of platelet-like

structure has not been observed. Second, working temperatures does not need to be kept below 0ºC, which simplifies the process.

The study of kinetics also revealed the achievement of different energetic states through the use of different pre-warming temperatures. For instance, when comparing 4% sample solutions pre-warmed at 46ºC and 50ºC, it is possible to observe that the former arrived to the equilibrium state faster than the later, while the same final equilibrium state was achieved in both cases.

Finally, the presence of different stiffness states achieved before the final equilibrium state (the observed peaks) remained opened to further studies. However, it is interesting to point that the studied gels achieved higher levels of stiffness (up to five fold) before the final plateau. Actually, the evolution of the delta angle (δ) (diphase between stress and deformation) along the gelation process (not shown) indicated that, during the non-equilibrium states found before the plateau, samples already acted like an almost pure Hookenian solid ($\delta^o \approx 0$). This means that, before achieving the plateau, gels were already formed but in a non-equilibrium state. Therefore, these results pointed to the possibility of obtaining stiffer gels (and potentially, stiffer scaffolds) by stopping the gelation process at some time point before the equilibrium state (like the maximum peak), through the precipitation of PLA in water.

Because the gelation of the PLA/EtLac solution responded to the packaging and ordering of the system molecules, which tried to find the lower energetic state, then it was expected to observe volume shrinkage during the gel formation. With the compensation of the normal force through the axial force control of the rheometer, and the consequent gap modification, it was possible to measure this shrinkage for the different concentrated solutions. Higher concentrations were correlated with higher volume shrinkages. This correlation would be explained by the presence of more polymer chains, which would be able to order and pack larger quantities of solvent. These shrinkage, which ranged from 0.8% to 3.5%, were small but of relevance in designing terms. For instance, for the formation of the dumbbell specimens, the thickness variation due to the shrinkages had to be considered in order to maintain the requirements defined on the ASTM guidelines.

After rheometric experiments, it was expected to correlate the distinct levels of G' with the distinct levels of polymer reticulation, this means, different network structure. It was logical to estimate that more concentrated solutions would form more dense nanofibrous networks. However, SEM images were not able to distinguish the differences clearly. Instead, they showed

on all samples a random nanofibrous structure with a porosity below the micron, which would be able to allow the diffusion of nutrients and metabolites, while restrict cell penetration. This characteristic could be useful on applications in which cells have to be compartmentalised, while other applications in which the scaffold have to be colonized by cells, would require the use of porogen agents to form larger cavities or the implementation of the technique into a SFF processing. The obtained continuous nano-fibrous network observed on SEM images, however, is a nanometric architecture that cannot be obtained by means of other techniques. Foams, particulate leaching and thermally induced phace separation can obtain fine structures and high porosities, but obtained matrices are different from natural ECM architecture. Indeed, structure and size of the obtained fibres closely resemble the structure and size of natural collagen fibrils (50-200 nm) [26].Furthermore, nano-fibrous matrices are a key factor to promote specific protein adsorption from serum, as well as to control cell attachment, proliferation, development and migration [27].

Because SEM imaging was not able to distinguish differences between different concentrations used, the ratio between the solid phase (fibrous PLA structure) and the liquid phase (entrapped water), was measured. This estimation confirmed the higher density of the solid phase on 10% samples and the high porosity obtained. Actually, for the lower concentrations, up to the 95% of the weight was water. Such a value is of high relevance because have strong consequences on the amount of material needed for the obtaining of scaffolds and the amount of water entrapped inside, as well as strong implications on the final specific surface area. For instance, for the PLA/THF system, the surface-to-volume ration obtained with this nanofibrous networks were up to two orders of magnitude higher than other techniques [18].

Related to the fibrous network densities, diffusion assays were able to detect differences between specimens, since higher sample concentrations reduced the diffusion rate of the dye, while lower sample concentration allowed deeper dye penetration. These results also pointed out the capability of this kind of system to produce scaffolds with desired molecules entrapped inside, which can be slowly released from it in a controlled manner, or to adjust their mass-transport properties to the targeted tissue.

From a mechanical point of view, the study of the tensile properties showed that the obtained porous structure allowed the creation of flexible PLA based scaffolds. These scaffolds, with poro-elastic properties, presented lower elastic modulus than compacted PLA, and different viscoelastic properties as well. These new conferred properties came, not only from the material itself, but also from the structure at the nanoscale. Actually, the nanofibrous structure was able to

distribute the applied stresses in such a way that forces could be shared and dissipated in part through the deformation of the network itself. The sum of these small deformations was able to contribute altogether to allow a more flexible deformation and avoid rigidness and brittleness. Thus, greater deformations without rupture could be achieved.

These mechanical properties, characterized by elastic modulus that could be tuned in the range of the 5-50 MPa and by maximum deformations around the 35%, made this material adequate to be used on the regeneration of soft tissues. Interestingly, different mechanical properties could be obtained by adjusting polymer concentration and consequently the matrix density.

However, despite the good mechanical properties shown before rupture, it was important to notice that the properties at the 0.2% yield offset were a limiting factor. The stresses, deformations and energies that the material was able to support before entering the plastic deformation range were remarkably lower than the ones that could support at the fracture limit. For instance, it is important to point that beyond deformations of about 1-3% (depending on the concentration used for the scaffold formation), the material entered into the plastic regime. Therefore, these short elastic ranges did not make suitable this material for applications that needed larger ranges of elastic deformation, such as skin (10-40%), blood vessels (30-70%), mesentery membrane (~100% deformation) and so on [28]. Still, the capability of tuning the mechanical properties by changing the concentration range of PLA/EtLac, and therefore the microscopic network densities, made this system a good option for the production of scaffolds with designed mechanical properties. Despite this study only covered a concentration range framed between 4% and 10% concentration, this could be extended to higher concentrations with proper machinery able to work at high concentrations (and viscosities). Moreover, the concentration limit imposed by the increasing levels of viscosity could be overpassed by using lower molecular weight polymer chains. In such a way, the inherent viscosity would be lowered, and higher concentration rates could be used, achieving stiffer porous materials made of exactly the same material. Actually, mixtures of long and short molecules of PLA could be also used in order to obtain a wider degree of tenability on the mechanical, viscoelastic, porous, diffusion and microstructure properties. However, it should be take into account, that the addition or change of the molecular size of the gelator would change as well the T_{GEL} and the gelation dynamics.

Another interesting property given by this nanofibrous network was the possibility of tuning and modifying the viscoelastic properties. Because the final obtained scaffold was constituted by a polymeric material, viscoelastic effects were expected. However, depending on

the network density, the applied stresses and deformations were distributed through different cross-sectional areas. This means that, same stresses applied at the macroscopic levels, were working different on the microscopic level. Therefore, it was possible to observe that specimens of lower concentration presented higher creep rates and relaxation ratios, while specimens of higher concentrations did the contrary. In such a way it was possible to accentuate the effect of the polymer relaxation on those scaffolds composed by lower concentration ratios, and vice versa.

Measured viscoelastic properties showed that the materials were not appropriate for applications in which stresses and deformations are constants and a deformation recovery is essential. Due to the high creep rates, a scaffold under a constant stress would be placed in the plastic region in a matter of hundreds hours, and once there, it could not recover properly the deformations and would not be functional anymore.

Still is very interesting to see that, like tensile properties, viscoelastic properties were able to be adjusted by only modifying the polymer concentration. Such an easy malleability showed potential uses for the designing of materials which are able to mimic the mechanical and viscoelastic properties of the aimed tissue. The control on both properties, and not only the mechanical, is showing everyday more relevance for the control and guidance of cell behaviour and phenotype, since it has been proved that viscoelastic properties directs as well characteristics like cell proliferation and cell differentiation [29].

5.5. Conclusions

This study has defined the values for the viscosity and T_{GEL}, which determined the working conditions. Viscosity as a function of shear rate has shown to behave like a Newtonian liquid in a range of stresses typical from moulding, pouring, mixing and pumping processes. The determination of T_{GEL} has allowed the optimization of the processing by keeping warming temperatures close to the T_{GEL} and gelating temperatures far from it. T_{GEL} showed as well the viability of performing at room temperature. The shrinkage factor has been measured and the constant equilibrium state of the obtained gels characterized. The role of the gelating and the pre-warming temperatures on the gelating kinetics has been defined as well.

Final properties of the obtained solid scaffolds were analysed and correlated with the initial gelator/solvent (PLA/EtLac) ratio. Despite all concentrations were able to produce scaffolds with a nano-fibrous structure and high porosity, the different gelator to solvent ratios were correlated to different structural network densities. Indeed, the nano-fibrous matrix density

was correlated with the modulation the different properties (porosity, diffusion rate, mechanical and viscoelastic properties). For instance, the micro-network architecture conferred to the PLA scaffolds a high flexibility and tuneable elastic modulus. Moreover, the distribution of stresses through the different networks, showed to affect and define both the mechanical and the viscoelastic properties. In such a way, scaffold produced with the same material but different network densities, was able to behave differently depending on initial used concentration.

Finally, the methodology here presented, based on the use of green, biocompatible, biodegradable and resorbable materials has proved to gather many of the requirements that scientific, physicians and engineers looks for. First, the resources and technology used are minimal. Second, the methodology applied is simple and the conditions used are soft compared to other non-woven fabric processing techniques. Third, the obtained fibrous network has a nanometric size and is interconnected in a continuous fashion. Forth, big and complex scaffolds can be obtained easily and fast by moulding. Fifth, the continuous network confers to the matrix unique mechanical properties. Sixth, the batch-to-batch consistency is easily achieved. Seventh, scaffolds can be designed with great control of their final properties. Moreover, the presented strategy can be applied on any PLA-based material. Thus, by gelating PLA copolymers, other properties like elasticity from PLC can be introduced into final scaffolds, opening the horizon to the treating of other tissues.

5.6. References

1. Ueda H, Tabata Y. Polyhydroxyalkanonate derivatives in current clinical applications and trials. Adv Drug Deliv Rev 2003;55(4):501-18.
2. Amass W, Amass A, Tighe B. A review of biodegradable polymers: uses, current developments in the synthesis and characterization of biodegradable polyesters, blends of biodegradable polymers and recent advances in biodegradation studies. Polym Int 1998;47:89-144.
3. Engelberg I, Kohn J. Physico-mechanical properties of degradable polymers used in medical applications: a comparative study. Biomaterials 1991;12(3):292-304.
4. Göpferich A. Mechanisms of polymer degradation and erosion. Biomaterials 1996;17(2):103-14.
5. Li S. Hydrolytic degradation characteristics of aliphatic polyesters derived from lactic and glycolic acids. J Biomed Mater Res 1999;48(3):342-53.
6. Schmitt EA, Flanagan DR, Linhardt RJ. Importance of distinct water environments in the hydrolysis of poly(DL-lactide-co-glycolide). Macromolecules 1994;27(3):743-48.
7. Vert M, Mauduit J, Li S. Biodegradation of PLA/GA polymers: increasing complexity. Biomaterials 1994;15(15):1209-13.
8. Middleton JC, Tipton AJ. Synthetic biodegradable polymers as orthopedic devices. Biomaterials 2000;21(23):2335-46.
9. Vert M, Li SM, Spenlehauer G, Guerin P. Bioresorbability and biocompatibility of aliphatic polyesters. J Mater Sci Mater Med 1992;3(6):432-46.
10. Madhavan Nampoothiri K, Nair NR, John RP. An overview of the recent developments in polylactide (PLA) research. Bioresour Technol 2010;101(22):8493-501.

11. Levato R, Mateos-Timoneda MA, Planell JA. Preparation of biodegradable polylactide microparticles via a biocompatible procedure. Macromol Biosci 2012;12(4):557-66.

12. Aparicio S, Alcalde R. The green solvent ethyl lactate: an experimental and theoretical characterization. Green Chem 2009;11:65-78.

13. Clary JJ, Feron VJ, van Velthuijsen JA. Safety assessment of lactate esters. Regul Toxicol Pharmacol 1998;27(2):88-97.

14. Mottu F, Laurent A, Rufenacht DA, Doelker E. Organic solvents for pharmaceutical parenterals and embolic liquids: a review of toxicity data. PDA J Pharm Sci Technol 2000;54(6):456-69.

15. Sahoo S, Kumar N, Bhattacharya C, Sagiri SS, Jain K, Pal K, Ray SS, Nayak B. Organogels: Properties and Applications in drug delivery. Des Monomers Polym 2011;14:95-108.

16. Murdan S. Organogels in drug delivery. Expert Opin Drug Deliv 2005;2(3):489-505.

17. Suzuki M, Hanabusa K. Polymer organogelators that make supramolecular organogels through physical cross-linking and self-assembly. Chem Soc Rev 2010;39(2):455-63.

18. Ma PX, Zhang R. Synthetic nano-scale fibrous extracellular matrix. J Biomed Mater Res 1999;46(1):60-72.

19. Hu J, Sun X, Ma H, Xie C, Chen YE, Ma PX. Porous nanofibrous PLLA scaffolds for vascular tissue engineering. Biomaterials 2010;31(31):7971-7.

20. Giordano RA, Wu BM, Borland SW, Cima LG, Sachs EM, Cima MJ. Mechanical properties of dense polylactic acid structures fabricated by three dimensional printing. J Biomat Sci-Polym 1996;E8:63-75.

21. Federal Register. Q3C Impurities: Residual Solvents. US Department of Health and Human Services: Food and Drug Administration. Federal Register 1997;62:67377-88.

22. Tosh SM, Marangoni AG. Determination of the maximum gelation temperature in gelatin gels. Appl Phys Lett 2004;84(21):4242-4.

23. Grillet AM, Wyatt NB, Gloe LM. Polymer Gel Rheology and Adhesion. In: De Vicente J. Rheology. InTech, 2012. p. 59-80.

24. Kim SY, Choi DG, Yang SM. Rheological Analysis of the Gelation Behavior of Tetraethylorthosilane/Vinyltriethoxysilane Hybrid Solutions. Korean J Chem Eng 2002;19(1):190-6.

25. Chambon F, Winter HH. Linear Viscoelasticity at the Gel Point of a Crosslinking PDMS with Imbalanced Stoichiometry. J Rheol 1987;31:683

26. Lee J, Cuddihy MJ, Kotov NA. Three-dimensional cell culture matrices: state of the art. Tissue Eng Part B Rev 2008;14(1):61-86.

27. Woo KM, Chen VJ, Ma PX. Nano-fibrous scaffolding architecture selectively enhances protein adsorption contributing to cell attachment. J Biomed Mater Res A 2003;67(2):531-7.

28. Fung YC. Elasticity of soft tissues in simple elongation. Am J Physiol. 1967 Dec;213(6):1532-44.

29. Cameron AR, Frith JE, Cooper-White JJ. The influence of substrate creep on mesenchymal stem cell behaviour and phenotype. Biomaterials 2011;32(26):5979-93.

CHAPTER 6

6. DEVELOPMENT AND CHARACTERIZATION OF AN OFF-THE-SHELF VESSEL GRAFT

The development of small-calibre vessel grafts has been pursued for decades. On small vessel substitutes, mechanical requirements become of high importance to prevent intimal hyperplasia and thrombotic effects. In this chapter, first steps toward the development of off-the-shelf vascular grafts are presented. Tubular scaffolds are fabricated combining the techniques of chapter 4 and 5. Obtained highly porous scaffolds are mechanically tested under transmural pressures. Elastic modulus and stiffness properties are calculated and analysed. Fatigue assays are performed to observe the effect of plastic accumulation. Cellular response is tested for functionalized and non-functionalized scaffolds. This chapter exposes the fabrication potential of this technique in order to obtain vascular scaffolds with tailored mechanical properties and good cell response.

6.1. Introduction

In western countries, one of the most frequent major surgeries found on the clinics is the grafting of a coronary artery bypass [1]. The current gold standard for this kind of surgery is the graft of the autologous saphenous vein and mammary arteries. However, approximately 20% of the cases have no available autologous grafts because they have already used them, or their integrity is compromised by some cardiovascular pathology [2]. The use of cadaveric allografts has proved low success because of the immunogenic problems and the aggressive processing required before their implementation [3]. Thus, the development of synthetic grafts available off-the-shelf has been under study for the last decades.

Synthetic vascular grafts can be already found on the clinics, which are normally fabricated from expanded polytetrafluoroethylene (ePTFE) or polyester (Dacron®). These synthetic materials perform well enough for substituting vessels with large diameters (>4 mm). However, the patency of small diameter vascular grafts is still a big concern due to the anastomotic intimal hyperplasia (IH) and thrombus formation [4,5]. On small calibre vascular grafts, the development of IH is commonly found on the anastomotic sites, especially on the distal anastomosis, and is related to the migration and proliferation of smooth muscles cells (SMC) into the luminal side and the generation of large amounts of extracellular matrix (ECM) [6,7].

It has also been detected that mechanical properties of vessel substitutes such as Young's modulus and compliance strongly influence the long-term patency of the grafts. Dacron and ePTFE are relatively rigid materials compared to native vessels, which causes mechanical properties mismatch at the anastomotic sites [8]. In this sense, from the mechanical point of view, there are two factors related to graft failure. The first one, the tubular compliance mismatch, is related to the loss of pulsatile flow energy during the propagation from a compliant artery to a non-compliant graft, and the increased shear stress on stiffer artificial grafts [9]. The second one, the anastomotic compliance mismatch, enhances the risk of IH due to (1) the increment of mechanical stress at the interface, which induces IH when the wall is injured [10]; (2) the stimulation of SMC growth and ECM production by means of cyclic stretching [11]; and (3) the low shear stress conditions, flow separation and prolonged flow residence time, which induce intimal thickening on the distal anastomosis [12,13]. In general, it is observed that compliance mismatch is inversely correlated with graft patency rate (Table 12), highlighting the importance of mechanics on artificial vessel design.

Table 12. Relationship between compliance and patency rate. Adapted from [14].

Graft Type	Compliance (% mmHg x 10^2)	Patency (%)
Host artery	5.9 ± 0.5	
Saphenous vein	4.4 ± 0.8	75
Umbilical vein	3.7 ± 0.5	60
Bovine heterograft	2.6 ± 0.3	59
Dacron	1.9 ± 0.3	50
ePTFE	1.6 ± 0.2	40

Matching mechanical properties is important to avoid the narrowing of the vessel lumen induced by IH, but preventing thrombogenic reactions is also a common cause of vessel reocclusion. Thus, enhancing endothelial cells adhesion and proliferation into the lumen has to be considered. Indeed, improving the luminal characteristics to generate a strong luminal endothelial layer that inhibits both platelet aggregation and SMC hyperproliferation after the implantation has proved to be a key parameter to enhance patency of small-calibre grafts [15-18].

Normally, graft endothelialisation starts with endothelial cell migration from the anastomoses, as well as from the recruitment of circulating endothelial progenitor cells. To enhance cell migration and recruitment, collagen grafts were firstly used, but they resulted to be thrombogenic as well as they were lacking enough mechanical properties [19,20]. An alternative strategy is to functionalized polymeric grafts with engineered proteins, like elastin-like proteins, which are able to promote the adherence of targeted cells while creating a non-fouling surface that reduces the risk of thrombogenesis.

On this chapter, biodegradable polymeric poly(lactic acid) (PLA) vascular grafts are fabricated by moulding Poly(lactic acid)/Ethyl lactate (PLA/EtLac) organogels into tubular shapes and precipitating the polymer into water. Resultant tubular scaffolds are functionalized with ELRs to improve interface properties. Finally, the mechanical properties and the in vitro biological response of the fabricated artificial grafts are evaluated and framed respect to the theoretical gold standard in order to discuss their potential as off-the-shelf small-diameter vascular grafts.

6.2. Materials and Methods

6.2.1. Materials

Poly–L/DL lactic acid 70/30 (Purasorb PLDL 70/38, inherent viscosity midpoint 3.8 dl/g, Mw≈ 850,000 Da) was purchased from Purac Biomaterials (The Netherlands).

Ethyl Lactate 99% photoresist grade was purchased from Sigma and used without further purification.

6.2.2. Scaffold Preparation

PLA was dissolved in EtLac at 54ºC and stirring conditions until complete dissolution. Then, the PLA/EtLac solution was poured into an open cylinder mould with the following dimensions: 50 mm length, 4.6 mm external diameter and 3 mm internal diameter. Filled mould was centrifuged to remove bubbles and placed at cold temperatures until complete gelation occurred. When the gel was completely formed, it was removed from the mould and immersed into milli-Q water to remove EtLac by means of diffusion into water and provoke polymer precipitation by phase separation. Finally, scaffolds were washed several times with water.

For in vitro cell studies, scaffolds were functionalized with the $HRGD_6$ molecule, an ELR with RGD sequences (see Chapter 4). Functionalization was carried out by physisorption. Tubes were soaked overnight with an ELR solution in PBS (100 μg/ml), and rinsed gently right after.

For long storages PLA tubular scaffolds were lyophilized and kept in dry conditions. Reconstitution was carried out by immersing lyophilized scaffolds into ethanol and exchanging the ethanol phase by water with several washing steps.

6.2.3. Scaffold Characterization

Scaffold microstructure was observed by Scanning Electron Microscope (SEM). Images were obtained by SEM at intensities between 3-10 kV with a Nova NanoSEM 230 microscope. Samples were covered with 10 nm gold by sputtering.

Pressure-diameter test were performed on tubular scaffold segments as described in previous works [21]. The specimens were tied at both ends on needles of appropriate diameter to prevent leakage. Two stainless steel fixtures joined the needles to the grips of an electromechanical tensile testing machine (Instron 4411, Instrom, Inc., Norwood, MA, USA) equipped with a 100N load cell (Instron 2525-806). The lower fixture was designed to permit

internal pressurization of the vascular segment through the needle. Specimens were placed in a PMMA transparent cell and immersed in phosphate-buffered saline (PBS) solution at constant physiological temperature (37ºC). Attached specimens were stretched to approximately 1.1 times of the length at rest. Intravascular pressure was applied via the lower needle and measured with a pressure transducer (Druck PMP 4000). The outer diameter of the specimen, measured at the midpoint section, was continuously recorded using an optical extensometer (Keyence LS-7500). Transmural pressure, i.e., the pressure difference between the inside and the outside of the vessel, was cycled first from 80 to 120 mmHg at a frequency of 0.4 Hz, and secondly from 0 to 200 mmHg at a frequency of 0.04 Hz, in both case for at least 8 minutes.

Mechanical analyses were carried out to calculate the Pressure-Strain Elastic Modulus (E_m) and Stiffness (k). For this purpose, the recorded pressure and the diameter values of each tested specimen were fit into a sine equation in order to eliminate intervallic variations produced by noise. The sine equation was described as follows:

$$Y = A \cdot \sin(2 \cdot \pi \cdot \nu \cdot t + \Phi) + (B \cdot t) + C$$

Where (Y) is the pressure or diameter value, (A) is the amplitude of the wave function, (ν) is the frequency of the wave function, (t) is the value of the time point, (Φ) is the phase of the sine function, (B) is the slope of the wave function and (C) is the DC offset. The sine function was fit for each specimen for a set of cycles comprised at 3, 5 and 7 minutes. Diameter values, the amplitude of the deformation, the accumulation of deformation (%ΔD) and the phase between the pressure pulse and the deformation wave were obtained from sine equation analyses. From the sine function it was also extracted a mean value for the diameter and pressure during the systolic (maximum) and diastolic (minimum) phases for the different time points (3, 5 and 7 minutes) which were used to calculate E_m and stiffness. Average E_m and stiffness (k) values were calculated using the following equations:

$$E_m = (P_{max}-P_{min}) \cdot D_{min} / (D_{max}-D_{min})$$
$$k = (P_{max}-P_{min}) / (D_{max}-D_{min})$$

Where (P) is pressure and (D) is diameter at the systolic (max) or diastolic (min) point. The inverse value of the E_m value is also known as Distensibility, and the inverse value of the Stiffness value is also known as Compliance [22].

Fatigue assay was carried out in a tensile testing machine (Instrom 4411, Instrom, Inc., Norwood, MA, USA) equipped with a 10 N load cell. Specimens were placed into a PMMA

transparent chamber and submerged in PBS solution heated at 37ºC by a thermostatic bath (Unitronic 6320200). Forces applied during the cyclic loadings were selected to match physiological stresses on graft walls. For the assay, extreme physiological ranges (50-200 mmHg) were chosen, assuming values of 0.71 mm and 7.2 mm for the thickness and width of specimen samples. Forces were calculated using Laplace's law:

$$\sigma = P \cdot r/h \text{ (Laplace's Law)}$$
$$F = \sigma/h \cdot z$$

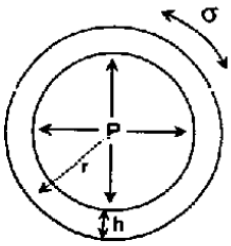

Where (σ) is circumferential tensile stress, (P) is radial pressure in the lumen, (r) is radius, (h) is wall thickness and (z) is width of the wall piece. Cyclic loadings were applied until rupture.

6.2.4. Cell Culture

Human Umbilical Vein Endothelial Cells (HUVECs) single donor cells (CC-2517, Lonza) were cultured on 6% tubular scaffolds with Supplemented Promocell® SMC Growth Medium 2 under static conditions. Cell adhesion was observed by fluorescence microscopy after 24h of culture (initial cell density: 100.000 cells/cm^2). Fluorescence labelling was carried out with DAPI (nuclei) and Rhodamine-Phalloidin (actin cytoskeleton) molecules.

Cell growth was studied during 13 days of culture (initial cell density: 10.000 cells/cm^2). For the observation of cell growth, cultured tubes were embedded into Paraffin and histological samples were cut along the longitudinal section of the tubes after 1, 5, 9 and 21 day. Cells were stained using Masson's trichrome protocol and observed under light microscopy.

6.2.5. Statistics

Pressure-diameter mechanical assays were performed on 3 to 4 different specimens for each condition, and for each specimen values were measured at 3 different time points. Values were expressed as mean values ± standard deviation. Fatigue assay was performed on 3 different scaffolds, but only one representative scaffold was plot. Cell culture was performed on 3 to 4 different specimens for each condition, and histological sections were cut and analysed on different randomly representative spots.

6.3. Results

6.3.1. Scaffold Characterization

Scaffold microstructure was analysed by SEM microscopy (Figure 36). SEM micrographs showed the expected nanofibrous structure resultant from the polymer precipitation of the gelated system (see section 5.3.2)

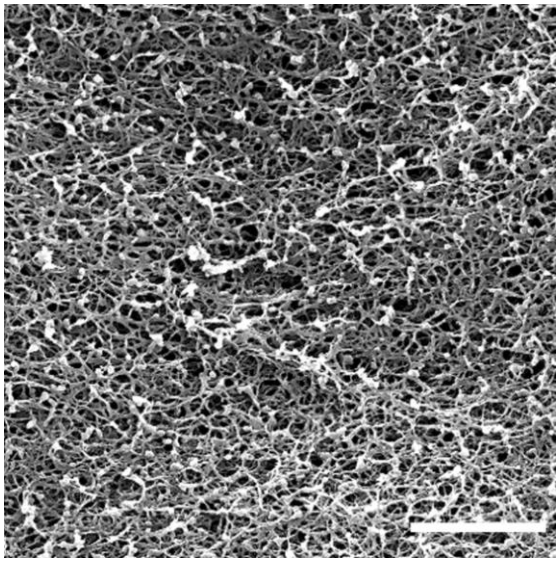

Figure 36. SEM micrograph of the lumen wall of a 4% PLA tubular scaffold (scale bar = 5 μm).

Mechanical properties were calculated from the analyses of pressure-diameter studies performed on artificial grafts subjected to flow pressures cycles. Figure 37A shows a typical representative Pressure-Diameter graph obtained from a tubular scaffold for a one load cycle at a 0-200 mmHg pressure interval. The graph showed that, during systolic phase (a), the diameter was subjected to a linear deformation. Instead, during the diastolic phase (b), the diameter deformation was relaxed following an exponential curve. Results also showed the existence of creep (c), which caused an accumulation of deformation. Figure 37B shows a typical pressure-strain graph from a normal artery obtained from [21].

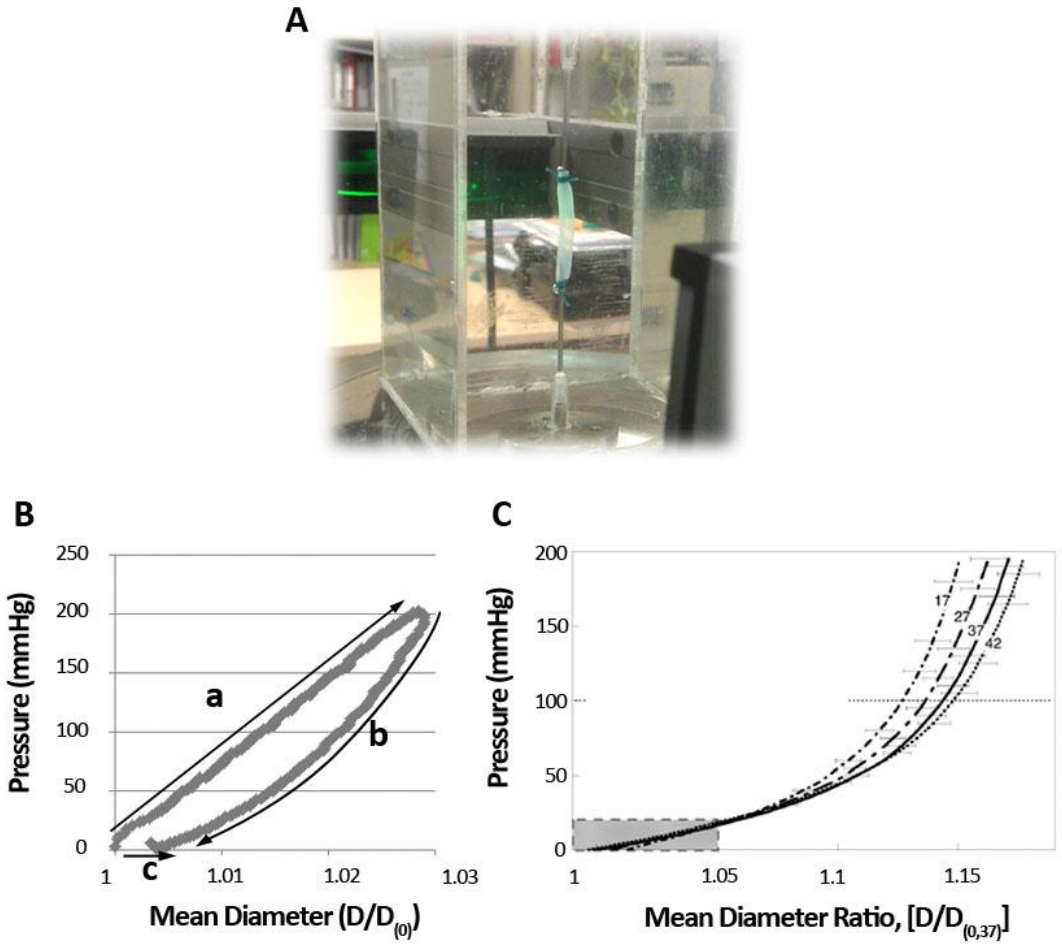

Figure 37. (A) Picture of a fabricated tubular scaffold during a pressure-diameter test. (B) Typical pressure-strain graph for one load cycle, at 0.04 Hz, on a 4% tubular scaffold. (a) represents the ascending pressure ramp during the systolic phase, (b) represents the descending pressure ramp during the diastolic phase, (c) represents resultant creep. (C) Pressure-strain graph for ascending pressure loads at 3 mmHg/s on human carotid arteries; obtained from [21]. Mean diameters were calculated dividing the actual outer diameter by that corresponding to zero pressure.

Figure 38A shows calculated E_m values for the different specimen types at different cyclic conditions. E_m values describe the distension of the graft wall during the cardiac cycle. Analyses were performed on different grafts fabricated from different PLA/EtLac concentrations. Results obtained from the 80-120 mmHg cyclic pressure conditions showed that fabricated grafts presented E_m between the ~4300 and the ~21000 mmHg for the 3.5% and 6% respectively. E_m obtained from 0-200 mmHg cyclic pressure conditions were framed between the ~5500 and the ~22200 mmHg for the 4% and the 6% respectively. The 3.5% scaffolds could not be tested under these conditions due to scaffold bursting at high pressures.

Figure 38B shows calculated stiffness values. At 80-120 mmHg cyclic conditions stiffness was framed between the ~1200 and the ~7000 mmHg/mm for the 3.5% and the 6% respectively. For the 0-200 mmHg cyclic conditions stiffness were framed between the ~1750

mmHg and the ~7300 mmHg for the 4% and the 6% respectively. The 3.5% scaffolds could not be tested under these conditions due to scaffold bursting at high pressures.

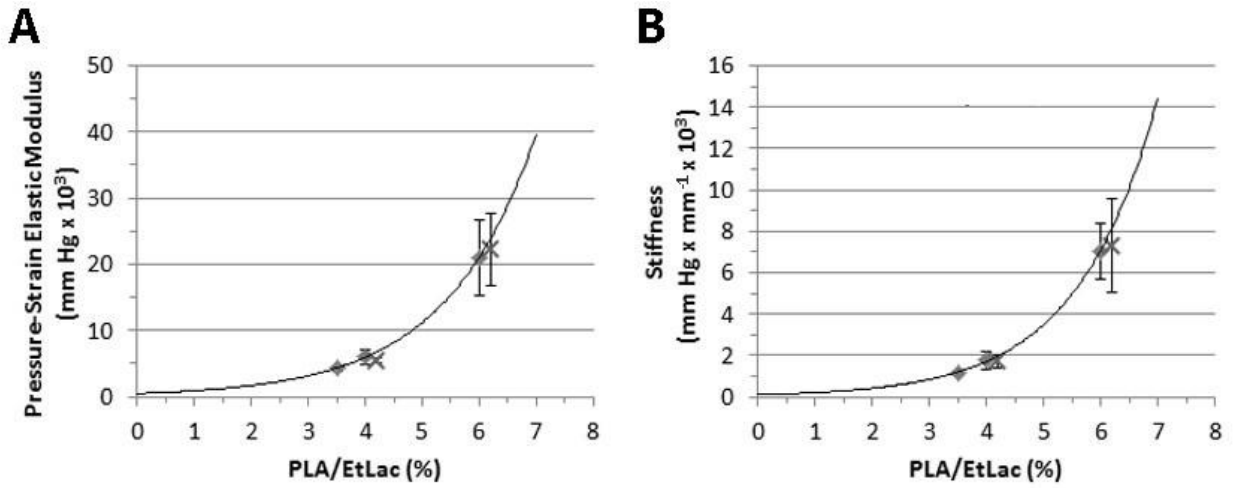

Figure 38. (A) Pressure-strain elastic modulus and (B) Stiffness values of 3.5%, 4% and 6% PLA tubular scaffolds tested at different conditions: (♦) 80-120 mmHg and 0.4 Hz; and (**x**) 0-200 mmHg and 0.04 Hz. The different cyclic conditions are represented displaced on the horizontal axis for better visualisation.

Diameter deformation during cyclic loadings along time was studied for the 80-120 mmHg cyclic conditions (Table 13). For this purpose, diastolic diameter was calculated at 0, 3, 5 and 7 minutes of cyclic loadings. Results showed that initial diameters at resting conditions (0 mmHg) were slightly different between the different specimen types as result of material shrinkage during scaffold fabrication (see section 5.3.1). However, when the different scaffolds were subjected to pressure conditions, differences on diameters substantially increased. The 3.5% PLA scaffolds presented a 3% diameter increase after 3 minutes of cyclic loading, while the 4% and the 6% PLA scaffolds presented a 2.7% and 0.3% increase respectively. Deformation accumulation persisted along time, which led to increased diameters at 5 and 7 minutes. Deformation accumulation was found larger for the 3.5% scaffolds than the 6% scaffolds. However, for all cases, the deformation accumulation ratio diminished along time ($\%\Delta D_{5min \rightarrow 7min} < \%\Delta D_{3min \rightarrow 5min}$).

Diameter amplitude was found to be constant during the cardiac pulse simulation for each specimen. Results showed that amplitude values were larger on 3.5% scaffolds than 6% scaffolds. Similarly, phase difference between the pressure wave and the deformation wave was found to be higher on the 3.5% than the 6% scaffold.

Table 13. Diameter analysis of the 3.5%, 4% and 6% PLA tubes tested at 80-120 mmHg/ 0.4 Hz.

PLA/EtLac	3.5%		4%		6%	
	Average	SD	Average	SD	Average	SD
$D_{initial}$ (mm)	4.294	0.151	4.242	0.062	4.165	0.020
D_{3min} (mm)	4.429	0.064	4.358	0.067	4.175	0.017
D_{7min} (mm)	4.594	0.102	4.432	0.091	4.176	0.019
Amplitude	0.013	0.002	0.009	0.002	0.003	0.002
$\%\Delta D_{3\rightarrow5min}$	2.3	0.7	1.1	0.4	0.04	0.03
$\%\Delta D_{5\rightarrow7min}$	1.3	0.1	0.5	0.2	0.01	0.01
ΔPhase	0.7	0.2	0.8	0.3	0.4	0.3

Diameter values correspond to the diastolic values.

Figure 39 shows a representative graph of the evolution of diameter deformation along time for a 4% scaffold during a fatigue assay. Fatigue assays were performed on pieces cut from the scaffold wall on the azimuth direction, which were subjected to forces that emulated the circumferential stresses caused by a 50-200 mmHg pressure cyclic loading. The range of 50-200 mmHg diastolic-systolic pressures were selected to include pathologic ranges. Results showed the presence of creep, which caused an accumulation of deformation and an eventual specimen failure after some minutes.

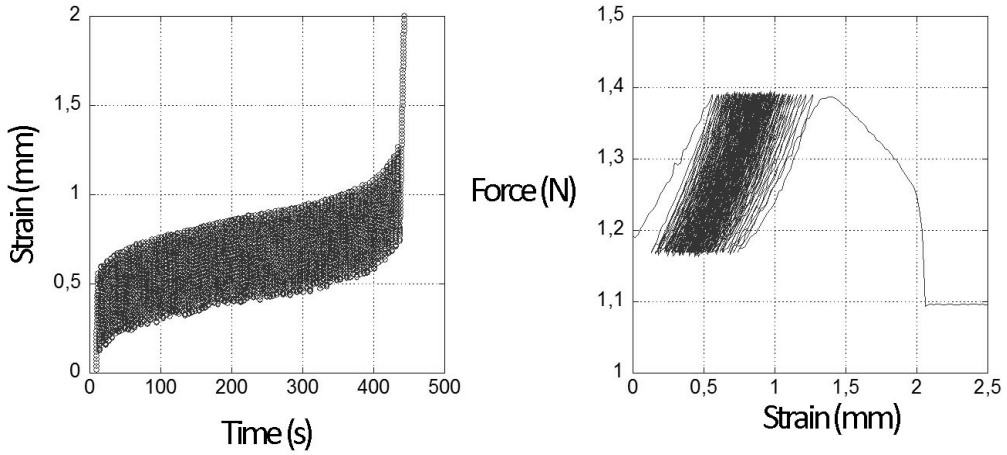

Figure 39. (A) Strain-time graph and (B) force-strain graph of a PLA 4% wall piece specimen subjected to load cycles that emulated an internal transmural pressure cycle framed at 50-200 mmHg at 0.2 Hz. Graphs revealed the existence of creep caused by the accumulation of plastic deformation, which ended with the specimen failure after 92 load cycles.

6.3.2. Cell Culture

In vitro cell response revealed that cells could firmly attach directly to the scaffold and develop an organized cytoskeleton with the presence of actin stress fibres (Figure 40A-B). On the other hand, histology sections of cultured tubes (Figure 40C-J) showed that cells seeded on the scaffolds could survive, grow and develop a continuous endothelium layer after 21 days of

culture. Proliferation studies performed on functionalized and non-functionalized scaffolds showed different cell behaviours. Scaffolds functionalized with ELR showed faster formation of the endothelial cells layer along the lumen. Indeed, functionalized scaffolds showed a continuous layer at day 5, while at day 9 a more robust, dense and thicker layer was observed. Instead, non-functionalized scaffolds presented a continuous layer at day 9 with the presence of some cell agglomerations. Moreover, after 21 days, non-functionalized scaffolds still present a lower-dense endothelial cell layer.

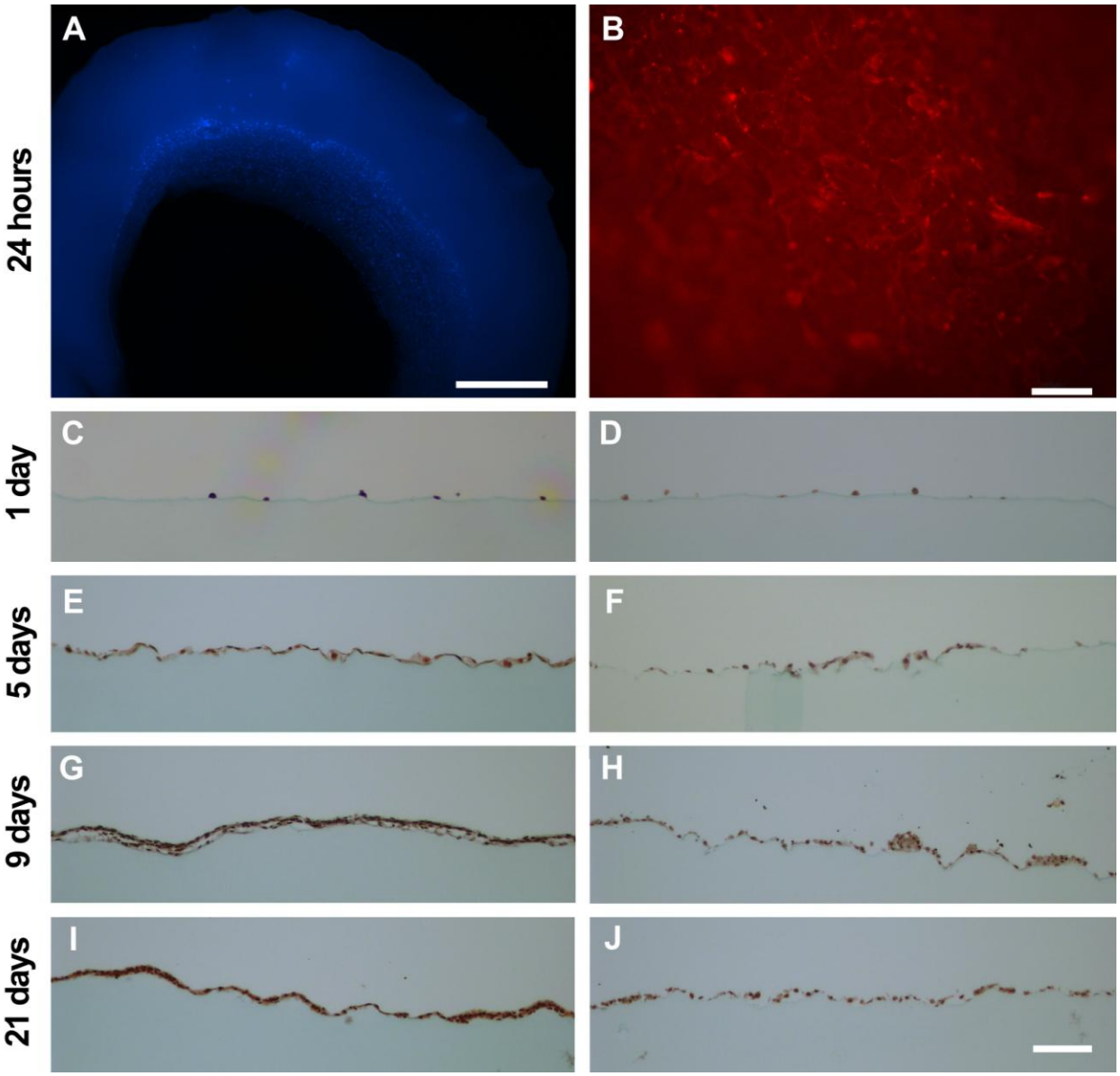

Figure 40. Fluorescence images of stained (A) nuclei and (B) actin cytoskeleton of HUVECs seeded into the lumen of a 6% tubular functionalized scaffold after 24 h of culture. (C-J) Histological images of HUVECs cultured into the lumen of tubular scaffolds after 1day, 5 days, 9 days and 21 days of culture for functionalized (C,E,G,I) and non-functionalized (D,F,H,J) scaffolds. Scale bars stands for 500 μm (A), 20 μm (B) and 200 μm (C-J).

6.4. Discussion

The fabrication of nano-fibrous scaffolds by means of PLA/EtLac gelation system (see chapter 5) was successful. Scaffold microstructure let to high porous tubular scaffolds able to rehydrate (Figure 36).

When scaffold mechanical behaviour was compared to normal human arteries (Figure 37), it was possible to detect important differences. The first difference was that deformation range was one order of magnitude different. While the mean diameter change of fabricated artificial scaffolds was between 1 and 1.03, normal arteries moved between the 1 and 1.15. Another important difference was that diameter deformation during the systolic ramp followed a linear behaviour, while arteries normally present an exponential increase. This artery mechanical behaviour is caused by a differential increase of compliance (decreasing stiffness) along decreasing pressure intervals. This behaviour responds to physiological needs at low pressure, when pulsatile energy has to be preserved during situations of shock to optimize the flow [23]. Thus, the absence of adjustable compliance properties in synthetic materials can be a factor of risk of failure [24]. Moreover, artificial grafts presented creep, whose consequences were observed on fatigue assays.

E_m, which is the inverse of vessel distensibility, defines the relative diameter change for a given pressure increment and is closely related to wall stiffness/compliance. A high E_m involves an increased wall stiffness which causes the acceleration of the propagation velocity of the pressure pulse along the vessel, also known as pulse wave velocity (PWV). PWV is related to arterial distensibility through the Moens-Korteweg equation [25], and calculates the travelling time of a pressure pulse between two vessel points. When a vessel graft has an increased E_m, the consequent rigidity of the vessel wall increases the flow velocity and therefore the shear stress at the interface. Such stress increment has negative impact on endothelial cell proliferation and viability. Moreover, the change of wall distensibility on the anastomotic site provokes a flow disruption, which is an important cause of the intimal hyperplasia development. Tested artificial vessel scaffolds presented E_m framed between the 4000-21000 mmHg for the 80-120 mmHg pressure range (Figure 38A). When compared with native arteries, measured lower values of fabricated tubes were one order of magnitude above normal values for human arteries. Indeed, human peripheral arteries present E_m between the 350 and 700 mmHg [26]. This means that 3.5-4% fabricated scaffolds show similar stiffness values (Figure 38B) than commercial devices made of Dacron or PTFE materials (~5000-6000 mmHg/mm; estimated from [27,28]), and therefore are subjected to the same associated troubles and risk of IH development. Also it is

interesting to notice that, on fabricated PLA scaffolds, neither elastic modulus nor stiffness seems to change within different pressure ranges (80/120 and 0/200), which is related with the absence of variable compliance on artificial grafts mentioned before, and which is far from real vessel walls [29,30].

Another aspect of vessel and flow mechanics to take into consideration is the phase angle between the pressure waveform (wall deformation) and the flow pulsation (deformation force). Despite few studies have been performed, there are indications that the pathologic effects of shear stress can be accentuated with an increased phase difference [31]. Results showed that, for PLA scaffolds, the phase difference was reduced on stiffer scaffolds (Table 13), which at same time presented less plastic deformation accumulation. Thus, aside from preventing plastic deformation accumulation, the elastic component was also important to keep a low phase difference between the pressure waveform and the flow pulsation.

Because important plastic deformation was detected at 7 minutes of cyclic loading, a fatigue assay was performed. Fatigue assay was done on tensile cyclic loading tests that emulated the forces caused by flow pressure on a circumferential portion of the graft wall. Forces were calculated to emulate a 50-200 mmHg diastolic-systolic cyclic pressures. This pressure range was selected to include extreme situations of shock, hypertension or other pathologic conditions. Fatigue tests performed on 4% PLA scaffolds showed that scaffolds broke after 92 cycles due to plastic deformation accumulation, which increased radius size and reduced wall thickness. The combination of both effects caused, as stated in Laplace's law, a fast increase of the circumferential tensile stress on the vessel wall, which eventually provoked the graft failure.

Finally, the proof-of-concept cell studies on tubular scaffolds proved that cells were able to attach, grow and proliferate under static conditions. In this case, HUVECs were seeded on the lumen of a PLA scaffolds obtained from the precipitation of a 6% PLA/EtLac organogel system. Fluorescence images showed that cells could firmly attach on the fibrous PLA network, spread and form an organized cytoskeleton. Histological images showed that cells could grow and develop into a continuous cellular endothelium, which covered the entire lumen. Differences were found between functionalized and non-functionalized scaffolds. While the former could form a continuous layer at day 5 and a more dense and thick layer at day 9, the latter took more time to form a continuous layer (day 9), presented cell aggregates, and after 21 days only was able to form a lower-dense cell layer. Thus, it was observed that functionalization of synthetic

scaffolds was necessary to obtain a good-quality endothelial cell layer in a short time, able to cover the inner vessel lumen and diminish the risk of graft failure.

6.5. Conclusions

This chapter proved the versatility of the system to produce highly-porous, nano-fibrous tubular scaffolds by moulding. High-dense cellular endothelial layer has been obtained by means of ELR functionalization under static conditions. However, mechanical properties still differ from clinical requirements. Stiffness and elastic modulus values have to be reduced one order of magnitude, and the elastic component of the material has to be increased in order to reduce plastic deformation accumulation along time, as well as to reduce phase difference. Importantly, this chapter proves the capacity to tune mechanical properties by means of polymer concentration, which allows tailoring of the scaffold mechanical properties according to the patient characteristics in order to match both.

In order to address these issues, future work will use blends of polymers and/or copolymers with a higher elastic component and reduced stiffness. Examples of this polymeric materials could be poly(lactide-co-caprolactone) or Poly(trimethylene carbonate), which, in the form of co-polymer or blend of polymers, can be processed through the same fabrication routes. Future studies also need to assess the in vitro cell response under dynamic conditions in order to assess cellular response under closer conditions to physiological environment.

6.6. References

1. Roger VL, Go AS, Lloyd-Jones DM, Adams RJ, Berry JD, Brown TM, et al. Heart disease and stroke statistics--2011 update: a report from the American Heart Association. Circulation 2011;123(4):e18-e209.
2. Goldman S, Sethi GK, Holman W, Thai H, McFalls E, Ward HB, et al. Radial artery grafts vs saphenous vein grafts in coronary artery bypass surgery: a randomized trial. JAMA 2011;305(2):167-74.
3. Axthelm S, Porter J, Strickland S, Baur G. Antigenicity of venous allografts. Ann Surg 1979;189(3):290-3.
4. Byrne J, Darling RC 3rd, Chang BB, Paty PS, Kreienberg PB, Lloyd WE, Leather RP, Shah DM. Infrainguinal arterial reconstruction for claudication: is it worth the risk? An analysis of 409 procedures. J Vasc Surg 1999;29(2):259-69.
5. Pomposelli FB Jr, Arora S, Gibbons GW, Frykberg R, Smakowski P, Campbell DR, Freeman DV, LoGerfo FW. Lower extremity arterial reconstruction in the very elderly: successful outcome preserves not only the limb but also residential status and ambulatory function. J Vasc Surg 1998;28(2):215-25.
6. Cho A, Mitchell L, Koopmans D, Langille BL. Effects of changes in blood flow rate on cell death and cell proliferation in carotid arteries of immature rabbits. Circ Res. 1997 Sep;81(3):328-37.
7. Langille BL. Blood flow-induced remodeling of the artery wall. In: Bevan JA, Kaley G, Rubanyi GM. Flow-dependent Regulation of Vascular Function. Oxford University Press, NY 1995. p. 277–299.
8. Greisler HP, Joyce KA, Kim DU, Pham SM, Berceli SA, Borovetz HS. Spatial and temporal changes in compliance following implantation of bioresorbable vascular grafts. J Biomed Mater Res 1992;26(11):1449-61.

9. Strandness DE, Summer DS. Hemodynamics for Surgeon. New York: Grune & Stratton, Inc., 1975.

10. Bassiouny HS, White S, Glagov S, Choi E, Giddens DP, Zarins CK. Anastomotic intimal hyperplasia: mechanical injury or flow induced. J Vasc Surg 1992;15(4):708-17.

11. Sottiurai VS, Sue SL, Feinberg EL 2nd, Bringaze WL, Tran AT, Batson RC. Distal anastomotic intimal hyperplasia: biogenesis and etiology. Eur J Vasc Surg 1988;2(4):245-56.

12. DePaola N, Gimbrone MA Jr, Davies PF, Dewey CF Jr. Vascular endothelium responds to fluid shear stress gradients. Arterioscler Thromb 1992;12(11):1254-7.

13. Tardy Y, Resnick N, Nagel T, Gimbrone MA Jr, Dewey CF Jr. Shear stress gradients remodel endothelial monolayers in vitro via a cell proliferation-migration-loss cycle. Arterioscler Thromb Vasc Biol 1997;17(11):3102-6.

14. Salacinski HJ, Goldner S, Giudiceandrea A, Hamilton G, Seifalian AM, Edwards A, Carson RJ. The Mechanical Behavior of Vascular Grafts: A Review. J Biomater Appl 2001;15(3):241-78.

15. Salacinski HJ, Tai NR, Punshon G, Giudiceandrea A, Hamilton G, Seifalian AM. Optimal endothelialisation of a new compliant poly(carbonate-urea)urethane vascular graft with effect of physiological shear stress. Eur J Vasc Endovasc Surg 2000;20(4):342-52.

16. Giudiceandrea A, Seifalian AM, Krijgsman B, Hamilton G. Effect of prolonged pulsatile shear stress in vitro on endothelial cell seeded PTFE and compliant polyurethane vascular grafts. Eur J Vasc Endovasc Surg 1998;15(2):147-54.

17. Kader K, Akella R, Ziats N, Lakey L, Harasaki H, Ranieri J, Bellamkonda RV. ENOS-overexpressing endothelial cells inhibit platelet aggregation and smooth muscle cell proliferation in vitro. Tissue Eng 2000;6(3):241-51.

18. Burkel WE. The challenge of small diameter vascular grafts. Med Prog Technol 1989;14(3-4):165-75

19. Weinberg CB, Bell E. A blood vessel model constructed from collagen and cultured vascular cells. Science 1986;231:397-400.

20. L'Heureux N, Paquet S, Labbe R, Germain L, Auger F. A completely biological tissue-engineered human blood vessel. FASEB J 1998;12:47-56.

21. Guinea GV, Atienza JM, Elices M, Aragoncillo P, Hayashi K. Thermomechanical behavior of human carotid arteries in the passive state. Am J Physiol Heart Circ Physiol 2005;288(6):H2940-5.

22. O'Rourke MF, Staessen JA, Vlachopoulos C, Duprez D, Plante GE. Clinical applications of arterial stiffness; definitions and reference values. Am J Hypertens 2002;15(5):426-44.

23. Henryk J. Salacinski, Sean Goldner The Mechanical Behavior of Vascular Grafts: A Review Journal of biomaterials Applications DOI: 10.1106/NA5T-J57A-JTDD-FD04

24. Schmitz-Rixen T, Hamilton G. Compliance: A critical parameter for maintenance of arterial reconstruction? In: Greenhalgh RM, Hollier LH. The Maintenance of Arterial Reconstruction. WB Saunders Company Ltd., 1991.

25. Callaghan FJ, Geddes LA, Babbs CF, Bourland JD. Relationship between pulse-wave velocity and arterial elasticity. Med Biol Eng Comput 1986;24(3):248-54.

26. Lee RT, Kamm RD. Vascular mechanics for the cardiologist. J Am Coll Cardiol 1994;23(6):1289-95.

27. Walden R, L'Italien GJ, Megerman J, Abbott WM. Matched elastic properties and successful arterial grafting. Arch Surg 1980;115(10):1166-9.

28. Kazuaki K, Artificial vessel and process for preparing the same. US Patent No. 4857069, 1984.

29. Bergel DH. The static elastic properties of the arterial wall. J Physiol 1961;156:445-57.

30. Dobrin PB. Mechanical properties of arteries. Physiol Rev 1978;58:397-460.

31. Pedrizzetti G, Domenichini F, Tortoriello A, Zovatto L. Pulsatile flow inside moderately elastic arteries, its modelling and effects of elasticity. Comput Methods Biomech Biomed Engin 2002;5(3):219-31.

CHAPTER 7

7. CONCLUSIONS AND FUTURE PERSPECTIVES

7.1. Conclusions

This Thesis presents an extensive study of two different methodologies for the fabrication of functionalized and highly-porous PLA-based scaffolds for tissue engineering. Below are summarized the main conclusions of the work reported in the experimental chapters (Chapter 3-6).

7.1.1. Chapter 3 & Chapter 4 – ELR surface functionalization

- Functionalization of polymeric surfaces (PMMA and PLA) using engineered proteins has been explored in Chapter 3 and 4.
- Functionalization methodology has been characterized and optimized.
- Successful functionalization with short peptides and larger polypeptides has been achieved.
- ELRs have shown to enhance cell-surface interaction in a stronger manner than short peptides (i.e., higher adhesion rates, better cell spreading, stronger attachment and faster proliferation).
- ELRs have shown to minimize the unspecific adsorption of proteins from the serum (albumin).
- ELRs have shown to regulate the selective attachment of specific cell types through the incorporation or not of specific integrin ligands.
- ELRs covalent functionalization has shown to improve cell spreading and proliferation.
- Covalent functionalization of ELRs has shown to permit a high degree of mobility (necessary for the development of cell adhesion focal points), while maintaining ELRs captured on surface.
- ELRs have shown to swell with water and increase wettability.
- ELRs have shown to be a viable alternative, presenting better and faster performances than the use of short peptides and native proteins.

7.1.2. Chapter 5 – Fabrication of high-porous PLA scaffolds

- Fabrication of high-porous nano-fibrous PLA scaffolds using the PLA/EtLac gelating system has been explored in Chapter 5.
- The gelation process for the system PLA/EtLac has been characterized.
- The viscosity behaviour of the PLA/EtLac system has shown to be constant for shear rate ranges of the typical manufacturing processes.
- The gelation temperature for the system PLA/EtLac has found to be 44.5ºC.

- The gelation temperature has shown to be independent from the polymer concentration.
- The equilibrium state of the obtained gel has shown to be independent of the gelling temperature and the gelation time.
- The speed of the gelation process has shown to be function of the warming temperature and polymer concentration.
- The gelation process has shown to cause shrinkage of the gel volume below the 4% and to be dependent of polymer concentration.
- Water-precipitation of PLA/EtLac gels has shown to form high-porous nano-fibrous structures that resemble ECM.
- The use of different polymer concentrations has shown to change the resultant structural network density.
- The micro-network architecture density has shown to control the properties of the resultant porosity, diffusion rate, mechanical and viscoelastic properties.
- The nano-fibrous architecture has shown to provide poro-elastic properties to the obtained scaffolds, which affected scaffold Young's Modulus and viscoelastic properties.
- Obtained PLA scaffolds presented Young's Modulus framed between the 5 MPa and 50 MPa.
- Obtained PLA scaffolds presented elastic deformations around 1-3% and maximum deformations around ~35%.
- A simple methodology to obtain flexible 3D scaffolds, with high porosity and a continuous nano-fibrous structure was obtained by means of green processes and soft conditions.

7.1.3. Chapter 6 – Development of artificial vessel grafts

- Tubular high-porous nano-fibrous PLA scaffolds were fabricated using the PLA/EtLac system and mechanically characterized.
- The mechanical characterization of artificial vessel PLA grafts has shown that the lower obtained E_m was on order of magnitude higher than E_m of normal arteries.
- Stiffness/compliance values of obtained artificial grafts have shown to be similar than commercial devices made of Dacron or PTFE materials.
- Obtained artificial grafts have shown not to have adjustable compliance properties as function of pressure.
- Obtained artificial grafts have shown to accumulate plastic deformation under cyclic loadings, which caused graft mechanical failure.

- Obtained artificial grafts have shown to present tuneable compliance properties as a function of polymer concentration.
- Functionalized artificial grafts with ELRs have shown to permit the development of a continuous endothelial layer after 5 days and a thick endothelial layer after 9 days under static conditions.
- Non functionalized artificial grafts have shown to develop a poor endothelial cell layer after 21 days.

7.2. Future perspectives

This Thesis has characterized two different approaches for the fabrication of scaffolds for tissue engineering: the surface functionalization by means of ELRs and the fabrication of PLA-based scaffolds using the properties of the PLA/EtLac system. Many aspects have been deeply analysed, such as the effects of the different functionalization strategies, the advantages of engineered proteins against short peptides, the enhanced surface properties obtained with ELRs, the characteristics of the PLA/EtLac gelation process, the conditions for the fabrication of highly porous nano-fibrous PLA-based scaffolds, the properties of the resultant scaffolds, the adjustability of such properties and the capability to produce different 3D shapes. As a consequence of the obtained results, new possible research lines are opened for further investigation. This section is devoted to expose some suggestions to be further developed in the future.

In Chapter 3 and 4 it has been observed that ELRs without integrin-ligands sequences can prevent the unspecific adhesion of cells and proteins on polymeric surfaces. In order to better understand the implications of this, further studies could analyse and quantify in more detail if there is any type of promotion towards the adhesion of certain types of proteins or not, since this can have important effects on cell response. Moreover, in order to trigger specific cell adhesion and proliferation, it is necessary to move towards different systems, since RGD is not specific for any cell-type. Instead, the REDV amino acid sequence is known to promote endothelial cells attachment and proliferation over smooth muscles cells [1]. The inclusion of this peptidic sequence into an ELR construct or any other construct with similar properties could be a strategic tool on the functionalization of synthetic vessel grafts to promote the endothelization of the graft lumen while preventing the spreading of smooth muscles cells.

In Chapter 5, the use of the PLA/EtLac system properties for the fabrication of porous scaffolds has been deeply studied. It is suggested that further studies consider exploring the

interaction of different PLA-based materials with EtLac. Indeed, results not shown on this Thesis has already proved that different biodegradable polymers can be dissolved in EtLac and gelate in a similar manner than PLA. In such a way, it is possible to incorporate new mechanical properties on the resultant scaffold (i.e., elastomeric properties), which may be useful for engineering vascular scaffolds. Furthermore, the different PLA-based gelating systems could be used in combination with other processing techniques, such as solid free-form or porogen leaching. It could be also possible to entrap different molecules inside the nano-fibrous matrix, like collagen or any other hydrogel, to include different capabilities and properties (i.e., drug delivery). The combination of different processing techniques and materials can be a powerful tool for the design of intelligent scaffolds. On a different perspective, it is also suggested to study the feasibility of obtaining nano-fibrous structures by lyophilizing the EtLac solvent, which would greatly simplify the process. Currently, there are no studies considering this approach. Thus, firstly it would be necessary to determine the feasibility of the process, and secondly determine if nanofibrous matrices can be similarly obtained.

In Chapter 6 the fabrication of off-the-shelf vessel grafts has been studied. Results suggest that used system must include elastomeric behaviour. For this approach it could be possible to work with PLA copolymers that include elastomeric polymers. In such a way, less rigid and more compliant scaffolds would be obtained. Also, dynamic cellular studies should be performed in order to assess cellular attachment, recruitment and proliferation under mechanical stress conditions.

7.3. References

1. Wei Y, Ji Y, Xiao L, Lin Q, Ji J. Different complex surfaces of polyethyleneglycol (PEG) and REDV ligand to enhance the endothelial cells selectivity over smooth muscle cells. Colloids Surf B Biointerfaces 2011;84(2):369-78.

ACKNOWLEDGEMENTS

When I was about to start this journey I had no clue of what was waiting for me. It has been an adventure that has put me into continuous contact with two things that I love the most in the world, people and knowledge. All things I have learned and experienced would have not been possible without the generosity and kindness of people I have met along the way. These words are addressed to them, to express my gratitude and love towards them.

First of all, I want to express my most honest gratitude to my thesis director, Dr. Miguel Ángel Mateos Timoneda. Miguel has been my guide during the entire journey. He has taken care of me, putting me on the wright way when I was lost, opening doors to me and being a helping hand every time I needed. The deep knowledge he has on the scientific field is something that I have always deeply admired and respected, and has been a reference for me. I owe him my outmost appreciation, for his guide, generosity and friendship along all these years.

I also want to express my thankfulness to Dr. Elisabeth Engel, the group leader of the Biomaterials for Regenerative Therapies group. She was the person that gave me the opportunity to join this excellent team, and has always put a lot of trust on me. I am extremely grateful to her for sharing her excellence with me. She has been a person always open to listen and understand. The difficult questions have been always easy to talk and discuss with her. Her trust towards me, her perseverance and positive actitude has motivated me to pursue my goals. I will be always grateful for her generosity and warm personality.

I also want to thank Prof. Josep A. Planell, the former director of the group and institute, for his effort and passion. He has provided to us a culture based on the effort and positive attitude that is still present in our group. I want to show as well my gratitude to Dr. Oscar Castaño and Dr. Soledad Pérez. They have been a really good company either professionally and personally, being always helpful and always kind.

It is impossible to imagine the greatness of all these years without my lab mates. First of all, I want to say, to all of them, how much I admire their professional dedication and effort. It has been easy to keep fighting against struggles at their side. They have been a source of strength, inspiration and happiness. Tiziano, Aitor, Nadege, Arlyng, Zaida, Marta, Irene, Claudia, Joan, Cris, Laura, Jenifer, Doug and, specially, Riccardo; they have made this travel

easier, better and funnier. I also want to give a special mention to Rodolphe, my first student. With him, I had one of my best times, and I am very happy to have seen his success in his life. I also want to thank Pablo and Maria for everything we shared, and for making me laugh during the hard and the good moments. I want also to express my thoughts to the members of BIBITE group, led by Prof. Maria Pau Ginebra, for all the help and support through all these years.

I also want to express my gratitude to Prof. Gustavo V. Guinea, from the Universidad Politécnica de Madrid, for giving me the opportunity to work in his lab. His friendly attitude made me feel welcome from the very beginning, and his scientific advice had a great impact over my experience. It was a pleasure to enjoy his passion towards science. I am also thankful to Dr. Didier Letourneur, from the UMR 1148 in Paris. During my stay in his lab, he was a very close person, always helpful and attentive. He helped me to overcome unexpected problems, and his scientific skills were of great value. I am also very thankful to Prof. Maria Lluisa Maspoch and Dr. Orlando Onofre, from Centre Català del Plàstic, for their priceless help and support on the development of my work.

Els meus més profunds agraïments al suport i la companyia dels meus amics. He crescut i m'he format com a persona al vostre costat. Amb vosaltres he après a estimar i he forjat els valors que em guien avui dia. Sense la vostra companyia, el vostre amor, la vostra amistat, i les nostres aventures, no es podria entendre perquè em llevo cada dia amb alegria. Víctor, Carol, Ivan, Rubén, Sergio, Helena, Marta, Riccardo, Edu, Moni, Patri, David, Alejandro; gràcies per ser com sou, us estimo enormement. Em doneu l'energia que he necessitat dia a dia per arribar fins aquí.

Toni, la teva arribada a la meva vida ha sigut tan inesperada com màgica. Compartir els moments amb tu és una de les millors alegries que he tingut mai. Fas que perseguir els somnis resulti senzill i divertit. La teva tendresa, alegria i capacitat de volar han sigut una inspiració. Gràcies per ajudar-me i acompanyar-me en aquesta etapa. T'estimo moltíssim.

Finalment volia dedicar els meus darrers pensaments a la meva família. Ells m'ho han donat tot. M'he sentit increïblement estimat i feliç. Ells m'han donat totes les eines i totes les forces necessàries per viatjar a través de la vida. Dels meus pares, Xavi i Montse; del meu germà Joan; de la meva tieta Agnès; i del meu avi Miquel; he après a estimar i a estimar-me, a ser crític, a ser persona, a ser humà, a ser independent, a ser valent, a disfrutar, a ser somiador, a ser lluitador, a respectar i a ser generós. Per ells, i gràcies a ells, m'esforço a ser millor persona. Em feu sentir orgullós de la família que tinc. Us estimo i admiro moltíssim.